Spin dynamics and quantum tunneling in Fe8 nanomagnet and in AFM rings by NMR

by

Seung-Ho Baek

A dissertation submitted to the graduate faculty

in partial fulfillment of the requirements for the degree of

DOCTOR OF PHILOSOPHY

Major: Condensed Matter Physics

Program of Study Committee:
Ferdinando Borsa, Co-major Professor
Marshall Luban, Co-major Professor
Joerg Schmalian
Joseph Shinar
Jianwei Qiu
Gordon J Miller Jr.

Iowa State University

Ames, Iowa

2004

Graduate College
Iowa State University

This is to certify that the doctoral dissertation of

Seung-Ho Baek

has met the dissertation requirements of Iowa State University

Co-major Professor

Co-major Professor

For the Major Program

사랑하는 아내 은지와 딸 라윤에게 바칩니다

To Eun-Ji and Flora

TABLE OF CONTENTS

IS-T 2015

CHAPTER 1 Introduction

1.1 Single molecule magnets (SMMs)

For a few decades, chemists have developed new classes of magnets based on molecules rather than on metals or oxides. The idea behind this is the challenge of creating new classes of materials from which new exciting properties may be expected (see, for example, Kahn [1]). It was only a decade ago when physicists realized that a particular class of molecular magnets (MM) i.e., single molecule magnets (SMMs) are excellent zero-dimensional model system for the study of the *nanoscopic* or *mesoscopic* magnetism. The prefix nano- or meso- indicates that SMMs are positioned at the frontier between single spin behavior and bulk magnetism. In this interesting regime, one can expect new physical phenomena arising from the coexistence of classical and quantum behaviors [2].

SMMs are exchange coupled clusters, at present, of two to thirty paramagnetic ions (e.g., iron dimer [3] to a giant cluster Fe30 [4]), usually from the first period of the transition metals.[1] The magnetic centers in the molecule are fairly well shielded (i.e., very weak intermolecular interaction) by large organic ligand shells, and thus the individual molecules are magnetically almost independent. The weak intermolecular interactions (or zero-dimensionality) in SMMs allow us to investigate the molecular magnetism, simply by the usual macroscopic measurement techniques. In fact, the macroscopic quantum phenomena observed in SMMs arises from the finite size system. Interestingly, some of SMMs can be viewed as *real* nanosize quantum dots. In this case, unfilled *molecular* orbitals, which are delocalized over the entire magnetic metal cores coupled by metal-metal bonding, provide another interesting class of molecular magnets

[1]Note that the term "single molecule magnets" is used here not only to the ferro- or ferri-magnetic clusters but also to non-magnetic rings or clusters.

in analogy with the traditional magnetism of unfilled *atomic* shells [5].

Thanks to the finite size of SMMs, one may sometimes perform first principles calculations from the Hamiltonian, and compare it with the experimental results. Although the exact diagonalization is limited to, for example, systems of eight spins 3/2 (in this case, the total degeneracy of the spin states is $(2S+1)^N = 65,536$), this feature is very attractive from a theoretical point of view. One of the big advantages of SMMs is that one can synthesize a molecular cluster at will, in principle if not in practice, for a specific purpose of investigation. Indeed, numerous different types of SMMs have been synthesized with different features: (1) the total spin of molecule in the ground state varies from zero up to 51/2; (2) the symmetry of structure ranges from simple one dimensional (e.g., rings) to complex three dimensional clusters (e.g., Fe8, Mn12ac); (3) the paramagnetic ions in a molecule are coupled via ferromagnetic (FM) or antiferromagnetic (AFM) interaction with various magnitude of the exchange constant J. Therefore, together with the ability to proceed with careful measurements and theoretical methods, SMMs present a wonderful laboratory to explore fundamental problems in magnetism such as spin correlation and exchange interactions at nanosize scale, which can be a key to understand the collective spin behavior in conventional magnetic materials.

Among the variety of molecular magnetic systems, here we will briefly review the general properties of the two classes of SMMs. (1) Ferrimagnetic clusters with a high spin ground state and a large uniaxial anisotropy such as Fe8 and Mn12ac; (2) Antiferromagnetic rings, which consist of an even number of metallic ions forming nearly perfect ring structures with isotropic nearest-neighbor exchange constant, such as the "ferric wheel" Fe10 [6]. For a comprehensive review of molecular magnetic clusters, we refer to Miller [7], Gatteschi [2, 8, 9], and Caneschi [10].

Antiferromagnetic rings

Antiferromagnetic (AFM) rings may be regarded as one-dimensional (1D) chains with periodic boundary conditions due to the perfect coplanar arrangement of the paramagnetic ions. The magnetic interaction between neighboring ions within individual molecules is of the antifer-

romagnetic Heisenberg type yielding a ground $S = 0$ state and dominates any other magnetic effect like single-ion and/or dipolar anisotropies. As a result, AFM rings are an attractive model system for the study of the quantum spin dynamics of one-dimensional antiferromagnetic Heisenberg magnetic chains [11]. Since the independent spin paramagnetic behavior at high temperature evolves towards a correlated collective spin system with decreasing temperature, one can obtain precious information with regard to the spin dynamics in this exactly solvable finite system as a function of temperature and external field. The obtained results can also be linked to a better understanding of the bulk system.

The magnetic properties of the AFM rings can be described well by the spin Hamiltonian [12, 13]

$$\mathcal{H} = -J\sum_{i=1}^{N}\mathbf{S}_i \cdot \mathbf{S}_{i+1} + D\sum_{i=1}^{N}S_{i,z}^2 + \mathrm{g}\mu_B\mathbf{H}\cdot\sum_{i=1}^{N}\mathbf{S}_i, \tag{1.1}$$

where J is an antiferromagnetic coupling ($J < 0$), the second term represents uniaxial single-ion anisotropies along the easy axis (z) ($D < 0$), N denotes the number of metal ions, and the last term is the Zeeman interaction. The magnetic anisotropy, which in most cases is assumed to be very small, plays an important role e.g., in quantum tunneling of the Néel vector [12, 14, 15].

By following systematic synthesis schemes one can obtain AFM rings with a wide variety of properties: (1) different size of the spin of the metallic ion: 1/2 (Cu^{2+}, V^{4+}), 3/2 (Cr^{3+}), 5/2 (Fe^{3+}, Mn^{2+}) etc, (2) different number of ions (odd numbered ring is in particular interesting because strong spin frustration effects are expected), (3) various strength of the exchange coupling J.

Apparently, the first AFM ring system that aroused the great interest in physics community is the molecular ferric wheel $[Fe(OMe)_2(O_2CCH_2Cl)]_{10}$ (in short Fe10) [6]. The structure of Fe10 is shown in Fig. 1.1. Magnetization measurements of Fe10 at low temperature show that the magnetization increases in a stepwise fashion [11] with increasing field. The first step in the magnetization is due to the level-crossing from $|S = 0, M = 0\rangle$ to $|S = 1, M = -1\rangle$, the second step is due to the level-crossing from $|S = 1, M = -1\rangle$ to $|S = 2, M = -2\rangle$, and so on. The field-induced level-crossing effect, which is a manifestation of quantum size effect, has

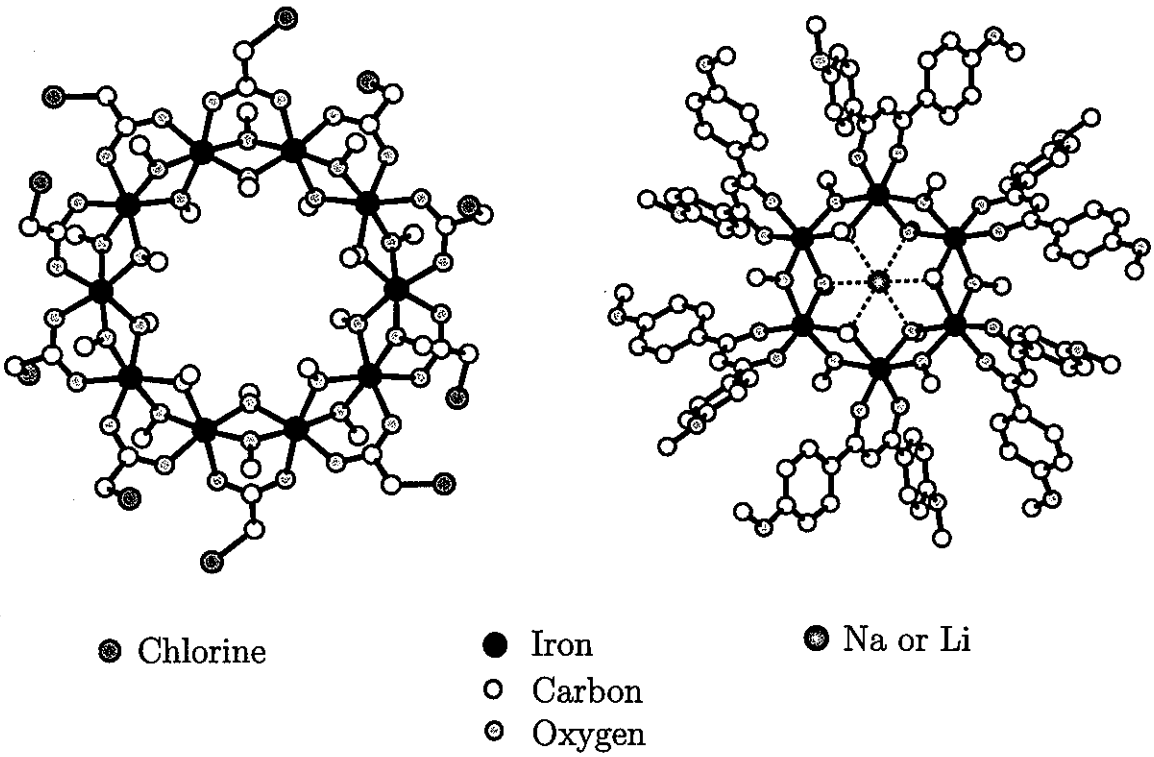

Figure 1.1 Structure of ferric wheels Fe10 (left) and Fe6(X) (right) with X=Na or Li. Hydrogen atoms were omitted for clarity.

been confirmed by NMR measurement [16]. Since the infinite magnetic chain does not show any step in the magnetization [17], the properties of the AFM rings can be extrapolated to the infinite chain by making larger and larger rings.

Smaller ferric wheels containing six Fe^{3+} ions, Fe6(Na) and Fe6(Li) also exhibit the field-induced "stepped" hysteresis behavior [18–20]. In these systems, the alkali-metal ion, Li^+ or Na^+, is hosted in the center of the ring, and plays an interesting role. Namely, the exchange constant J changes from 14 K to 21 K by replacing Li^+ with Na^+. Also the magnetic anisotropy is affected by the replacement of the alkali-metal ion [18]. These significantly different magnetic properties in the two derivatives may arise from the distortions induced by the alkali-metal ion on the ring by the so called "host-guest interaction". Therefore, these Fe6 derivatives can provide valuable information regarding the origin of the magnetic anisotropy as well as the spin dynamics itself.

Another interesting AFM ring is a "chromic wheel" $Cr_8F_8Piv_{16}$ (Cr8) where HPiv is pivalic

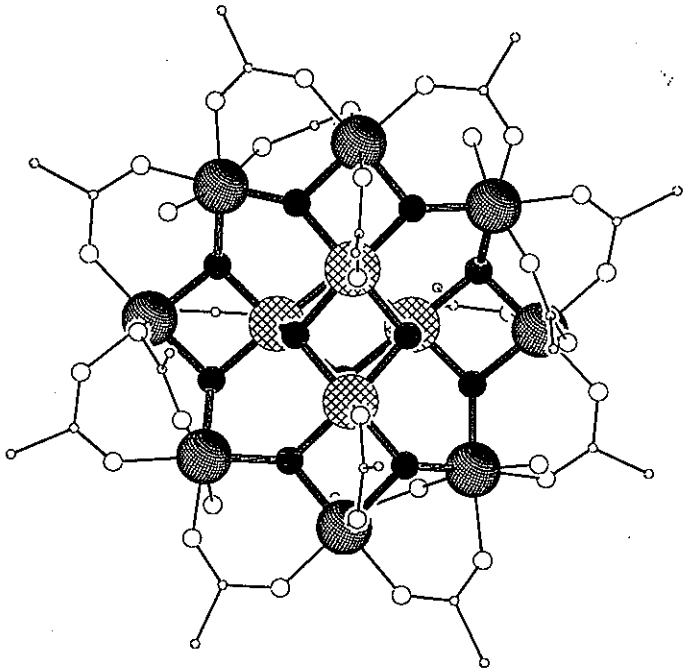

Figure 1.2 Structure of the Mn12ac clusters (taken from Ref. [10]). The large symbols denote manganese ions [inner 4 ions are Mn^{4+} ($s = 3/2$), outer 8 ions are Mn^{3+} ($s = 2$)], small dark gray circle denotes oxygen bridge, and open circles forms the acetate ligands.

acid, which consists of eight Cr^{3+} ($s = 3/2$) [21]. It has been found that Cr8 exhibits the level-crossing effect by specific heat measurement [22] and by NMR measurement [23]. Regarding spin dynamics, $s = 3/2$ system could be regarded as a link between *quantum* spin 1/2 and *classical* spin 5/2 systems. (Unfortunately, there is no *bona fide* spin 1/2 AFM ring.) Our NMR study of AFM rings in this thesis has been motivated by the interesting spin dynamics via spin-lattice relaxation rate $1/T_1$ as a function of temperature and external field.

Ferrimagnetic high-spin clusters

The magnetic properties of these systems are discussed in detail in chapter 3. Here we limit ourselves to a brief description of the two main clusters of this class and to a mention of their potential applications.

SMMs such as $[Mn_{12}O_{12}(CH_3COO)_{16}(H_2O)_4]$ (Mn12ac) [24] and $[Fe_8O_2(OH)_{12}(tacn)_6]^{8+}$

(Fe8) [25], where both clusters have the ground spin $S = 10$, show the interesting phenomenon of superparamagnetism i.e., slow relaxation of the magnetization [26, 27]. These molecules can be magnetized at low temperatures, and will remain magnetized even after removal of the external field. This property is usually associated with bulk magnets. However, it was shown that this property in SMMs is truly due to the individual molecule, and not to long range interactions. The physical properties of SMMs are very interesting, due to the size of the systems. The properties of a bulk magnet with a large spontaneous magnetization can be described in a classical framework, using well known theories. On the other hand, a single large spin is clearly a quantum system. The area between these two limiting regimes is very interesting from a physical point of view, and it is exactly there that molecular magnets with the total spin $S = 10$ are located. Certainly, the discovery of the slow relaxation of the magnetization in Mn12ac [26] can be regarded as a major breakthrough in SMMs. The second breakthrough may be the experimental observation of the quantum tunneling of the magnetization in Mn12ac [28, 29] and Fe8 [30]. For Fe8, the pure quantum tunneling has been observed for the first time below 0.4 K. These quantum phenomena have been under intensive investigation, resulting in a substantial body of literature related with those subjects in the last ten years [31].

Since these molecules are bistable, in the sense that they can be magnetized along two directions, applications in data storage devices have been proposed. The maximum theoretical data density would be enormous, since every molecule can be considered as a bit of data. This information density could be of the order of 100 Tbit/in^2, which is three to four orders of magnitude larger than what is currently possible. For this idea to be realized, a significant challenge is the development of methods for reading and writing such a tiny magnetic moment. Another challenge is related with the synthesis of SMMs having larger energy barrier for the reorientation of the magnetization, which would permit storage of information at accessible temperatures. Although the quantum tunneling is fascinating feature from a physical point of view, its effect should be suppressed for the application of the data storage because the tunneling means loss of information. Beyond that, applications in the memory components

of quantum computation [32] are possible. A single crystal of the molecules could potentially serve as the storage unit of a dynamic random access memory device in which fast electron spin resonance pulses are used to read and write information [33, 34]. It has also been suggested that these high-spin ferrimagnetic clusters might be utilized as low-temperature refrigerants utilizing the magnetocaloric effect [35, 36]. The idea for this application arises from the fact that a large entropy variation, which depends on the sweeping rate of the magnetic field, takes place around the blocking temperature.

1.2 Nuclear magnetic resonance as a tool to investigate SMMs

Nuclear magnetic resonance (NMR) is a powerful tool to investigate the local static and dynamic properties of magnetic systems. Among the many successes achieved by NMR technique in various magnetic materials, we give a few examples related with the motivation for the investigation of single molecule magnets by NMR. Firstly, NMR has been proved to be a suitable tool as a local probe to study spin dynamics due to the fact that the nuclei are very sensitive to the fluctuations of the local field produced by the localized magnetic moments. The nuclear spin-lattice relaxation ($1/T_1$) probes the long time behavior of the spin correlation function since NMR detects the low frequency part of the spin fluctuation spectrum. For example, in 1D Heisenberg magnetic chains, the long-time persistence of spin correlation has dramatic consequences on the field dependence of $1/T_1$ [37, 38]. Secondly, NMR spectrum gives us information on the hyperfine interactions of the nuclei with the local magnetic moments, and its field dependence provides information of the internal magnetic structure [39–42]. Thirdly, NMR is a powerful tool for the investigation of quantum tunneling effect [43, 44].

We have studied both static and dynamic properties of SMMs by NMR taking advantage of the above mentioned potentiality of the technique.

1.3 Organization of the dissertation

We began this thesis with a general introduction to single molecule magnets and to nuclear magnetic resonance (NMR) in Chapter 1. In Chapter 2, we introduce the basic concepts of

NMR focusing on the nuclear spin-lattice relaxation mechanisms which are applied for single molecule magnets. Chapter 3 is devoted to the magnetic properties and the spin dynamics in Fe8 molecular cluster. In particular, the quantum tunneling of the magnetization phenomena will be described in detail with some novel calculations and insights. ^{57}Fe NMR measurements in Fe8 at low temperatures are presented in Chapter 4. There we analyze the ^{57}Fe NMR spectrum and the nuclear relaxation rates as a function of external field and temperature in terms of the hyperfine field and its fluctuations via spin-phonon interactions and tunneling mechanism. We discovered that the relaxation rate of ^{57}Fe in zero field or weak fields at low temperature is due to a strong collision mechanism and thus it measures directly the effective tunneling rate of the magnetization.

Chapter 5 is concerned with the temperature and field dependence of the proton $1/T_1$ in antiferromagnetic ring clusters. There we present a scaling formula that is in excellent agreement with the peak of $1/T_1$ observed near the temperature which is comparable to the magnetic exchange energy J/k_B and we provide an underlying physical picture in terms of broadening of the magnetic levels due to acoustic phonons.

CHAPTER 2 Nuclear magnetic resonance and relaxation

Nuclear magnetic resonance (NMR) has established itself as a powerful technique for the study of the local static and dynamic properties of magnetic materials. In this chapter we discuss the basic concepts of NMR, nuclear spin relaxation mechanism, and pulse NMR methods, restricting ourselves to the topics which are necessary to understand NMR in single molecule magnets.

2.1 Magnetic resonance theory

For the discussion in this section we are referring to Abragam [45] and Slichter [46].

2.1.1 Isolated nuclear spins

Consider a nucleus with total spin angular momentum $\mathbf{I}\hbar$. The relation between the angular momentum and nuclear magnetic dipole moment $\boldsymbol{\mu}$ is given by $\boldsymbol{\mu} = \gamma_n \hbar \mathbf{I}$, where γ_n is the gyromagnetic ratio. The Hamiltonian which describes the Zeeman interaction between $\boldsymbol{\mu}$ and a magnetic field $\mathbf{H}_0$ can therefore be written as

$$\mathcal{H} = -\boldsymbol{\mu} \cdot \mathbf{H}_0. \tag{2.1}$$

The energies of the $2I+1$ eigenstates $|m\rangle$ of Eq. (2.1) are given by $E(m) = -\gamma_n \hbar H_0 m$, where m are the eigenvalues of I_z, and z denote the direction of $\mathbf{H}_0$. Since the magnetic dipole transition is allowed for $\Delta m = \pm 1$, we have $\Delta E = \gamma_n \hbar H_0 = \hbar \omega_n$, giving the Larmor frequency $\omega_n = \gamma_n H_0$. From the Larmor theorem, the magnetic moment $\boldsymbol{\mu}$ obeys the classical equation of motion in a magnetic field,

$$\frac{d\boldsymbol{\mu}}{dt} = \boldsymbol{\mu} \times (\gamma_n \mathbf{H}_0). \tag{2.2}$$

Thus, the expectation value of μ_z is time independent while those of μ_x and μ_y vary sinusoidally with Larmor frequencies ω_n.

Now we introduce a transverse, linearly oscillating magnetic field of the form $\mathbf{H}_1(t) = H_1(\hat{x}\cos\omega t + \hat{y}\sin\omega t)$. It is convenient to transform Eq. (2.2) to a new coordinate system x', y', z' in which $\mathbf{H}_0 \parallel z'$; the x', y' axes rotate about z' with constant angular velocity ω, and H_1 is taken to lie along x'. One can write the time derivative $\delta\boldsymbol{\mu}/\delta t$ in the rotating frame as $\delta\boldsymbol{\mu}/\delta t = d\boldsymbol{\mu}/dt + \boldsymbol{\mu}\times\boldsymbol{\omega}$, which yields

$$\frac{\delta\boldsymbol{\mu}}{\delta t} = \gamma_n\boldsymbol{\mu}\times\left[\hat{x}'H_1 + \hat{z}'\left(H_0 + \frac{\omega}{\gamma_n}\right)\right], \tag{2.3}$$

where $\hat{x}'$ and $\hat{z}'$ denote unit vectors. The resulting motion of $\boldsymbol{\mu}$ in the rotating frame, about an effective field $\mathbf{H}_{\text{eff}} = \hat{x}'H_1 + \hat{z}'(H_0 + \omega/\gamma_n)$ is illustrated in Fig. 2.1. If $\boldsymbol{\mu}$ is oriented initially along z' it will always return to that direction periodically. Thus, there is no net energy transfer, on the average, between the H_1 field and the magnetic moment. At resonance ($\omega = -\gamma_n H_0$) the effective field is simply H_1 and $\boldsymbol{\mu}$ precesses about x' at a rate $\omega_1 = -\gamma_n H_1$. If H_1 were applied only for duration τ such that $\theta = \pi/2 = \gamma_n H_1\tau$ (90° pulse), the magnetic moment is initially turned along y' direction and remains at rest in the rotating frame. Of course, the moment precesses with the Larmor frequency in xy plane in the laboratory frame.

For a system of N identical, non-interacting spins in a volume V, the total nuclear magnetization is simply expressed as $\mathbf{M} = V^{-1}\sum_{i=1}^{N}\boldsymbol{\mu}_i$. Eq. (2.3) is also valid by replacing $\boldsymbol{\mu}$ with the total magnetization $\mathbf{M}$.

2.1.2 Relaxation

From the discussion in previous subsection, one would predict that the magnetization (after applying $\pi/2$ pulse) should precess indefinitely in the xy plane at the Larmor frequency. In any real system, however, the transverse magnetization decays to zero and the longitudinal magnetization relaxes to its equilibrium state along the z axis as a consequence of interactions among the nuclear spins and between them and their environments. One can usually distinguish two types of relaxation; the spin-spin and spin-lattice relaxation.

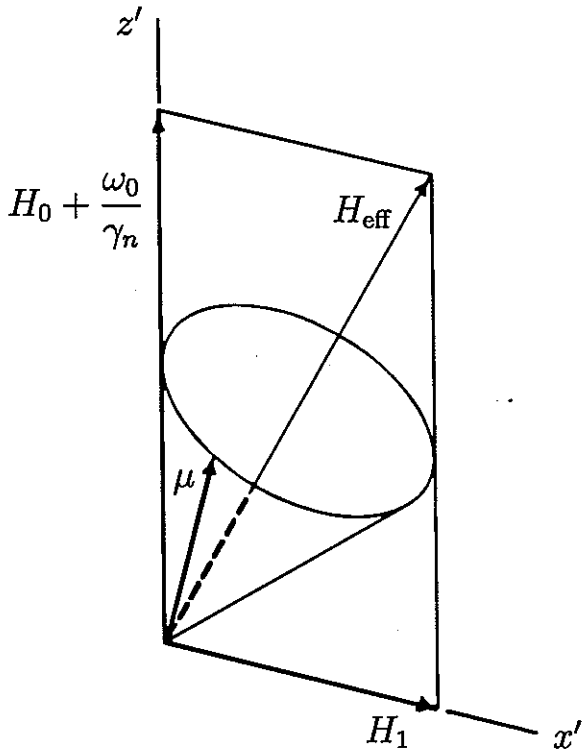

Figure 2.1 Motion of the magnetic moment μ in the rotating coordinate system.

2.1.2.1 Spin-spin relaxation

The spin-spin interactions (e.g. the classical magnetic dipolar coupling between the nuclear moments) tend to maintain thermal equilibrium within the nuclear spin system. This interaction leads to the decay of the transverse magnetization in the static field. The characteristic time of the *irreversible* decay of the transverse magnetization is defined by the spin-spin (or transverse) relaxation time T_2. The T_2 process for solids is generally associated with the spread in the local fields (thus the spread of the Larmor frequencies) produced by the nearby nuclear spins. If the distance between the nearest neighbors is r, $1/T_2$ is given as order of magnitude by:

$$1/T_2 \sim \gamma_n H_{\text{loc}} \sim \frac{\gamma_n^2 \hbar}{r^3}. \tag{2.4}$$

2.1.2.2 Spin-lattice relaxation

The spin-lattice interactions provide contact between the nuclear spins and a "lattice" consisting of the other internal degrees of freedom of the system (e.g. phonons, conduction electrons). Since the specific heat of the lattice is generally much greater than that of the nuclear spin system, the lattice serves as a heat reservoir of temperature T_L. Here we assume that the spin-spin couplings are strong enough to maintain the thermal equilibrium among the nuclear spins during the relaxation with a common "spin temperature" T_s. Thus, in the absence of external perturbations, $T_s = T_L$. When the perturbation is initially applied, $T_s > T_L$. After removal of the perturbation, the spin temperature (i.e. the longitudinal magnetization) will tend to reach the lattice temperature (i.e. the equilibrium magnetization) with a characteristic spin-lattice relaxation time T_1.

Consider a spin system in thermal equilibrium described by a spin temperature T_s. The probability that the system is found in the energy state i is given by

$$p_i = \frac{1}{Z}\exp(-\beta_s E_i), \tag{2.5}$$

where the partition function $Z \equiv \sum_i \exp(-\beta_s E_i)$ with $\beta_s \equiv 1/k_B T_s$, and the sum is extended over the entire states. Then the total average energy

$$\overline{E} = \sum_i p_i E_i \tag{2.6}$$

can be related at any time to a unique β_s. For convenience, we define a zero of energy such that $\mathrm{Tr}(E_i) = 0$, where Tr denotes a trace over the spin eigenstates. The time dependence of β_s can be derived from

$$\frac{d\beta_s}{dt} = \frac{d\overline{E}/dt}{d\overline{E}/d\beta_s}. \tag{2.7}$$

We assume that the p_i's obey simple linear rate equations of the form (so called "master" equation)

$$\frac{dp_i}{dt} = \sum_j \left(p_j W_{ji} - p_i W_{ij}\right), \tag{2.8}$$

where W_{ij} is the transition probability from state i to j. Since each term in the sum in Eq. (2.8) vanishes when $dp_i/dt = 0$ (i.e. when $\beta_s = \beta_L$),

$$W_{ij} = W_{ji} \exp\left[-\beta_L \left(E_j - E_i\right)\right]. \tag{2.9}$$

In the high temperature approximation (i.e. $\gamma_n \hbar H_z \ll k_B T_s$), only states for which $|E_i| \ll k_B T_s$ contribute significantly to the resonance behavior of the system. In this limit, the partition function becomes the total number of states, $Z = Z_\infty = (2I+1)^N$. Combining Eqs. (2.6)–(2.9) yields

$$\frac{d\beta_s}{dt} = \frac{\beta_L - \beta_s}{T_1}, \tag{2.10}$$

where

$$\frac{1}{T_1} = \frac{1}{2} \frac{\sum_{ij} (E_i - E_j)^2 W_{ij}}{\sum_i E_i^2}. \tag{2.11}$$

If the perturbation is very weak compared to the Zeeman Hamiltonian i.e. $\mathcal{H}_1(t) \ll \mathcal{H}_0$, one can apply the first-order time-dependent perturbation theory to calculate the relaxation transition probabilities. In this limit (also called weak collision limit), W_{ij} in Eq. (2.11) is given by,

$$W_{ij} = \frac{2\pi}{\hbar} |\langle i|\mathcal{H}_1|j\rangle|^2 \delta(E_i - E_j - \hbar\omega), \tag{2.12}$$

where $\mathcal{H}_1$ is the Hamiltonian of the perturbation. Eq. (2.12) is useful only when the energy levels of the lattice are exactly known. It can also be used at low temperature when the energy levels can be approximated by a given dispersion relation e.g. spin wave theory, phonon states, etc. It is sometimes more convenient to calculate the transition probability from the correlation function $G_{ij}(t)$ of $\mathcal{H}_1$. In this semi-classical approach, particularly valid at high temperature, we can rewrite Eq. (2.12) by using the relation $\delta(x) = 1/2\pi \int_{-\infty}^{+\infty} \exp(ixt)dt$ and the Heisenberg operator representation, $A(t) = e^{i\mathcal{H}t/\hbar} A(0) e^{-i\mathcal{H}t/\hbar}$,

$$W_{ij} = \frac{1}{\hbar^2} \int_{-\infty}^{+\infty} dt G_{ij}(t) e^{i\omega t}, \tag{2.13}$$

where $\omega = (E_i - E_j)/\hbar$. For a stationary (or weakly time dependent) perturbation, the correlation function can be defined by

$$G_{ij}(t) \equiv \langle \mathcal{H}_1(t)\mathcal{H}_1(0)\rangle = \overline{\langle i|\mathcal{H}_1(t)|j\rangle\langle j|\mathcal{H}_1(0)|i\rangle}, \tag{2.14}$$

where the bar denotes an ensemble average. If $\mathcal{H}_1(t)$ is a randomly varying quantity in time, the correlation function decays exponentially with a correlation time τ_c [i.e. $G(t) \propto \exp(-\tau_c/t)$]. The correlation function $G_{ij}(t)$ is also related to the spectral density function $\mathcal{J}_{ij}(\omega)$ as

$$G_{ij}(t) = \frac{1}{2\pi}\int_{-\infty}^{+\infty} d\omega \mathcal{J}_{ij}(\omega)\exp(i\omega t). \tag{2.15}$$

$\mathcal{J}(\omega)$ and $G(t)$ have an inverse relationship. In other words, $\mathcal{J}(\omega)$ contains frequencies up to the order of $1/\tau_c$. For example, if $G(t)$ decays slowly (i.e. long τ_c), $\mathcal{J}(\omega)$ is all bunched up for small ω, while if $G(t)$ decays rapidly (i.e. short τ_c) $\mathcal{J}(\omega)$ is distributed in large range of ω. From Eqs. (2.13) and (2.15), we have

$$W_{ij} = \frac{\mathcal{J}_{ij}(\omega_n)}{\hbar^2}. \tag{2.16}$$

For the case of $I = \frac{1}{2}$, one can write

$$\frac{1}{T_1} = W_{\frac{1}{2},-\frac{1}{2}} + W_{-\frac{1}{2},\frac{1}{2}} = 2W, \tag{2.17}$$

where we utilized the fact that in the high temperature limit $W_{ij} \cong W_{ji}$ [see Eq. (2.9)]. It must be emphasized that Eqs. (2.11) and (2.17) are only valid if the spin system can be described by a spin temperature.

If we have information on the physical basis of the fluctuation of the interaction, $1/T_1$ can be evaluated from Eqs. (2.13) and (2.17).

2.1.3 Generalized nuclear susceptibilities

Let us assume that the rotating field of amplitude H_1 is actually produced by a linearly polarized field $H_x(t) = 2H_1 e^{i\omega t}$. Note that $2H_1$ is the peak value of a linearly polarized field while H_1 is the magnitude of the two counter-rotating fields into which $H_x(t)$ can be decomposed. If H_1 is sufficiently small, the linear response $M_x(t)$ of the spin system can be described by a complex susceptibility, $\chi = \chi' - i\chi''$:

$$M_x = 2H_1 \mathrm{Re}\{\chi e^{-i\omega t}\} = 2H_1(\chi' \cos\omega t + \chi'' \sin\omega t). \tag{2.18}$$

The establishment of a transverse magnetization corresponds to an average power dissipation

$$\overline{P} = \frac{\omega}{2\pi}\int_{t=0}^{t=2\pi/\omega} H_x(t) dM_x = 2\omega\chi'' H_1^2 \tag{2.19}$$

per unit volume.

On the other hand, the power absorbed by the system per unit volume can be calculated by the perturbation theory,

$$\begin{aligned}\overline{P} &= \hbar\omega \sum_{ij}(p_i - p_j)W_{ij} \\ &= 2\pi\omega H_1^2 \sum_{ij}(p_i - p_j)|\langle i|\mu_x|j\rangle|^2 \delta(E_i - E_j - \hbar\omega).\end{aligned} \tag{2.20}$$

Since $|E_i - E_j| \ll k_B T_s$ in most experiments we have

$$(p_i - p_j) = \frac{1}{Z} e^{-E_i\beta_s}\left(e^{(E_i - E_j)\beta_s} - 1\right) \approx \frac{\hbar\omega\beta_s}{Z}. \tag{2.21}$$

Substituting Eq. (2.21) into Eq. (2.20) and comparing the resulting expression with Eq. (2.19) yields

$$\chi'' = \pi\hbar\omega\beta_s f(\omega), \tag{2.22}$$

where $f(\omega)$ is the shape function defined by

$$f(\omega) = \frac{1}{Z}\sum_{ij}|\langle i|\mu_x|j\rangle|^2 \delta(E_i - E_j - \hbar\omega). \tag{2.23}$$

Eq. (2.22) may also be expressed as an integral form by the same method used when deriving Eq. (2.13)

$$\chi'' = \frac{1}{2Z}\omega\beta_s \int_{-\infty}^{+\infty} dt G(t) e^{i\omega t}, \tag{2.24}$$

where $G(t) = \mathrm{Tr}(\mu_x(t)\mu_x(0))$.

The real part of χ can be obtained from Eq. (2.22) by means of the Kramers-Kronig relation

$$\chi'(\omega) = \frac{1}{\pi}\mathcal{P}\int_{-\infty}^{+\infty} \frac{d\omega'\chi''(\omega')}{\omega' - \omega}, \tag{2.25}$$

where $\mathcal{P}$ means the principal part.

A phenomenological solution to the problem of the NMR response of a many-spin system is provided by the Bloch formulation. In this formulation the equation of motion of the macroscopic magnetization ($d\mathbf{M}/dt = \gamma_n \mathbf{M} \times \mathbf{H}$) is modified by the addition of damping terms of the form $-M_x/T_2$, $-M_y/T_2$, and $(M_0 - M_z)/T_1$, where M_0 is the thermal equilibrium

magnitude of M. The solution to the resulting equations is given by the Bloch susceptibilities

$$\chi'(\omega) = \frac{1}{2}\chi_0\omega_n T_2 \frac{T_2(\omega_n - \omega)}{1 + T_2^2(\omega_n - \omega)^2 + \gamma_n^2 H_1^2 T_1 T_2}, \tag{2.26}$$

$$\chi''(\omega) = \frac{1}{2}\chi_0\omega_n T_2 \frac{1}{1 + T_2^2(\omega_n - \omega)^2 + \gamma_n^2 H_1^2 T_1 T_2}, \tag{2.27}$$

where χ_0 is the static nuclear susceptibility and $\omega_n = \gamma_n H_0$ is the resonance frequency. One can easily see that Eqs. (2.26) and (2.27) do not fulfill the Kramers-Kronig relation since these susceptibilities depend on the strength of H_1. It is only in the limit $\gamma_n^2 H_1^2 T_1 T_2 \ll 1$ (so called "linearity condition") when the H_1 dependence may be ignored and the frequency response takes on the characteristic Lorentzian form. If H_1 is large, the response of the system is maximized when $\gamma_n^2 H_1^2 T_1 T_2 \approx 1$. The phenomenon is known as *saturation.*

2.1.4 Nuclear dipolar broadening and methods of moments

The nuclear dipole-dipole interaction is written as

$$\mathcal{H}_{\text{dip}} = \sum_{j>k} \frac{\hbar^2\gamma_n^2}{r_{jk}^2}\left[\mathbf{I}_j \cdot \mathbf{I}_k - 3\frac{(\mathbf{I}_j \cdot \mathbf{r}_{jk})(\mathbf{I}_k \cdot \mathbf{r}_{jk})}{r_{jk}^2}\right]. \tag{2.28}$$

This interaction produces a homogeneous broadening of the resonance line of the order of $\mathcal{H}_{\text{dip}}/\hbar$ (in frequency unit). In solids, a reasonable picture of the real situation is given by the "rigid lattice" approximation, in which nuclear positions are fixed. A quantitative evaluation of the broadening of the resonance lines due to nuclear spin-spin coupling can be obtained by calculating the moments with respect to $\langle\omega\rangle = \omega_n$,

$$M_n = \int_0^\infty (\omega - \omega_n)^n f(\omega) d\omega, \tag{2.29}$$

where $f(\omega)$ is the normalized shape function defined by Eq. (2.23). If the interactions are known, the moments can be calculated exactly.

In the case of a Gaussian line shape (i.e. the function $\chi''(\omega)$ decreases very fast as $|\omega - \omega_n|$ increases), the width of the line corresponds to $\sqrt{M_2}$. The second moment due to the dipole-dipole interaction between like nuclei is given by Van Vleck [47]:

$$(M_2)_{II} = \frac{3}{4}\gamma_I^4\hbar^2 I(I+1)\sum_k \frac{(1 - 3\cos^2\theta_{jk})^2}{r_{jk}^6}, \tag{2.30}$$

where r_{jk} is the distance between the spin $\mathbf{I}_j$ and $\mathbf{I}_k$, and θ_{jk} is the angle between $\mathbf{r}_{jk}$ and the external field $\mathbf{H}$. The coupling between unlike spins is

$$(M_2)_{IS} = \frac{1}{3}\gamma_I^2\gamma_S^2\hbar^2 S(S+1)\sum_k \frac{(1-3\cos^2\theta_{jk})^2}{r_{jk}^6}. \tag{2.31}$$

Eq. (2.31) can be interpreted that the local magnetic field seen by nuclei I is proportional to the magnetic moment $\gamma_S\hbar\sqrt{S(S+1)}$ of the other species.

2.1.5 Hyperfine interaction

The nuclear magnetic dipole moment can interact with the electronic spin and orbital magnetic moments via hyperfine coupling mechanism. In view of the character of the coupling, we can distinguish the interaction into magnetic and quadrupole ones. Here we will discuss only the magnetic interactions since the quadrupole interaction, which occurs only with the nuclear spin $I > 1/2$, does not appear in this thesis.

The magnetic interactions can be represented by a hyperfine field $H_{\rm hf}$. The total magnetic interaction is then given by the Hamiltonian

$$\mathcal{H}_T = -\gamma_n\hbar\mathbf{I}\cdot(\mathbf{H}_0 + \mathbf{H}_{\rm hf}). \tag{2.32}$$

A nuclear moment at the origin would see a magnetic field produced by an electron,

$$\mathbf{H}_{\rm hf} = -g\mu_B\left[\frac{\boldsymbol{\ell}}{r^3} - \frac{r^2\mathbf{s} - 3(\mathbf{r}\cdot\mathbf{s})\mathbf{r}}{r^5} + \frac{8\pi}{3}\delta(\mathbf{r})\mathbf{s}\right], \tag{2.33}$$

where μ_B is the Bohr magneton, and $\mathbf{s}$ and $\boldsymbol{\ell}$ are the electronic spin and orbital angular momentum operators, respectively. The first term in Eq. (2.33) describes the orbital coupling arising from the electronic currents. The second term is the dipolar field due to the electronic spin magnetic moment. In many cases, the orbital term vanishes due to the quenching of the orbital momentum of the electron, and the dipolar term disappears in a cubic symmetry of the electron cloud. The third term is called the Fermi contact term. The contact term is non-zero only if the electronic density at the nucleus sites is non-zero. Therefore, the term will survive only if unpaired s-electrons are present. However, ions with no unpaired s-electrons sometimes show very large hyperfine interactions. For example, Mn^{2+} and Fe^{3+} ions are not expected to

have the hyperfine interactions, because both ions have no orbital mechanism (orbital singlet state) so that there is no dipolar and no orbital hyperfine interactions. Experimentally, however, a huge hyperfine field has been observed in the ions. A qualitative explanation is that the exchange interaction between the core s-electrons and the unpaired d-electrons produce a slight difference between the electronic densities of the core s-electrons with different spin orientations. This effect is called *core polarization* hyperfine interaction and is important, in particular, for transition elements where the unpaired electrons have no s-character [48].

2.2 NMR in molecular magnets

Basing on the discussion in the previous section we concentrate now on the relation between spin dynamics and nuclear spin-lattice relaxation in single molecule magnets. We consider separately the high temperature region ($k_BT \gg J$) where the nuclear relaxation is driven by the uncorrelated spin dynamics and is thus similar to any paramagnet except for the effect of the reduced dimensionality, and the intermediate and low temperature region ($k_BT \leq J$) where the $1/T_1$ reveals features which are very specific to SMMs being related to the discrete nature of the magnetic energy levels.

2.2.1 High temperature region ($k_BT \gg J$)

SMMs are characterized by exchange constants J, which are generally of the order of $1-30$ K [except a few species like Cu8 where it can be very large (~ 1000 K)]. In the high temperature region ($k_BT \gg J$), we treat SMMs as non-metallic paramagnets. In this case, the coupling between the electronic spin system and the lattice is so strong that the electronic spin system can be considered as a part of the lattice i.e. in thermal equilibrium at T_L [49]. Then the fluctuating local field produced by the fluctuation of the electronic spins induces the nuclear transition probabilities. The perturbation Hamiltonian for a nuclear spin I can be expressed by $\mathcal{H}_1 = \sum\{\mathcal{H}_i^{\text{dip}} + B_i \mathbf{I}\cdot\mathbf{S}^i\}$ where B_i is a hyperfine coupling constant, the two terms represent the dipolar and the scalar hyperfine interaction, respectively [see Eq. (2.33)]. Then from Eq. (2.13) together with Eqs. (2.16) and (2.17), $1/T_1$ can be expressed in terms of the spectral densities

of the spin fluctuations as [49–51],

$$\frac{1}{T_1} = 2\gamma_n^2\gamma_e^2\hbar^2 S(S+1)\left\{\sum_{jj'}\alpha_{jj'}\mathcal{J}_{\pm}^{jj'}(\omega_e) + \sum_{jj'}\beta_{jj'}\mathcal{J}_z^{jj'}(\omega_n)\right\}, \tag{2.34}$$

where j, j' number the electronic spins, ω_e and ω_n are the Larmor frequencies of the electron and of the nucleus respectively, $\alpha_{jj'}$ and $\beta_{jj'}$ are geometrical factors related to the dipolar and scalar hyperfine interaction, and $\mathcal{J}_{\pm,z}^{jj'}$ are the transverse and longitudinal spectral densities of the spin fluctuations.[1] Eq. (2.34) can also be expressed in terms of collective q-variable as shown in Appendix A.

In the high temperature limit, one can neglect correlation between the magnetic spins. Then the pair correlation terms can be set equal to zero and one can rewrite Eq. (2.34) in terms of the uniform static susceptibility χ as

$$\frac{1}{T_1} = \frac{(\hbar\gamma_n\gamma_e)^2}{4\pi g^2\mu_B^2}k_B T\chi\left[\frac{1}{2}A^{\pm}\Phi^{\pm}(\omega_e) + A^z\Phi^z(\omega_n)\right], \tag{2.35}$$

where $\Phi^{\alpha}(\omega)$ are the Fourier transforms of the auto-correlation function of the transverse ($\alpha = \pm$) and longitudinal ($\alpha = z$) components of the electronic spin. On the assumption of a rapid decay of the correlation function at short times followed by a much slower decay at long time due to the almost isotropic Heisenberg nature of the Hamiltonian and the zero dimensionality $\Phi(\omega)$ is peaked at low frequency. However, even small anisotropic terms can introduce a cut-off frequency at low frequencies. Thus one can model the spectral density as the sum of two Lorentzian [38, 52, 53] :

$$\Phi^{\pm}(\omega) = \Phi^z(\omega) = \frac{\Gamma_D}{\omega^2+\Gamma_D^2} + \frac{\Gamma_A}{\omega^2+\Gamma_A^2}, \tag{2.36}$$

where Γ_D is the frequency characterizing the initial fast decay and Γ_A is the cut-off frequency which limits the slow decay of the correlation function at long times. If we assume that

[1] It should be emphasized that in this case the spectral density function is the Fourier transform of the correlation function of the electronic *spin* instead of the Hamiltonian or the *local field*. Since only the transverse component of the local field fluctuations can contribute the nuclear spin-lattice relaxation, Eq. (2.34) could be written as

$$1/T_1 \propto \int_{-\infty}^{\infty} dt e^{i\omega_n t}\langle H_{\pm}(0)H_{\pm}(t)\rangle.$$

This formula is more general than Eq. (2.34). If we know the physical basis of the fluctuations of the local field, we can derive the simple equation directly from above formula, as we will see in the next subsection.

$\omega_n \ll \Gamma_A, \Gamma_D$ and $\Gamma_A < \omega_e < \Gamma_D$, we can approximate Eq. (2.35) as

$$\frac{1}{T_1} = \frac{(\hbar\gamma_n\gamma_e)^2}{4\pi g^2\mu_B^2} k_B T\chi \left[\frac{1}{2}A^{\pm}\left(\frac{\Gamma_A}{\omega_e^2+\Gamma_A^2}+\frac{1}{\Gamma_D}\right)+A^z\left(\frac{1}{\Gamma_D}+\frac{1}{\Gamma_A}\right)\right] = \frac{A}{B+H^2}+C. \quad (2.37)$$

This simple formula has been proved to be successful in describing $1/T_1$ as a function of external fields for SMMs at room temperature [54, 55].

2.2.2 Low temperature region ($k_BT \ll J$)

At low temperature the SMMs occupy the lowest magnetic energy states described by the total spin value S. If one uses Eq. (2.12) to calculate $1/T_1$ one finds no nuclear relaxation due to the large energy difference among the molecular quantum states compared with the nuclear Zeeman energy. Of course the situation would change if one introduces a broadening of the levels (i.e. replace the δ functions in Eq. (2.12) with Lorentzians or Gaussians) as will be explained in the following section. An alternative approach is to use a semi-classical theory whereby one describes the relaxation in terms of fluctuations of the magnetization associated with the probability of a molecule to make a transition from a quantum state to another. We will first describe this simple model and at the end of the section we will consider a very interesting case which occurs at very low temperature when the magnetic fluctuations are dominated by quantum tunneling. This latter case gives rise to nuclear relaxation by a non-perturbative mechanism which is referred to as strong collision.

We express $1/T_1$ in these systems in terms of the correlation function of a perturbation Hamiltonian $\mathcal{H}_1$. From Eqs. (2.13)–(2.17), we have

$$\begin{aligned}\frac{1}{T_1} = 2W &= \frac{2}{\hbar^2}\int_{-\infty}^{+\infty} dt\langle\mathcal{H}_1(t)\mathcal{H}_1(0)\rangle e^{i\omega_n t} \\ &= \frac{\gamma_n^2}{2}\int_{-\infty}^{+\infty} dt\langle H^{\pm}(t)H^{\pm}(0)\rangle e^{i\omega_n t},\end{aligned} \quad (2.38)$$

where $\langle H^{\pm}(t)H^{\pm}(0)\rangle$ is the correlation function of the transverse local field $H^{\pm}$, and the longitudinal field component has been omitted since it does not induce nuclear transitions. A phenomenological model derived from Eq. (2.38) based on the assumption that the hyperfine field is proportional to the magnetization and the assumption of an exponential decay of the

correlation function of the magnetization has been used for the analysis of the temperature dependence of $1/T_1$ in Fe8 and Mn12ac [54, 56–59]:

$$\frac{1}{T_1} = \frac{A}{Z} \sum_{m=+10}^{m=-10} \frac{\tau_m}{1+\omega_n^2 \tau_m^2} \exp(-E_m/k_B T), \tag{2.39}$$

where A is a parameter related with the average square of the fluctuating hyperfine field (i.e. $\gamma_n^2 \langle \Delta H_\pm^2 \rangle$), Z the partition function, and τ_m is the lifetime of the m magnetic quantum state expressed in terms of the spin-phonon transition probabilities.

In this thesis, we will adopt a slightly different formula than Eq. (2.39) in the analysis of ^{57}Fe $1/T_1$ data obtained in a very low temperature region ($T < 2$ K). In fact for the low temperature case one can consider only the fluctuations of the two hyperfine field values corresponding to $m = \pm 10$ and $m = \pm 9$. The derivation of the formula for $1/T_1$ in this simple case is illustrated in detail in Appendix B. Finally, the ^{57}Fe NMR at zero and low fields can be explained mostly by tunneling mechanism that overwhelms the spin-phonon contribution. (The spin-phonon contribution reappears when we apply a longitudinal field due to rapid decay of the tunneling contribution.) In this case, we find that the weak collision approximation, which has been assumed throughout this chapter so far and is valid in most NMR experiments, fails for the relaxation due to the tunneling mechanism. In this very rare case, the strong collision formula should be used since each tunneling event induces the nuclear transition so that $1/T_1$ is directly related to the tunneling rate. The nuclear relaxation in the strong collision limit is illustrated in detail in Appendix C and will be discussed in Chapter 4.

2.2.3 Intermediate temperature region ($k_B T \sim J$)

When the temperature is comparable to the magnetic exchange constant J/k_B, SMMs show very interesting features. In particular, AFM ring clusters are characterized by an enhancement of $1/T_1$ near a temperature of the order of J/k_B. An analytic expression of $1/T_1$ based on a first-principles perturbative treatment of the hyperfine field can be derived either quantum mechanically [from Eq. (2.12)] or semi-classically [from Eq. (2.34)]. Let's consider the latter case. It can be shown that the correlation function in the Heisenberg model systems consists of several terms whose time dependence is of the form $\exp(\pm i\Omega t)$, where Ω is either

zero or the frequencies Ω_{ex} associated with transitions between energy levels with different S. The longitudinal components of the spectral density $\mathcal{J}_z^{ij}$ reduces to a sum of terms which can be expressed as $f^{ij}(T,\Omega)\delta(\omega_n - \Omega)$. Neglecting second-order effects of the field H, it follows that the transverse components of the spectral density $\mathcal{J}_\pm^{ij}$ are sums of terms of the form $f^{ij}(T)\delta(\omega_n - \Omega \pm \omega_e)$ where ω_e is the electronic Larmor frequency. However, given that $\omega_n, \omega_e \ll \Omega_{ex}$, the only terms which might realistically contribute to $1/T_1$ are $f^{ij}(T)\delta(\omega_n)$ and $f^{ij}(T)\delta(\omega_e \pm \omega_n)$. This corresponds to the fact that only quasi-static fluctuations allow for energy-conserving nuclear transitions at $\omega_n, \omega_e \pm \omega_n$. In actual fact we expect that these δ functions are somewhat broadened to Lorentzians in the real material. Thus we obtain the following expression for the temperature and field dependence of $1/T_1$ [60]:

$$\frac{1}{T_1}(T,H) = F_{zz}(T)\left[\frac{\omega_0}{\omega_n^2+\omega_0^2} + B\frac{\omega_0}{\omega_e^2+\omega_0^2}\right], \tag{2.40}$$

where ω_0 is a frequency measuring the broadening of the energy levels, B is a constant which measures the ratio between components of the magnetic dipole interaction tensor [see Eq. (2.34)], and $F_{zz(T)}$ is a T-dependent function.[2] At high temperature $\omega_0 \gg \omega_n$ and thus the field dependence of $1/T_1$ is due to the second term in Eq. (2.40) containing $\omega_e = \gamma_e H$.[3]

In chapter 5, we will show that the first Lorentzian term in Eq. (2.40) is responsible for the enhancement of $1/T_1$ at intermediate temperature ($k_B T \sim J$) and that the characteristic frequency ω_0 has a power law T dependence: $\omega_0 \propto T^\alpha$ with $\alpha = 3.5$. The power law dependence of $\omega_0(T)$ indicates that the lifetime broadening of the Heisenberg energy levels originates from the coupling of the paramagnetic ions with *acoustic* phonons. It is surprising that the broadening frequency decreases rapidly and reaches the order of the nuclear Larmor frequency at intermediate temperature (10–30 K). This remarkable finding proves that NMR is indeed a unique tool for detecting such low frequency fluctuations.

[2] It turns out that $F_{zz}(T)$ is equivalent to $A\chi T$ with a constant A.

[3] A quantum-mechanical approach based on Eq. (2.12) also gives rise to the same form as Eq. (2.40) by the analytical calculation of the matrix elements [61].

2.3 Detection methods

2.3.1 Free induction decay (FID) and spin echoes

The magnetization $M_z = M_0$ can be tipped into the transverse plane by an rf pulse of frequency ω_n and duration $\tau(< T_2)$ such that $\gamma_n H_1 \tau = \pi/2$. Following the $\pi/2$ pulse, the magnetization in the rotating frame decays at a rate $\sim 1/T_2^* \sim 1/T_2 + \gamma_n \Delta H$, where T_2^* is the time constant which describes the decay of the magnetization in the xy-plane and ΔH is the spread in static field over the sample due to inhomogeneity of the applied field H_0 and/or of internal hyperfine fields. It should be emphasized that T_2^* is related to the dephasing of the magnetization in the xy plane, while T_2 is related to the irreversible decay of the transverse magnetization.

As a result of the spread due to field inhomogeneity, some of the components of the magnetization start getting ahead of average and some getting behind. The resulting signal envelope is called the free induction decay (FID). The characteristic time of the decay of FID corresponds to T_2^*. In order to remove the effect of the field inhomogeneity, the *spin echo* technique is widely used in pulse NMR experiment. The idea is the following. Suppose that a $\pi/2$ pulse is applied along x' axis in the rotating frame. The magnetization is initially along y' axis, and shortly after it will dephase. If we apply a π pulse along x' axis after a delay τ that is shorter than T_2, the dephasing spins are rotated π altogether. The result is refocusing of the spins along $-y'$ axis at time 2τ, giving rise to the *echo*. The echo formation is illustrated in Fig. 2.2.

In the following two subsections we illustrate the basic methods used to measure T_2 and T_1 in the simplest case. It should be stressed that in SMMs and in general in broad line NMR there are many complications which may make the measurement more involved as will be discussed in specific cases in Chapters 4 and 5.

2.3.2 Measurement of spin-spin relaxation time, T_2

The spin echo does not recover the full height of the FID but decays with the intrinsic relaxation time constant T_2. The advantage of the use of spin echo is obvious since the decay of spin echo is not affected by the field inhomogeneity. The typical pulse sequence for the

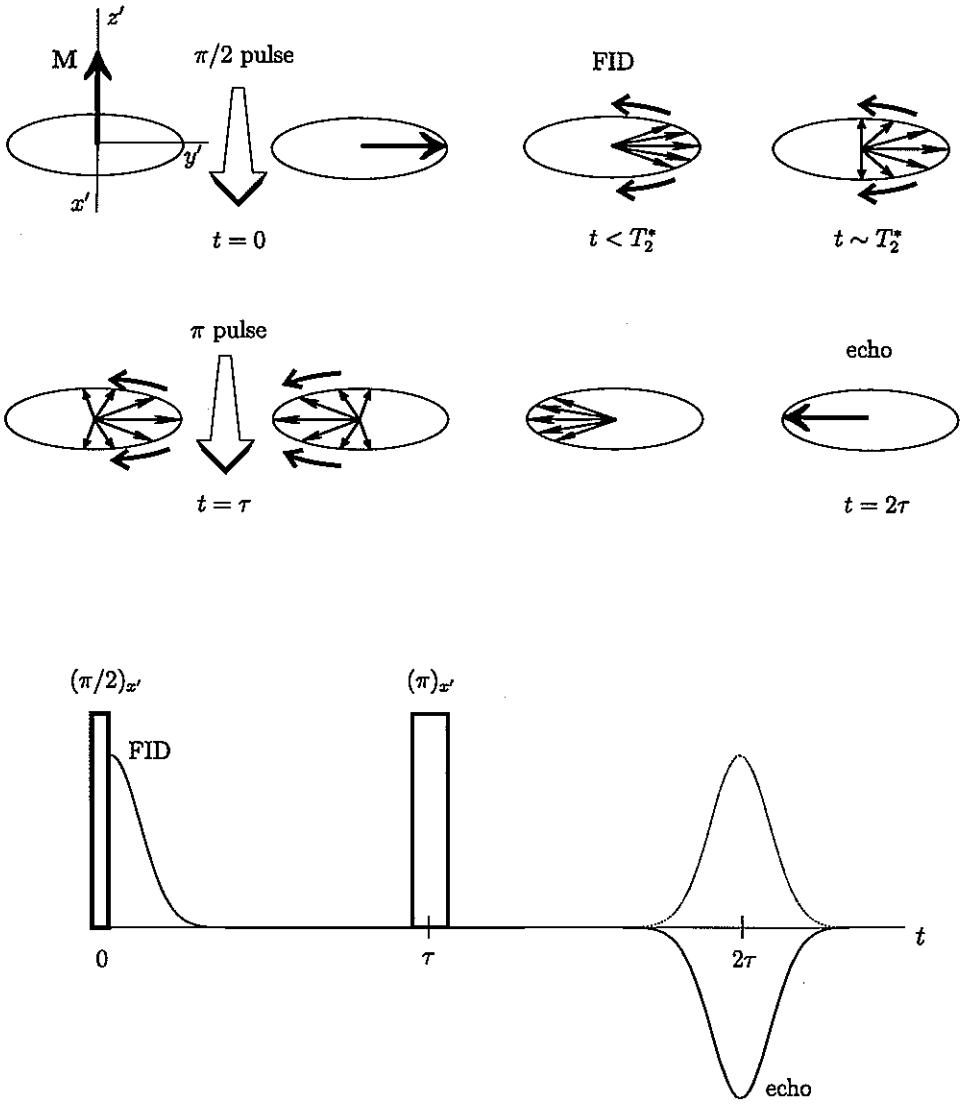

Figure 2.2 Schematic diagram for the formation of spin echo in a $(\pi/2)_{x'} - \tau - (\pi)_{x'}$ pulse sequence in the rotating frame. Note that the echo is formed in the opposite direction to the initial FID since the reconstruction of the magnetization occurs in $-y'$ direction.

measurement of T_2 is

$$\pi/2 - \tau - \pi - \tau - \text{echo}. \tag{2.41}$$

It is necessary to capture a number of data points by repeating the above sequence with different values of τ and to wait between each sequence for a time of the order of $5T_1$ for the equilibrium M_0 (within 1 % of it) to be established. We can find T_2 by measuring the spin echo intensity $I(2\tau)$ as a function of the delay 2τ i.e.

$$I(2\tau) = \exp(-2\tau/T_2). \tag{2.42}$$

2.3.3 Measurement of spin-lattice relaxation time, T_1

The longitudinal magnetization M_z recovers in a time T_1 following a $\pi/2$ pulse. Thus, in order to measure T_1 we should monitor the recovery of M_z. This can be done by rotating by a $\pi/2$ pulse the magnetization in the xy plane so as to make $M_z = 0$ (saturation) and then monitoring the growth of M_z towards equilibrium by a second $\pi/2$ pulse. A better method for measuring T_1, particularly suitable for broad lines, consists of saturating the resonance with a series of $\pi/2$ pulses and measuring the height of the spin echo, which corresponds to the magnitude of $M_z(t)$, following the saturating "comb" and a subsequent pulse sequence [Eq. (2.41)] i.e.

$$\underbrace{\pi/2 - \tau_1 - \pi/2 - \tau_1 - \cdots - \tau_1 - \pi/2}_{\text{saturating "comb" pulses}} - \tau - \underbrace{\pi/2 - \tau_2 - \pi - \tau_2 - \text{echo}}_{\text{detecting pulse sequence}}, \tag{2.43}$$

where the delay τ_1 must fulfill the condition $T_2 < \tau_1 \ll T_1$, τ is the variable delay time for the measurement of T_1, and τ_2 is a fixed delay. τ_2 should be short compared with T_2 (but long compared T_2^*) in order to maximize the signal intensity. The use of the comb pulses has the advantage that the system can always be prepared in an initial state of definite spin temperature ($T_s = \infty$). Moreover, it is not necessary to wait $5T_1$ before starting next sequence with different τ. The wait time can be of the order of T_1 giving another advantage, in particular, for long T_1. The recovery of M_z then follows a time dependence

$$M_z(t) = M_0 \left[1 - \exp(-\tau/T_1)\right], \tag{2.44}$$

where T_1 is given by Eq. (2.17).

CHAPTER 3 Magnetic properties and spin dynamics in Fe8 molecular cluster

In this chapter we review the known experimental results for Fe8 and the theoretical description of the spin dynamics. In doing so we revisit some aspects of the magnetic properties and propose some new interpretative schemes. After a short introduction of the Fe8 cluster and the theoretical basis relevant to interpret the magnetic properties, we analyze the experimental magnetic susceptibility data. In the low temperature range we used the total spin model Hamiltonian to perform calculations of the magnetization and the magnetic susceptibility as a function of external field and temperature. The comparison with the experimental data is given, showing the good agreement between the theory and the experiments. The quantum tunneling of magnetization (QTM) is the main subject in this chapter. We will review and discuss the well-known tunneling phenomena found in Fe8 and their physical interpretations. In particular, tunnel splitting and its oscillations for the field applied along hard axis will be studied in detail. We propose a simple way to estimate the temperature and the field regime in which the tunneling can take place, from the calculated static transverse magnetization as a function of transverse field and temperature.

3.1 Introduction

3.1.1 Structure of Fe8

Fe8 with the formula $[Fe_8O_2(OH)_{12}(tacn)_6]^{8+}$ (tacn= $C_6N_3H_{15}$) [25] is one of the best studied clusters due to its spectacular quantum effects, such as pure quantum tunneling of magnetization and coherent quantum oscillations [30].

Fig. 3.1 shows the structure of Fe8 cluster, which consists of eight Fe^{3+} ($s = 5/2$) ions almost

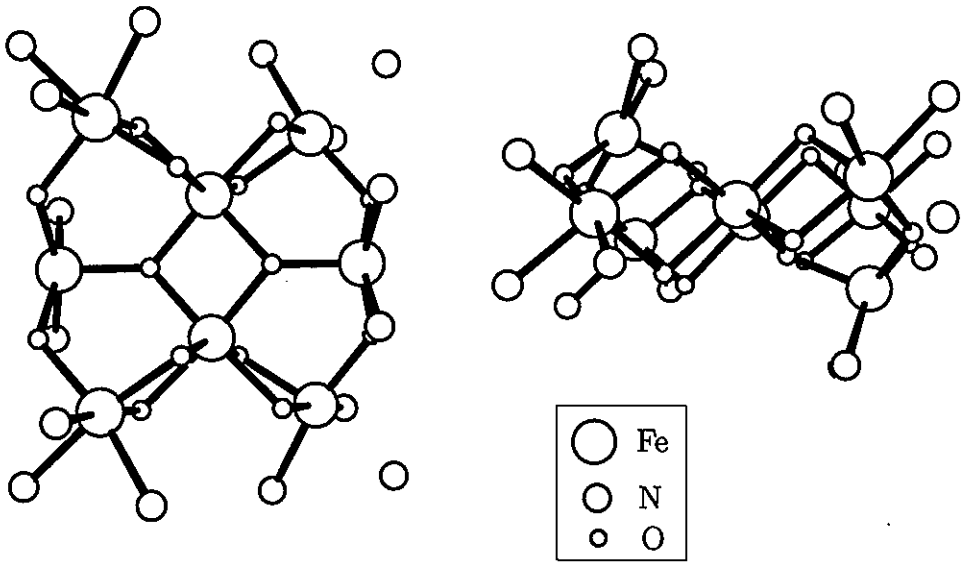

(a) (b)

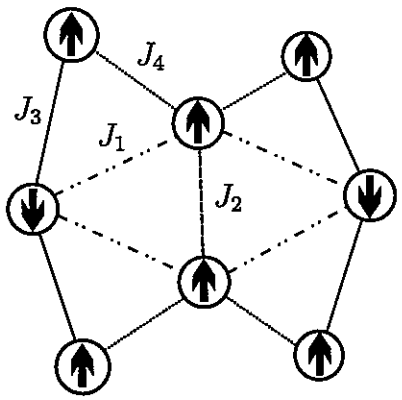

$J_1 = -195$ K
$J_2 = -30$ K
$J_3 = -52.5$ K
$J_4 = -22.5$ K

(c)

Figure 3.1 Schematic diagrams of structure of Fe8 cluster. (a) top view (b) side view (c) exchange pathways connecting Fe^{3+} centers and the values of the exchange constants from Ref. [62].

in a plane. There is no rigorous symmetry but it forms approximate D_2 symmetry. The four ions in the middle of the molecule are in the so-called butterfly arrangement, which is similar to that of an iron oxide (hydroxide). The inner core of the molecule can be regarded as the first step toward the formation of a triangular planar lattice. Hydroxo bridges connect the central core to the four peripheral Fe^{3+} ions, while the presence of the organic ligands prevents the growth of the iron hydroxide. Also the organic ligands separate the Fe8 molecule in the crystal, resulting in a typical intermolecular dipolar fields of the order of 0.05 T [63]. Fe8 crystallizes in the acentric $P1$ space group with $a = 10.522$ Å, $b = 14.05$ Å, and $c = 15.00$ Å and the unit cell contains one molecule [25]. The magnetic ground state of the Fe8 cluster is determined by the paths of intramolecular exchange interactions:[1] $J_1 \sim -195$ K, $J_2 \sim -30$ K, $J_3 \sim -52.5$ K, and $J_4 \sim -22.5$ K [62, 64]. The intramolecular exchange coupling scheme is shown in Fig. 3.1(c) together with the spin structure of Fe^{3+} ions in the ground state $S = 10$. The spin structure of the ground state with $S = 10$ has been suggested by the temperature dependence of the magnetic susceptibility [65], and confirmed by the polarized neutron diffraction (PND) [62] and ^{57}Fe nuclear magnetic resonance (NMR) spectrum [40]. The ground state are largely split into $2S + 1 = 21$ magnetic sublevels in such a way that the $m = \pm 10$ components lie lowest [27, 66].

3.1.2 Magnetization and magnetic susceptibility

A sample containing 1 mol of a molecular compound in a magnetic field H acquires a molar magnetization M related to H through[2]

$$\frac{\partial M}{\partial H} = \chi, \tag{3.1}$$

where χ is the molar magnetic susceptibility. If H is weak enough, then χ becomes independent of H, i.e., $M = \chi H$. Although χ is the algebraic sum of two contributions (paramagnetic and diamagnetic), χ will refer to the paramagnetic susceptibility only hereafter.

[1] In this thesis, we use the convention that the interaction energy is written as the form of $\mathcal{H} = -\sum_{ij} J_{ij} \mathbf{S}_i \cdot \mathbf{S}_j$, where J_{ij} is the exchange energy between i and j ion spins. Therefore, the interaction is ferromagnetic for $J_{ij} > 0$ and antiferromagnetic for $J_{ij} < 0$.

[2] Most elements of the discussion in this subsection can be found in Kahn [1].

Let's consider a molecule with an energy spectrum E_n ($n = 1, 2, \cdots$.) in the presence of a magnetic field H. We can define a microscopic magnetization μ_n for each energy level n as

$$\mu_n = -\frac{\partial E_n}{\partial H}, \tag{3.2}$$

then we can write the macroscopic molar magnetization M:

$$M = N\langle\mu_n\rangle = N\frac{\sum_n(-\partial E_n/\partial H)\exp(-E_n/k_BT)}{\sum_n \exp(-E_n/k_BT)} \tag{3.3}$$

where k_B is the Boltzmann constant, N is the Avogadro's number, and $\sum_n \exp(-E_n/k_BT)$ can be defined as the partition function Z. Finally, M and χ can be expressed in terms of the partition function Z,

$$M = Nk_BT\frac{\partial \ln Z}{\partial H}, \tag{3.4}$$

and

$$\chi = Nk_BT\frac{\partial^2 \ln Z}{\partial H^2}. \tag{3.5}$$

If each spin under consideration has an independent magnetic moment i.e., no interaction between the spins, the susceptibility is inversely proportional to the temperature T, which is known as the Curie law:

$$\chi = \frac{C}{T} \tag{3.6}$$

with

$$C = n\left(\frac{N\mu_B^2}{3k_B}\right)\mathrm{g}^2 S(S+1) \tag{3.7}$$

where n is the number of the moments per molecule, g the gyromagnetic ratio, and S the spin of each moment. It is very useful to remember that $N\mu_B^2/3k_B$ in the cgsemu unit is $0.125048612 \sim 1/8$. If there is an interaction between the magnetic moments, Eq. (3.6) should be modified leading to the Curie-Weiss law:

$$\chi = \frac{C}{T-\Theta}. \tag{3.8}$$

The Weiss temperature or Weiss constant Θ is given by

$$\Theta = \frac{zS(S+1)J}{3k_B}, \tag{3.9}$$

where z is the number of nearest neighbors and J is the exchange constant.

3.2 Magnetic properties of Fe8

The static magnetic susceptibility was measured with a SQUID magnetometer (Quantum Design MPMS) on a sample of non-oriented powders in a field of 0.01 T [57]. The temperature dependence of the magnetic susceptibility multiplied by T, χT, is shown in Fig. 3.2(b). At room temperature χT is about 20 (emu/mol K), which is much smaller than the Curie constant 35 (emu/mol K) expected for eight independent $s = 5/2$ spins with g = 2. This is due to the presence of antiferromagnetic coupling among Fe^{3+} ions. On cooling, χT increases steadily toward a maximum value of 50.6 (emu/mol K) at about 10 K. The maximum value is close to but smaller than 55 (emu/mol K) expected for a single total spin $S = 10$. This discrepancy may be due to the fact that in polycrystalline powders one measures a statistical average for the direction of the magnetic anisotropy axis oriented in all direction. Below 10 K a small decrease is observed. The decrease of χT can arise from (i) the magnetic anisotropy (i.e., zero-field splitting) and/or (ii) intermolecular antiferromagnetic interactions, whereby the first explanation has been assumed in the literature to be the most relevant [15, 67]. In the course of the present research we have revisited the problem and found that the effect of intermolecular interactions may also be relevant. We give in the following details of our analysis.

Let's start from $1/\chi$ vs T plot [Fig. 3.2(a)]. At high temperatures (above 150 K), $1/\chi$ is almost linear versus temperature T, being extrapolated to a negative value at $T = 0$, which may be indicative of a ferromagnetic coupling among the spins. Since the Curie-Weiss (CW) law is valid only in the temperature range satisfying the condition $k_B T \gg J$, the effective exchange energy $zJ = -270$ K, which was estimated from the four exchange constants reported in Refs. [62, 64, 65], does not fulfill the condition even at room temperature. However, one can conjecture another possibility. What if the spin of Fe^{3+} is an intermediate spin 3/2, or what if an equilibrium state between the high spin 5/2 and the low spin 1/2 is formed? In this case, the interpretation of χT should be changed. From the fit by Eq. (3.8) from 150 to 300 K [solid line in Fig. 3.2(a)], one can obtain $C = 15.82$ (emu/mol K) and $\Theta = 58.13$ K, corresponding to an effective spin $s_{\text{eff}} = 1.55 \sim 3/2$ and an effective exchange constant $zJ = 44.04$ K. It may be interpreted that $s = 3/2$ spins interact ferromagnetically with each other via the exchange

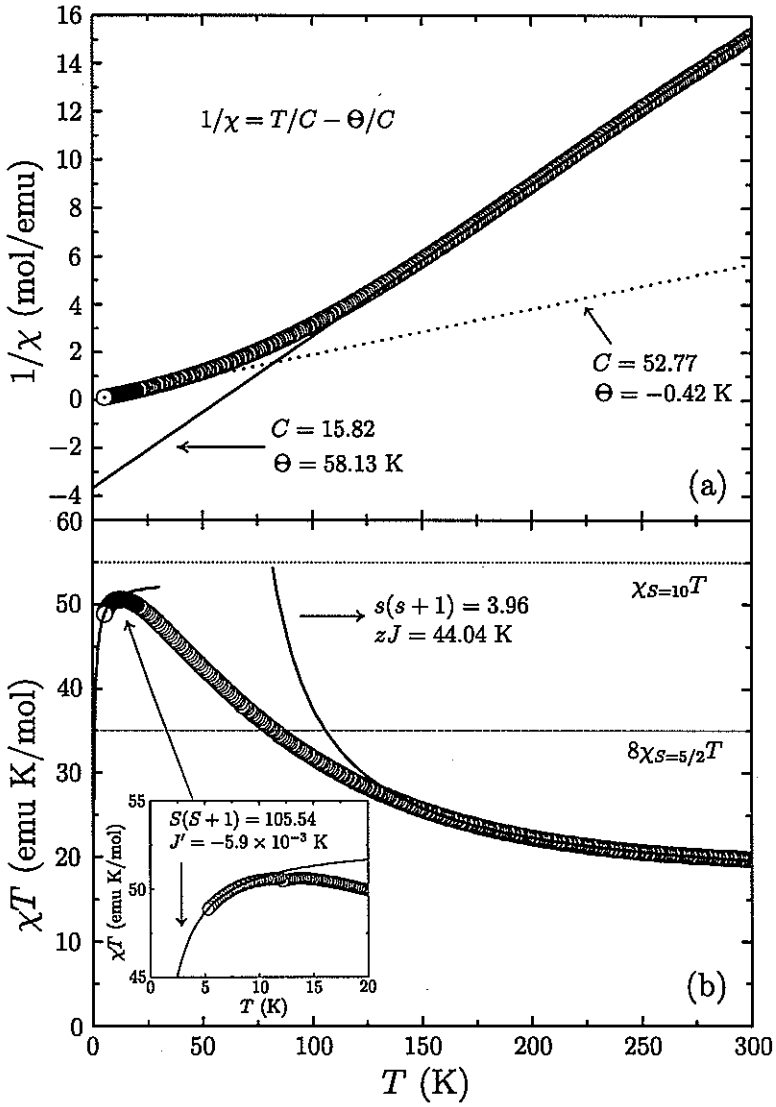

Figure 3.2 Magnetic susceptibility measured at 0.01 T in polycrystalline powers (a) $1/\chi$ vs T plot. The fit by the Curie-Weiss law gives rise to $C = 52.77$ (emu/mol K) and $\Theta = 58.13$ K (solid line), and $C = 15.82$ (emu/mol K) and $\Theta = -0.42$ K (dotted line). (b) χT vs T plot. Two theoretical curves represent the Curie-Weiss law with the parameters obtained in (a). From C and Θ values, the effective spin and the effective exchange constant can be derived, as designated in (b). For the discussion of the validity of the use of the CW law, see text.

energy $zJ = 44.04$ K. Although the occurrence of low-spin high-spin transition is unlikely, its possibility cannot be completely ruled out unless the high temperature (> 1000 K) data are available.

In any cases, the above analysis is useful for a rough estimate of the crossover temperature for the collective total spin. The fact that the curve deviates rapidly from the experimental data below 160 K implies that a *ferrimagnetic* order among all Fe^{3+} ions starts to take place, leading to the ground spin $S = 10$ at low temperatures. Since the energy gap between $S = 10$ and $S = 9$ is about 36 K [15, 64], at sufficiently low temperature compared to the energy gap, each molecule in Fe8 can be described with the total spin $S = 10$. In fact χT value, or equivalently the total magnetic moment of the molecule, is saturated to a constant value at around 15 K. In the very low temperature region (below 10 K), $1/\chi$ is almost linear versus T. If one assumes that the molecules which have a single spin $S = 10$ are coupled via intermolecular dipolar interaction, then the interaction may be expressed as $\mathcal{H} = -J' \sum_{ij} \mathbf{S}_i \cdot \mathbf{S}_j$, where J' is the interaction energy between molecules, and $\mathbf{S}$ is the total spin operator. As long as $J' \ll k_B T$, the Curie-Weiss (CW) law could be used. The fit by the CW law gives rise to $C = 52.77$ (emu/mol K) and $\Theta = -0.42$ K [dotted line in Fig. 3.2(b)]. From Eqs. (3.7) and (3.9), one can obtain $J' = -5.9 \times 10^{-3}$ K, which is reasonably small for the intermolecular interaction, and $S_{\text{eff}} = 9.8$, which is surprisingly close to the expected total spin $S = 10$. The negative J (or the negative Θ) indicates an antiferromagnetic coupling among the molecules leading to the decrease of χT at low temperatures. The result is also drawn in the inset of Fig. 3.2(b).

A rough estimate of the dipolar field $(z\langle\mu\rangle/r^3$, where $\langle\mu\rangle$ is taken as $gS\mu_B = 20\mu_B$, and the nearest neighbors are 2 for Fe8 with the separation length of ~ 10.5 Å between centers of the molecules) yields $H_{\text{dip}} = 2\mu/r^3 = 0.043$ T, which is in good agreement with the reported value (0.05 T) [63]. On the other hand, from the mean field approximation, one can express the local field as $H_{\text{loc}} = zJ'S/(g\mu_B)$. Using J' and S_{eff} obtained above one has $H_{\text{loc}} = 0.086$ T. Although H_{loc} is a factor of 2 larger than H_{dip}, the agreement between the two fields estimated independently could be considered to be satisfactory. A very interesting issue in

SMMs is the possibility of observing long range ordering (LRO) at low temperature due to the intermolecular dipolar interaction among the high spin S molecules. The main obstacle to the establishment of LRO appears to be the fact that the intermolecular dipolar interaction energy is so small that the predicted ordering temperature falls below the freezing temperature of the SMM's magnetization. However, in Fe8 the presence of a large in-plane anisotropy makes the tunneling between individual easy directions very effective and thus the possibility of the establishment of a ground state with ferromagnetic dipolar order below 0.13 K has been suggested [68]. In fact, the experimental observation of the dipolar ordering in Mn6 molecular cluster has been reported for the first time by Morello *et al.* [69].

We consider now in detail the magnetization results at low temperature where quantum effects may be relevant. Fig. 3.3 shows the field dependence of the magnetization measured on the single crystal in the external fields along the a axis at 2.0 K (empty circle) and perpendicular to a axis at 1.8 K (empty triangle) (data taken from Ueda *et al.* [70]).[3]

As mentioned above, in the strong coupling limit at low temperatures (roughly below 20 K), the cluster can be described by the simple model Hamiltonian with the total spin $S = 10$.

$$\mathcal{H} = DS_z^2 + E(S_x^2 - S_y^2) + \mathrm{g}\mu_B \mathbf{S} \cdot \mathbf{H}, \tag{3.10}$$

where S_x, S_y, and S_z are the components of the total spin operator, $D = -0.293$ K is the axial anisotropy and $E = 0.047$ K is the in-plane anisotropy [66], and the last term is the Zeeman energy associated with an external field H.

The exact diagonalization of Eq. (3.10) gives rise to the $(2S + 1) = 21$ energy levels of the magnetic quantum number $m = -10, -9, \cdots, 9, 10$. The field dependences of the energy levels in the $S = 10$ ground state are shown in Fig. 3.4. From this energy level scheme, it is possible to calculate the magnetization directly from Eq. (3.4). First, we performed the calculations of the magnetization M and the magnetic (differential) susceptibility $\partial M/\partial H$ by using Eqs. (3.4)

[3]The purpose of the magnetization measurements in Ref. [70] was to obtain information regarding the relationship between the anisotropy axes and the crystal axes in Fe8. Therefore the parallel field $H_\parallel$ in Ref. [70] means that the field is applied along a-axis, one of the crystal axes (a, b, c) not along the easy z axis. Also in Ref. [70] the sample is rotated around the a axis so that the transverse magnetization is an average value in xy-plane which is tilted off the perpendicular field to a axis. However, we found that one could use a fixed azimuthal angle $\phi = 63°$ from the best fitting procedure.

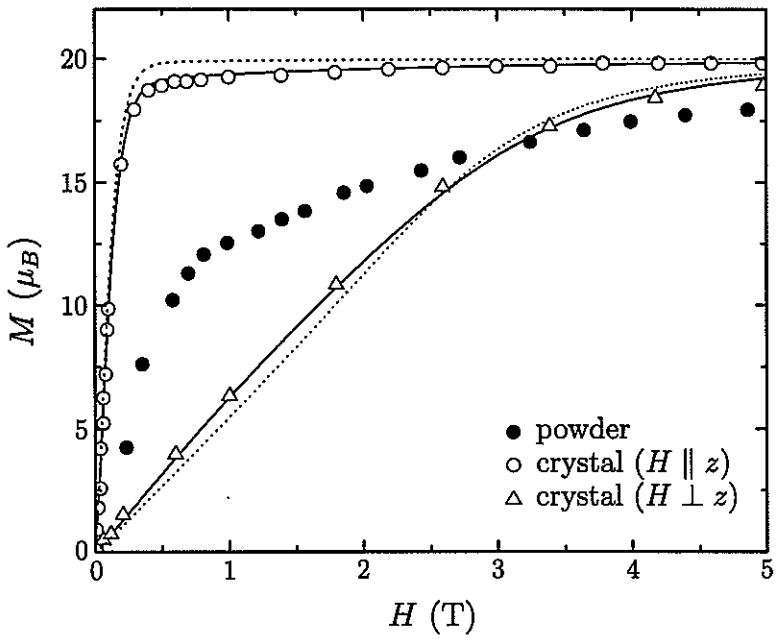

Figure 3.3 Field dependence of the magnetization for the single crystal and the polycrystalline powders in Fe8. Empty circles: $H \parallel z$ axis at 2.0 K, empty triangles: $H \perp z$ axis at 1.8 K. Both the data were taken from Ref. [70]. The data of the powder sample, extracted from Ref. [65] (filled circle), are in-between the two data sets of the single crystal, as expected from the average effect of the distribution of orientation of the molecules. Dotted lines were obtained from Eq. (3.4) for the applied field along the easy z axis and xy plane with $\phi = 63°$, respectively. The discrepancies between the dotted lines and the experiment is eliminated by introducing a *misalignment* of 15° for H_z and 3.5° for $H_\perp$ (solid lines).

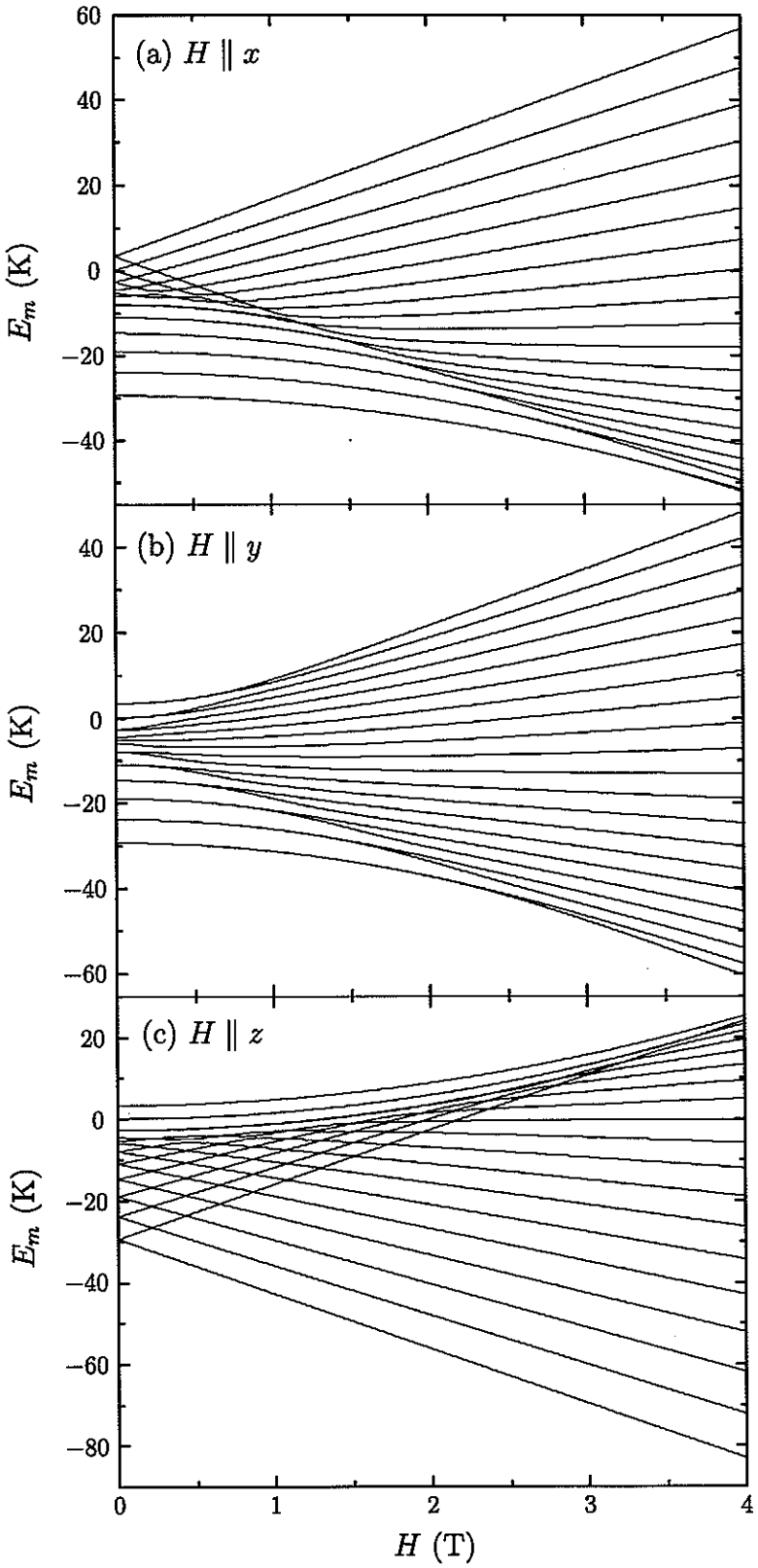

Figure 3.4 Energy level spectrum vs external fields, calculated from Eq. (3.10). (a) $H \parallel x$ (hard axis) (b) $H \parallel y$ (medium axis) (c) $H \parallel z$ (easy axis).

and (3.5) as a function of an external field that is applied along one of three anisotropy axes. The results are shown in Fig. 3.5 for the longitudinal field and Fig. 3.6 for the transverse field at various temperatures designated in the figures. For H applied along easy axis, M saturates rapidly to $20\mu_B$ and $\partial M/\partial H$ decreases accordingly, and both M and $\partial M/\partial H$ depend strongly on the temperature.

For H applied along medium and hard axes, the saturation of M takes place at much higher field as expected, but there appears to be an interesting feature. The magnetization curves show an abrupt increase at some field value, which results in a peculiar peak in $\partial M/\partial H$ curves as shown in Fig. 3.6. The peak of $\partial M/\partial H$ is much more pronounced at lower temperature (below 0.5 K). With increasing temperature, the peak shifts to lower field and broadens, and finally it disappears above a certain temperature (note that there is no peak at 8 K in Fig. 3.6). The field value at which the peak occurs depends on the orientation of H with respect to the anisotropy axis. If the E term is zero, the peak positions for both x and y axes coincide at an intermediate field value. This means that the peak itself is not due exclusively to the presence of a transverse anisotropy term. The peak of $\partial M/\partial H$ was also derived and investigated in the other high total spin ($S = 10$) cluster Mn12ac [71]. The authors in Ref. [71] ascribed the origin of the peak to *quantum fluctuations*. An enhancement of the amplitude of quantum fluctuations can indeed influence the susceptibility as will be shown in subsection 3.3.3.3 with a different approach than used in Ref. [71].

With the assumption that the magnetization data were obtained without any misalignment effects, we get the dotted lines in Fig. 3.3. For the case of $H \parallel z$, we introduced an angle between the easy z axis and the field direction, and increased it until we get the correct curve. The good agreement of the theory with the data (solid line) was obtained with $\theta \sim 15°$, which angle indeed corresponds to the angle between crystal a axis and easy anisotropy axis. Whereas the transverse magnetization data were accurately fitted with the "misalignment" angle $\sim 3.5°$ off xy plane and the azimuthal angle $\phi = 63°$. Here we used an effective *average* angle rather than taking into account the effect of the rotation of the sample, and it is found that this simplification works very well, as shown in Fig. 3.3. Also the magnetization measured in

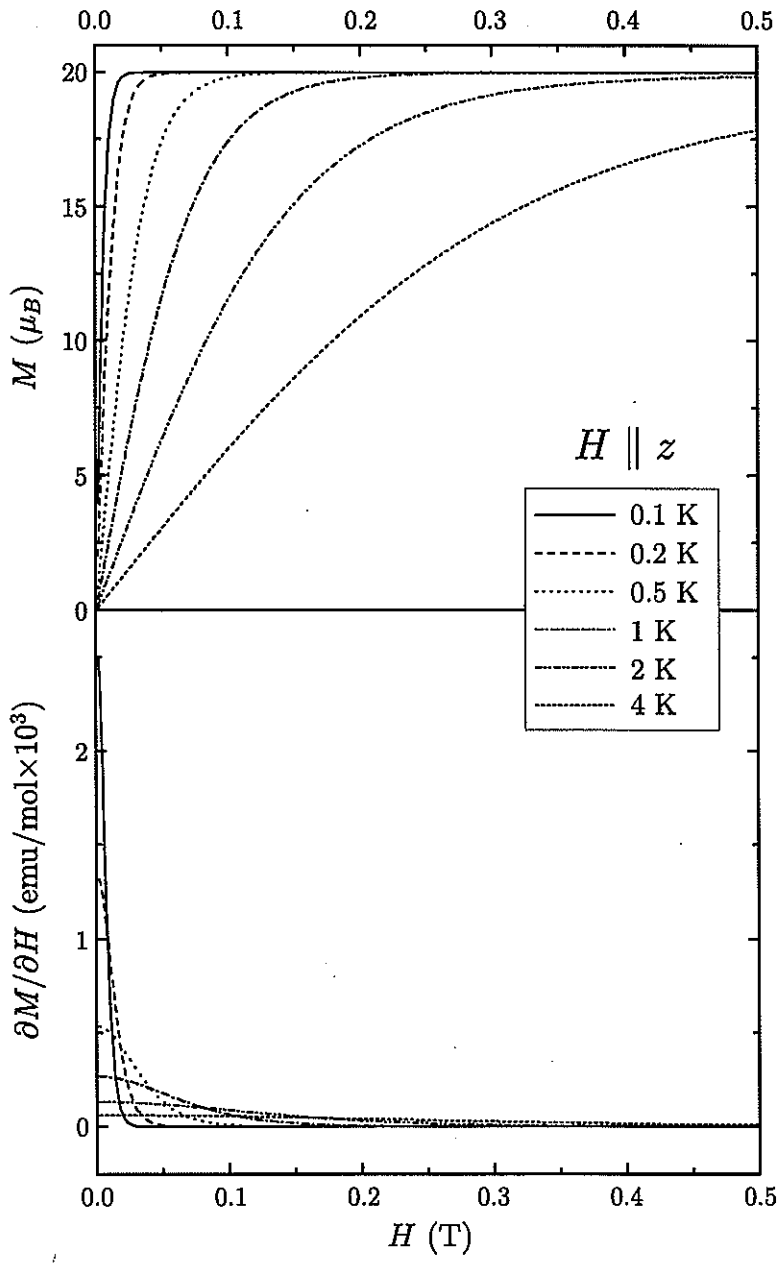

Figure 3.5 Plot of magnetization M and $\partial M/\partial H$ versus an external field H along easy z axis in Fe8.

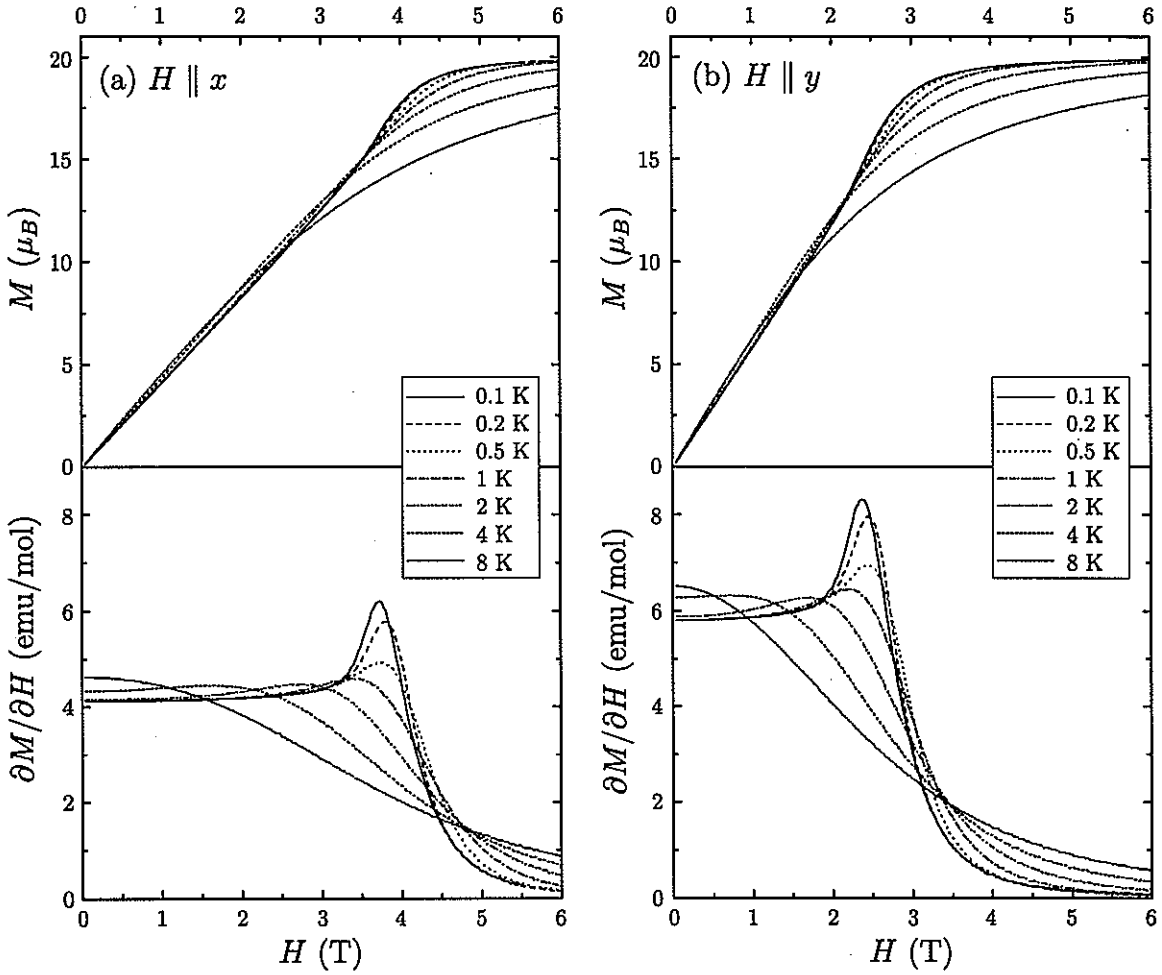

Figure 3.6 Plot of magnetization M and $\partial M/\partial H$ vs the external field H along hard x (a) and medium y axes (b) in Fe8.

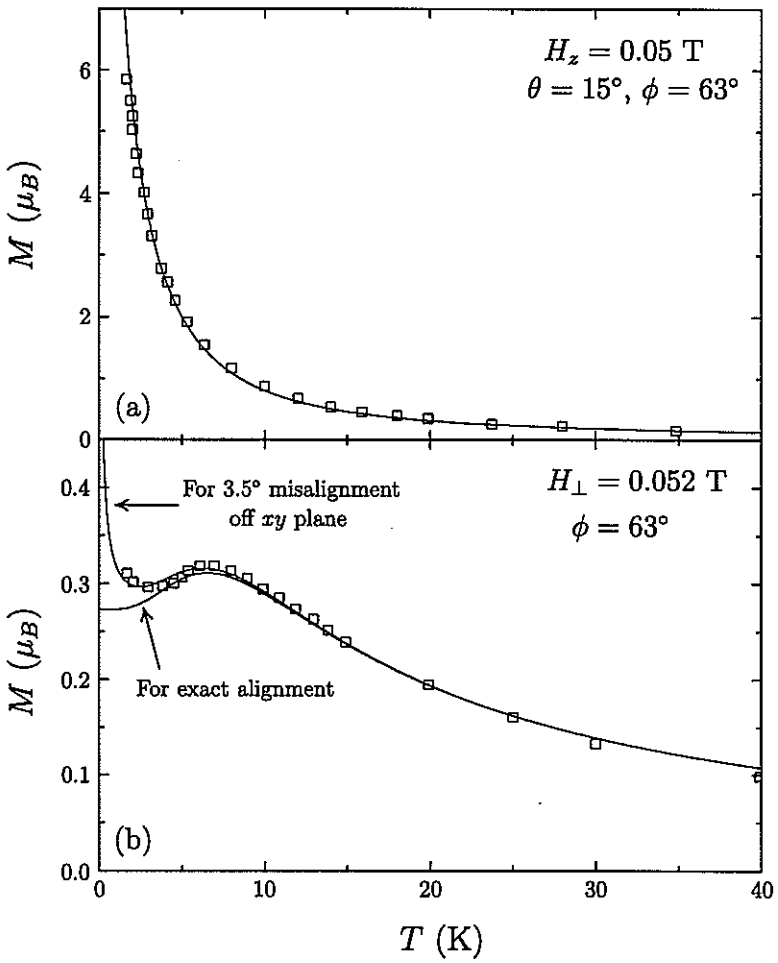

Figure 3.7 Temperature dependence of the magnetization at 0.05 T in Fe8, taken from Ref. [70]. (a) $H \parallel z$ with $\theta = 15°$. (b) $H \perp z$ with the tilting angle 3.5° off xy-plane and effective azimuthal angle $\phi = 63°$. Note that in (b) we used a bit larger field value than reported for a better fit. In both cases, the solid lines were calculated from Eq. (3.4).

polycrystalline powders at 2 K (filled circle) taken from Delfs *et al.* [65] is shown in Fig. 3.3 for the comparison.

The temperature dependence of the magnetization at 0.05 T is shown in Fig. 3.7. In (a), the solid curve was obtained by taking into account the angle between the field direction and z axis, 15°. It turns out that the temperature dependence of the transverse magnetization in Fig. 3.7(b) is very sensitive to the given field value. In order to improve the quality of the fit, we used the field value 0.052 T instead of 0.05 T reported. The transverse magnetization exhibits complex behavior in the low temperature region. Namely, it makes a broad peak at around 7 K and increases again at around 3 K. The upturn of the transverse magnetization at very low temperature is due to the field component along z axis. In fact, the calculation of the magnetization for the field applied along the xy plane (no z component) does not show the upturn but becomes T independent at sufficiently low temperature, as drawn in Fig. 3.7(b).

Our calculations for the field and the temperature dependence of the magnetization are in good agreement with the experimental results in Ref. [70]. Since, however, the measurements in Ref. [70] have been performed with applied fields along the crystal axes, which do not coincide with the anisotropy axes, the confirmation of the peak of $\partial M/\partial H$ is not established. The theoretical prediction of the peak of $\partial M/\partial H$ could be verified with the accurate measurement of the magnetization. For Mn12ac, the measurement of the magnetization may be very difficult because the relaxation time of the magnetization is extremely long in the low temperature region. However, Fe8, for which the magnetization could be measured even at the temperature below 0.1 K, is a good candidate for the investigation of this interesting quantum effect.

3.3 Quantum tunneling of the magnetization

During the last two decades, there has been a considerable interest in the phenomena associated with macroscopic quantum tunneling (MQT) of the magnetization in small magnetic particles. For the observation of MQT, it is required that we have a "macroscopic" variable controlled by a "microscopic" energy [72]. In this sense, a molecular magnet is a unique system for the observation of MQT. The magnetization of Fe8 could be treated as a "macroscopic"

variable since the spin $S = 10$ of the molecule is associated with many internal degrees of freedom (8 individual spins of $s = 5/2$). Whereas the energy involved is the exchange energy J and the single ion anisotropy.

In 1993, Sessoli *et al.* [26] reported that the relaxation time of the magnetization measured in oriented Mn12ac powder follows an exponential law at low temperature, which gives rise to magnetic hysteresis of purely molecular origin. Three years later, the magnetic hysteresis was best observed in a single crystal of Mn12ac with the distinct steps that demonstrate the fast relaxation originating from the tunneling mechanism [29]. Ever since the remarkable findings, quantum tunneling of magnetization (QTM) has been one of the most active research subject in molecular magnets. Fe8 is an even better cluster than Mn12ac for studies of QTM due to following reasons: (i) the relaxation time of the magnetization is much shorter than Mn12ac so that it can be measured at all accessible temperatures; (ii) it has a sizeable in-plane anisotropy which is crucial for QTM to take place. In this section, we will deal with the theoretical aspects of QTM expected in Fe8, basing the calculations exclusively on the single total spin model approximation.

3.3.1 Tunneling in zero field

3.3.1.1 Easy axis magnetic anisotropy and superparamagnetism

In Eq. (3.10), if $D < 0$, z is the easy axis of magnetization and the term $|D|S_z^2$ corresponds to the height of the energy barrier.[4] In zero field the energy barrier separates a set of degenerate states $|+m\rangle$ and $|-m\rangle$ with the energy $E_{+m} = E_{-m}$, each state being localized on the left or right side of the barrier, as shown in Fig. 3.8(a). When the thermal energy is larger than the energy barrier, the molecule behaves like a paramagnet i.e., the magnetization flips freely and its time average is zero. Upon further cooling, the relaxation rate of the magnetization τ^{-1} becomes slow giving rise to superparamagnetic behavior. The relaxation rate follows the Arrhenius law:

$$\tau^{-1} = \tau_0^{-1} \exp(-U/k_B T), \tag{3.11}$$

[4]For a half-integral spin state, the height of the barrier should be expressed as $(S_z^2 - 1/4)|D|$.

where τ_0^{-1} is the constant rate at infinite temperature[5] and U/k_B is the energy barrier for the reorientation of the magnetization. It should be noted that the measured $U/k_B \cong 22.2$ K [27] in Eq. (3.11) is lower than the expected barrier height calculated from $|D|S_z^2$, owing to the effects of quantum tunneling of the magnetization.

3.3.1.2 Transverse magnetic anisotropy and tunnel splitting

The transverse term $E(S_x^2 - S_y^2)$ is responsible for QTM because the term is non-diagonal and does not commute with S_z, and thus significantly splits the pairs of states with $\pm m$ providing possible tunneling window. Due to the presence of the non-diagonal term in the Hamiltonian, an eigenstate should be an admixture of the different m states.

Let us consider the new basis $|m'\rangle$ which is spanned in the basis of the eigenstates $|m\rangle$ of S_z, i.e.,

$$|m'\rangle = \sum_{m=-10}^{+10} c_m |m\rangle. \tag{3.12}$$

The coefficients $c_m = \langle m|m'\rangle$ in zero field are tabulated in Tab. 3.1. As it can be seen in Tab. 3.1, for larger m', $|m'\rangle$ is a superposition of the pair of states $|+m\rangle$ and $|-m\rangle$. For example, $|-10'\rangle$ and $|+10'\rangle$ states can be written approximately,

$$\begin{aligned} |-10'\rangle &= \frac{1}{\sqrt{2}}(|+10\rangle + |-10\rangle) \\ |+10'\rangle &= \frac{1}{\sqrt{2}}(|+10\rangle - |-10\rangle). \end{aligned} \tag{3.13}$$

Thus the new ground states are just the pair of symmetric and antisymmetric wavefunctions of the actual ground states with the energy gap (or tunnel splitting) Δ. From Tab. 3.1 it is clear that a simple expression such as Eq. (3.13) is not valid for small m' states. In particular the states $|m'| < 5$ are so strongly admixed that $S_z = m$ is no longer a good quantum number. However, at very low temperatures, all the molecules can occupy only a few lower energy states close to the ground states, and thus one can keep using this energy level scheme as a good

[5] τ_0^{-1} is sometimes called the relaxation *attempt* frequency, the frequency with which the magnetization fluctuates in a potential well before jumping to the other orientation. The obtained value $\tau_0 \sim 2 \times 10^{-7}$ s for both Fe8 [27] and Mn12ac [26] is a few orders of magnitude larger than the value observed in classical bulk superparamagnets ($\tau_0 \sim 10^{-10} - 10^{-13}$ s) [73], indicating that the slow relaxation is not a bulk phenomenon but of molecular origin.

approximation. Also we can see in Tab. 3.1 the mixture of states differing by 2 in m due to the second order transverse term.

At first sight, the admixture of $|+10\rangle$ and $|-10\rangle$ seems impossible in the first approximation of the perturbation theory because the second order transverse term couples m states only by $\Delta m = \pm 2$. In fact, only the tenth order perturbation theory can lead to the coupling between the two lowest states. This explains the extremely small tunnel splitting in the ground doublet, $\Delta_{10} \sim 10^{-9}$ K, and the much larger splitting for smaller m states (see Fig. 3.13). It also explains the very high power dependence of the tunnel splitting from the perturbation terms and/or the transverse field as will be discussed further on.

The energies of the m sublevels of the $S = 10$ ground state for Fe8 in zero field are shown in Fig. 3.8(a). It is easily seen that the energy levels $|m| < 5$ is heavily admixed in zero field, and the highest energy does not simply associate with the $m = 0$ state alone, as also shown in Tab. 3.1. This implies that in Fe8 the height of the energy barrier is not well-defined. However the energy level scheme has been quite successful in describing the quantum phenomena in the low temperature region. This is because only the states close to the ground states $m = \pm 10$ can be populated at very low temperature.

If the temperature is much less than the energy difference between the ground states and the first excited states, then only the ground states will be occupied. The tunneling process between two degenerate m states across the barrier can occur coherently or incoherently depending on the dissipation mechanism caused by the environmental effects such as the spin-phonon interaction, the intermolecular dipolar interaction, and the hyperfine interaction of the electron spins with nuclear spins. Coherent process means that if we prepare an initial wavefunction, for example $|+10\rangle$ which is localized in right well, the time evolution of the wavefunction will be

$$\begin{aligned} e^{-i\mathcal{H}t/\hbar}|+10\rangle &= \left(e^{-iE_+t/\hbar}|+10'\rangle + e^{-iE_-t/\hbar}|-10'\rangle\right)/\sqrt{2} \\ &= e^{-iE_+t/\hbar}\left(|+10'\rangle + e^{-i\Delta t/\hbar}|-10'\rangle\right)/\sqrt{2}, \end{aligned} \tag{3.14}$$

where $E_\pm$ are energies for eigenstates $|\pm 10'\rangle$, and $\Delta = E_+ - E_-$. After a time $t = \pi\hbar/\Delta$, the initial state $|+10\rangle$ makes transition to the final state $|-10\rangle$. Hence the wavefunction

Table 3.1 The coefficient $c_m = \langle m|m'\rangle$ obtained from the diagonalization of the model Hamiltonian Eq. (3.10) in zero field. The significant digits were taken up to 3. Thus 0 in this table means just negligible mixture of the states.

$\|m\rangle$	$\|-10'\rangle$	$\|+10'\rangle$	$\|-9'\rangle$	$\|+9'\rangle$	$\|-8'\rangle$	$\|+8'\rangle$	$\|-7'\rangle$	$\|+7'\rangle$	$\|-6'\rangle$	$\|+6'\rangle$
$\|+10\rangle$	0.706	0.706	0	0	-0.045	-0.045	0	0	0.003	-0.003
$\|+9\rangle$	0	0	-0.702	0.702	0	0	-0.084	0.084	0	0
$\|+8\rangle$	-0.045	-0.045	0	0	-0.694	-0.694	0	0	0.127	-0.127
$\|+7\rangle$	0	0	0.083	-0.083	0	0	-0.678	0.678	0	0
$\|+6\rangle$	0.006	0.006	0	0	0.125	0.125	0	0	0.644	-0.652
$\|+5\rangle$	0	0	-0.014	0.014	0	0	0.176	-0.175	0	0
$\|+4\rangle$	0	0	0	0	-0.028	-0.027	0	0	-0.240	0.231
$\|+3\rangle$	0	0	0.003	-0.003	0	0	-0.050	0.048	0	0
$\|+2\rangle$	0	0	0	0	0.006	0.006	0	0	0.098	-0.073
$\|+1\rangle$	0	0	0	0	0	0	0.018	-0.009	0	0
$\|0\rangle$	0	0	0	0	-0.003	0	0	0	-0.062	0
$\|-1\rangle$	0	0	0	0	0	0	-0.018	-0.009	0	0
$\|-2\rangle$	0	0	0	0	0.006	-0.006	0	0	0.098	0.073
$\|-3\rangle$	0	0	-0.003	-0.003	0	0	0.050	0.048	0	0
$\|-4\rangle$	0	0	0	0	-0.028	0.027	0	0	-0.240	-0.231
$\|-5\rangle$	0	0	0.014	0.014	0	0	-0.176	-0.175	0	0
$\|-6\rangle$	0.006	-0.006	0	0	0.125	-0.125	0	0	0.644	0.652
$\|-7\rangle$	0	0	-0.083	-0.083	0	0	0.678	0.678	0	0
$\|-8\rangle$	-0.045	0.045	0	0	-0.694	0.694	0	0	0.127	0.127
$\|-9\rangle$	0	0	0.702	0.702	0	0	0.084	0.084	0	0
$\|-10\rangle$	0.706	-0.706	0	0	-0.045	0.045	0	0	0.003	0.003

$\|m\rangle$	$\|-5'\rangle$	$\|+5'\rangle$	$\|-4'\rangle$	$\|+4'\rangle$	$\|-3'\rangle$	$\|+3'\rangle$	$\|-2'\rangle$	$\|+2'\rangle$	$\|-1'\rangle$	$\|+1'\rangle$	$\|0'\rangle$
$\|+10\rangle$	0	0	0	0	0	0	0	0	0	0	0
$\|+9\rangle$	-0.008	0.008	0	0	0	0	0	0	0	0	0
$\|+8\rangle$	0	0	0.021	0.017	0	0	-0.004	0	0	0	0
$\|+7\rangle$	-0.174	0.179	0	0	-0.058	-0.031	0	0	-0.007	0	0
$\|+6\rangle$	0	0	0.239	0.240	0	0	-0.110	-0.040	0	0	-0.005
$\|+5\rangle$	-0.562	0.617	0	0	-0.369	-0.295	0	0	-0.132	-0.032	0
$\|+4\rangle$	0	0	0.430	0.591	0	0	-0.495	-0.312	0	0	-0.106
$\|+3\rangle$	0.328	-0.284	0	0	-0.334	-0.594	0	0	-0.527	-0.253	0
$\|+2\rangle$	0	0	-0.422	-0.306	0	0	-0.316	-0.633	0	0	-0.462
$\|+1\rangle$	-0.216	0.079	0	0	0.499	0.242	0	0	-0.452	-0.660	0
$\|0\rangle$	0	0	0.398	0	0	0	0.535	0	0	0	-0.743
$\|-1\rangle$	0.216	0.079	0	0	-0.499	0.242	0	0	0.452	-0.660	0
$\|-2\rangle$	0	0	-0.422	0.306	0	0	-0.316	0.633	0	0	-0.462
$\|-3\rangle$	-0.328	-0.284	0	0	0.334	-0.594	0	0	0.527	-0.253	0
$\|-4\rangle$	0	0	0.430	-0.591	0	0	-0.495	0.312	0	0	-0.106
$\|-5\rangle$	0.562	0.617	0	0	0.369	-0.295	0	0	0.132	-0.032	0
$\|-6\rangle$	0	0	0.239	-0.240	0	0	-0.110	0.040	0	0	-0.005
$\|-7\rangle$	0.174	0.179	0	0	0.058	-0.031	0	0	0.007	0	0
$\|-8\rangle$	0	0	0.021	-0.017	0	0	-0.004	0	0	0	0
$\|-9\rangle$	0.008	0.008	0	0	0	0	0	0	0	0	0
$\|-10\rangle$	0	0	0	0	0	0	0	0	0	0	0

oscillates in time between the states $|+10\rangle$ and $|-10\rangle$ with the tunneling frequency, $\omega_T = \Delta/\hbar$. This phenomenon is also known as Rabi oscillations. On this account, Δ is called the tunnel splitting. In incoherent tunneling, the spin can tunnel with a finite probability but without oscillations due to the damping associated with the environmental effects mentioned above. In fact, one can observe only incoherent tunneling in Fe8, since the extremely small tunnel splitting compared to the broadening of the energy levels cannot lead to the coherence.

3.3.1.3 Tunnel splitting and tunneling in the ground state in zero field

The Δ_m in zero field can be expressed in terms of the anisotropy constants and the total spin [74],

$$\Delta_m = \frac{8(|D| - E)}{[(m-1)!]^2}\frac{(S+m)!}{(S-m)!}\left(\frac{E}{8(|D|-E)}\right)^m. \tag{3.15}$$

For Fe8 cluster, Eq. (3.15) gives rise to $\Delta_{10} = 2.2 \times 10^{-9}$ K, $\Delta_9 = 3.7 \times 10^{-7}$ K, and $\Delta_8 = 2.62 \times 10^{-5}$ K. The results are consistent with the values obtained from the exact diagonalization of the Hamiltonian (see Fig. 3.11). Although Δ_m with decreasing m increases rapidly ($\Delta_5 \sim 0.3$ K), the tunnel splitting with large m is very small. At very low temperature where the lifetime broadening of the levels becomes very small one can hope to observe the pure quantum tunneling regime in the ground state. However, even a minute longitudinal magnetic field can lift the degeneracy of the two $\pm m$ states and prevent the tunneling. For example, 10^{-9} T corresponds to the energy, $g\mu_B S_z \times 10^{-9} = 1.3 \times 10^{-8}$ K $> \Delta_{10}$, which is large enough to cause the molecules out of resonance. In particular, the intermolecular dipolar field of about 0.05 T introduces significant longitudinal field components, which destroy the resonance condition. This can be easily seen by a variational argument [75, 76]. Let's consider the ground states $|\pm m'\rangle$ and their energy E_+ and E_-. It was already shown that those states can be written as a superposition of $|\pm m\rangle$ [Eq. (3.13)]. In order to apply variational principle, let's write the ground state as

$$|\psi\rangle = \sin\alpha|+m'\rangle + \cos\alpha|-m'\rangle, \tag{3.16}$$

and the Hamiltonian as $\mathcal{H} = \mathcal{H}_0 + \mathcal{H}_{\text{dip}} = \mathcal{H}_0 - \gamma_z S_z$, where $\gamma_z = g\mu_B H_{\text{dip,z}}$ with the longitudinal component of the dipolar field $H_{\text{dip,z}}$. Using the fact that $\langle +m'|S_z|-m'\rangle = \langle -m'|S_z|+m'\rangle \cong m$

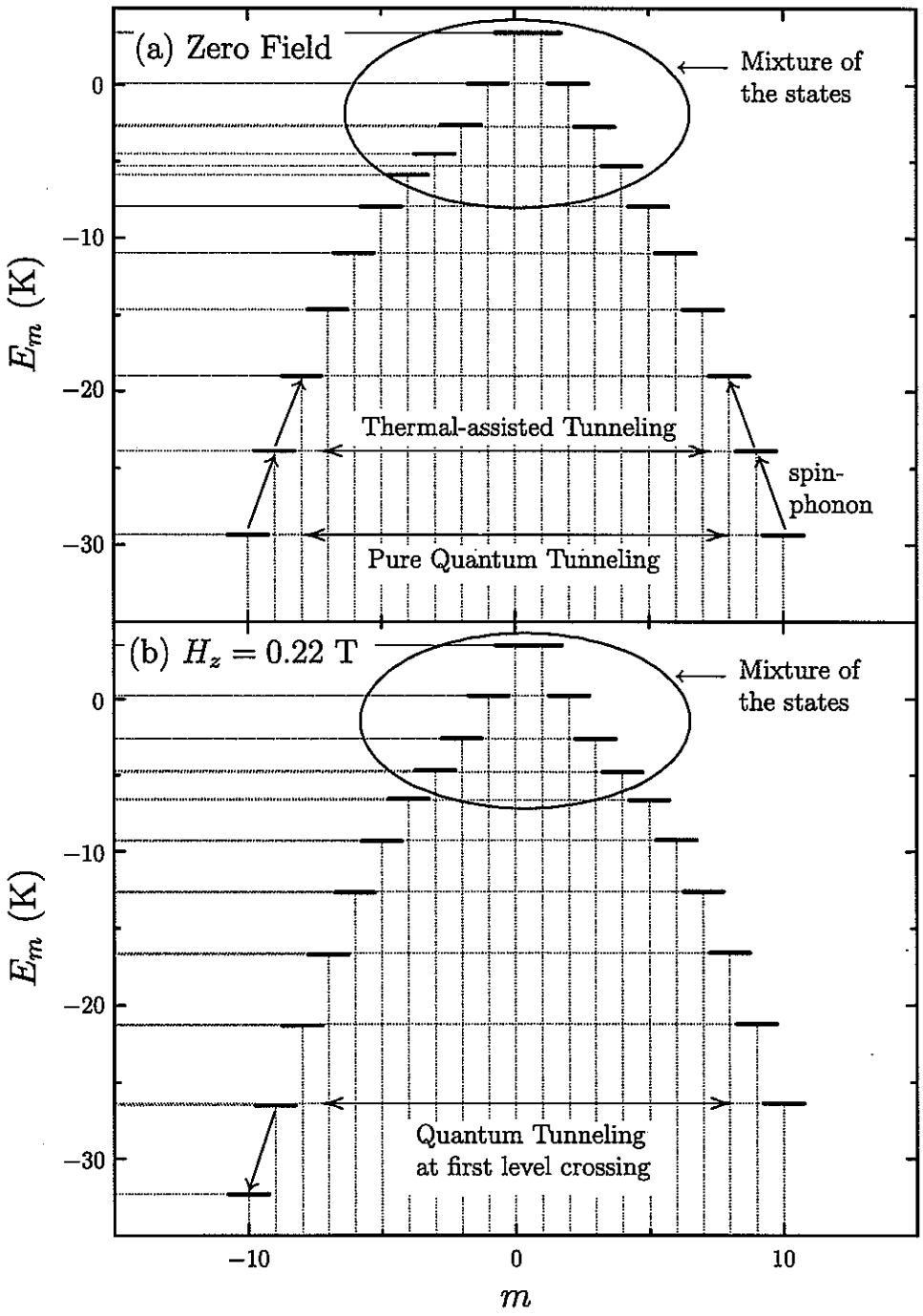

Figure 3.8 The energy level scheme for the model Hamiltonian Eq. (3.10) at (a) zero field (b) $H_z = 0.22$ T.

and $\langle +m'|S_z|+m'\rangle = \langle -m'|S_z|-m'\rangle = 0$, we have

$$\langle\psi|\mathcal{H}|\psi\rangle = \langle +m'|\mathcal{H}_0|+m'\rangle + \Delta_m \sin^2\alpha - m\gamma_z \sin 2\alpha. \tag{3.17}$$

The minimization of Eq. (3.17) with respect to α leads to,

$$\tan 2\alpha = -\frac{\gamma_z m}{\Delta_m}, \tag{3.18}$$

where Δ_m is the tunnel splitting for $S_z = m$. Since $\gamma_z \gg \Delta_m$, the allowed values of α are only $\pm\pi/4$. Therefore, the ground states are localized in either side of the potential well i.e., either $+m$ or $-m$, and the tunneling cannot occur.

The above argument, however, is in contrast with the experimental observation of QTM. The matching of the energies of the $\pm m\rangle$ states can be restored by a distribution of hyperfine interactions at low T where lifetime broadening due to spin-phonon interaction can be neglected. This explanation was advanced by Prokofe'v and Stamp (PS) [77, 78]. The fundamental idea is the following. Initially, the rapidly fluctuating hyperfine fields bring a fraction of the molecules to resonance. The tunneling relaxation of the fraction of the molecules modifies the dipolar fields and brings the initially off-resonant molecules into resonance. In this way, the experimental observation of the tunneling effect can be possible. Indeed, a Gaussian lineshape for the distribution of the tunneling rate due to the hyperfine fields was observed experimentally using an array of micro-SQUIDs by Wernsdorfer *et al.* [63, 79]. The half linewidth 0.8 mT of the Gaussian is in agreement with the predicted value of 0.3 mT by Prokof'ev and Stamp. The relationship between the width of the distribution and a typical hyperfine energy was theoretically probed by the use of Monte Carlo simulations [80]. Also the crucial role of the hyperfine fields in the tunneling process was confirmed by the remarkable isotope effect: enrichment with ^{57}Fe ($s = 1/2$) enhances both the tunneling rate and the linewidth, while the enrichment of ^{2}H ($s = 1$) causes slower rate and smaller linewidth [81, 82].

At a given low field and at short times, PS theory predicts that the magnetization should relax as $M(t) \propto 1 - \sqrt{t/\tau_{\rm sqrt}}$ where the rate $1/\tau_{\rm sqrt}$ is proportional to the energy bias distribution $P(\xi_H)$. Indeed, $\sqrt{t}$ relaxation has been observed in Fe8 [63, 83] and Mn12ac [84, 85].

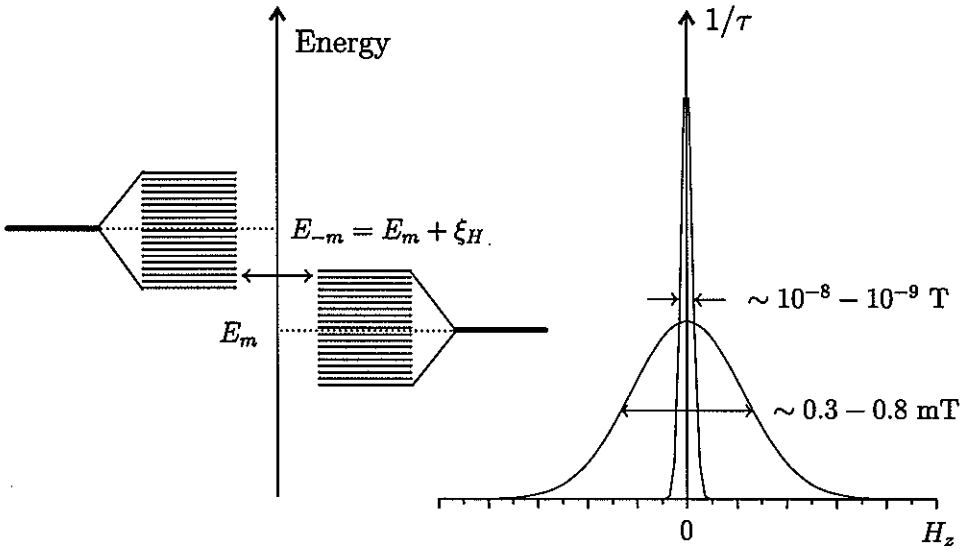

Figure 3.9 Schematic diagram for the tunneling mechanism by hyperfine interaction. The energies of the states $\pm m$ are separated by the bias energy ξ_H arising from dipolar interactions among the molecules. Each state is broadened by the rapidly fluctuating hyperfine field, allowing the tunneling between two states. The Gaussian distribution of the tunneling rate by the hyperfine field for each state is compared with the otherwise very narrow tunnel window.

3.3.1.4 Incoherent tunneling and tunneling in the excited states

At temperatures higher than 0.1 K, the lifetime broadening of the magnetic levels prevents any coherent tunneling. Also as the temperature is increased the lower m values become populated and quantum tunneling between excited m states can occur [see Fig. 3.8(a)]. Since this requires phonon absorptions and emissions, it is called phonon assisted tunneling. The tunneling process by the thermal assistance is very important mechanism because the tunnel splitting is much larger for the excited states. In fact, the experimental observations of QTM in both Mn12ac and Fe8 at $T > 1$ K are mostly associated with this mechanism. Thus the reversal of the total magnetization M at temperature comparable to the barrier is a complex phenomenon resulting from the combination of thermal excitation to the lower m values (higher energy states) combined with tunneling in the excited states. The calculation of the relaxation

of M in this regime called mixed thermal and tunneling regime or phonon-assisted relaxation has been performed by many authors [75, 76, 86–90]. In our case we are interested in the calculation of the tunneling probability between quasi-degenerate m states due to a phonon-assisted mechanism or incoherent tunneling.

In 1980, Kagan and Maksimov [91] showed that two-well tunnel kinetics of the particle, in the presence of the interaction only with the phonons, can be solved by taking into account the one- and two-phonon processes, separately. Recently, their derived formulas were reinterpreted by Tupitsyn and Barbara [92], and the incoherent tunneling rate is expressed as:[6]

$$\Gamma_{m,m'} = \frac{\Delta^2_{m,m'} W_m}{\xi^2_{m,m'} + \Delta^2_{m,m'} + W^2_m}, \tag{3.19}$$

where W_m is the lifetime broadening due to spin-phonon interaction, $\Delta_{m,m'}$ is the tunnel splitting, and $\xi_{m,m'}$ is the longitudinal bias field,

$$\xi_{m,m'} = E_m - E_{m'} + \xi_{\text{int}}, \tag{3.20}$$

where $E_m - E_{m'}$ is the longitudinal bias caused by the external field H_z (zero when $H_z = 0$) and ξ_{int} is the longitudinal bias arising from both hyperfine and dipolar fields.

A similar formula has been derived by Villain *et al.* [88, 93], and later by Leuenberger and Loss, independently [89, 90]. Neglecting slight differences between the two formalism, we can express the tunneling rate between m and m' states as:

$$\Gamma_{m,m'} = \frac{\Delta^2_{m,m'} W_m}{(E_m - E_{m'})^2 + W^2_m}. \tag{3.21}$$

We can see that as compared to Eq. (3.19) Eq. (3.21) does not have the internal bias energy ξ_{int} and $\Delta^2_{m,m'}$ in the denominator. Since $\Delta_{m,m'}$ is expected to be much smaller than the broadening W_m for Fe8 system, it is the term ξ_{int} that gives rise to the difference between Eqs. (3.19) and (3.21).

[6] It is worth pointing out that Kagan and Maksimov have presented two relaxation rates (longitudinal and transverse) for the molecular magnetization. Eq. (3.19) corresponds to the longitudinal relaxation rate, which can be associated directly with $1/T_1$. On the other hand, the transverse relaxation rate (not presented here and which is the analogue of the NMR $1/T_2$) is much smaller than the longitudinal one.

The PS theory [77, 94] discussed earlier for the tunneling in the ground state also leads to a prediction for the incoherent tunneling rate:

$$\Gamma_{10}(\xi) = \frac{2\Delta_{10}^2}{\sqrt{\pi}\tilde{\Gamma}} e^{-|\xi|/\xi_0}, \tag{3.22}$$

where both ξ_0 and $\tilde{\Gamma}$ are of the order of the amplitude of the hyperfine bias field. Eq. (3.22) and (3.21) are almost identical in zero field ($\xi = 0$ i.e., $E_m - E_{m'} = 0$) and $\tilde{\Gamma} = W_m$. However, one should note that the PS tunneling mechanism is quite different since no spin-phonon broadening is considered and the tunneling takes place as the hyperfine bias field sweeps through the matching condition for the ± 10 states leading to a Landau-Zener tunneling probability.

Since there is not yet a consensus about the mechanism for incoherent tunneling in SMMs we adopt an expression which approximates all three expressions Eqs. (3.19), (3.21), and (3.22):

$$\Gamma_{m,m'} = \frac{\Delta_{m,m'}^2 W_m}{\xi_{m,m'}^2 + W_m^2}. \tag{3.23}$$

The crucial conceptual difference with Eq. (3.21) is that the resonance width is determined not only by the phonons but also by the internal bias. W_m in Eq. (3.21) is just phonon transition probability, while W_m in our simplified model Eq. (3.23) represents the level-broadening whatever the origin is. The width W_m in higher energy states should increase due to the large density of states of phonons. For the ground state tunneling, the use of Eq. (3.23) is still valid, because W_m can be defined as the hyperfine broadening, which must be regarded as an intrinsic broadening. Then W_{10} has the same meaning as $\tilde{\Gamma}$ in Eq. (3.22). In fact, $W_{10} = 2.5 \times 10^8$ (rad/s) estimated in Chapter 4 from the NMR measurements corresponds to 2 mK, which is a correct order of magnitude of the hyperfine energy taking into account the ^{57}Fe enriched sample measured. It should be emphasized that ξ_{int} is actually time dependent since, according to PS theory, each tunneling event modifies the internal bias. The extra dynamics of the bias is hardly implemented in the theoretical model. Fortunately, the dynamics could be treated as a quasi-static because the change of the bias must be slow compared to typical experimental time. Then it would be reasonable if we interpret ξ_{int} as a half-width of the average internal field distribution.

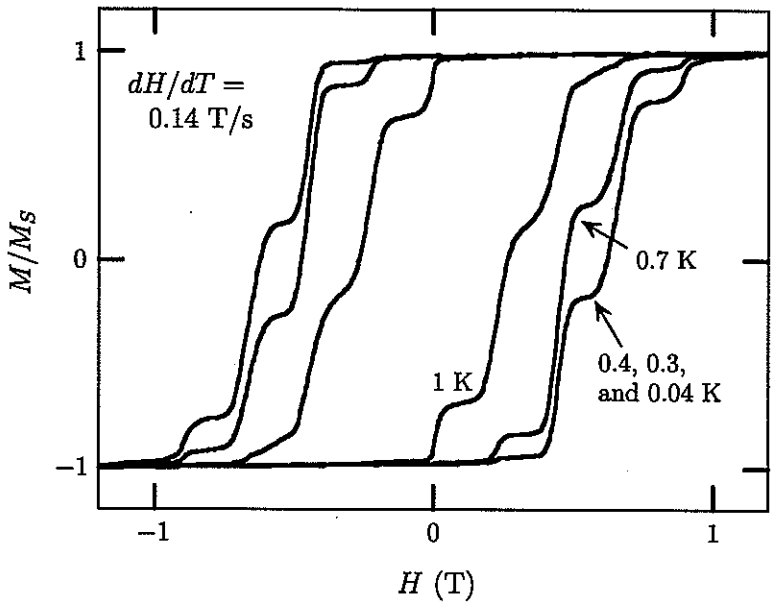

Figure 3.10 Hysteresis loops measured in a single crystal Fe8 at the constant field sweep rate of 0.14 T/s. The figure was extracted from Ref. [10].

Finally, the total effective tunneling rate can be obtained by summing up $\Gamma_{m,m'}$ multiplied by the Boltzmann factor,

$$\Gamma = \sum_m \Gamma_{m,m'} e^{-E_m/k_B T}. \tag{3.24}$$

3.3.2 Tunneling in a longitudinal field

If a magnetic field is applied along the z axis the energy levels of the m states change rapidly with a slope equal to $mg\mu_B$ as shown in Fig. 3.4(c). Since the degeneracy is removed, the tunneling is blocked. The tunneling condition, however, can be restored when $+m$ and $-m+n$ levels come into resonance (i.e., level crossing) at a field value given by

$$H_z(n) = nD/g\mu_B, \tag{3.25}$$

where n is an integer. For example, the first level crossing will occur at ~ 0.22 T as depicted in Fig. 3.8(b).

The stepped hysteresis observed in Fe8 [10, 30] is an experimental proof of the above argument. The steps are separated by about 0.22 T and equally spaced, as shown in Fig. 3.10.

The flat regions correspond to field at which the relaxation is slow, and the sharp steps are attributed to fast relaxation, determined by resonant quantum tunneling between $+m$ and $-m+n$ states. At different values of the field, QTM is suppressed due to the energy mismatch. Therefore, the stepped hysteresis are strong evidence of the phonon-assisted QTM. Moreover, the hysteresis curve becomes temperature independent below $\sim$ 0.4 K, being in excellent agreement with the temperature independent relaxation time of the magnetization below 0.36 K [95]. These observations demonstrate that a pure quantum tunneling region is attained at such a low temperature. On the other hand, for Mn12ac, no clear evidence of the pure quantum tunneling regime was observed.[7] It is obvious that the difference of the tunneling mechanism in the two clusters arises from the fact that the transverse magnetic anisotropy is large enough to establish the tunnel window for the pure QTM region in Fe8 but not in Mn12ac.

3.3.3 Tunneling in a transverse field

3.3.3.1 Tunnel splitting with an applied field along medium axis

The tunnel splitting can be increased enormously by applying a transverse field along medium y axis as shown in Fig. 3.11. For sufficiently large transverse field, the tunnel splitting of the ground state Δ_{10} can become larger than the level broadening $\delta \sim 0.03$ K. Our calculation without taking into account the fourth order anisotropy shows that $\Delta_{10} = 0.037$ K $> \delta$ at 2 T. Under this condition, the coherent QTM can be established. It has been reported that the observation of the coherence was made experimentally at a transverse field $>$ 2 T and in the temperature range of a few tenth of mK in Fe8 [96–98]. It should be stressed, however, that the enhancement of Δ_m by the transverse field does not hold when the symmetry in the energy level scheme is broken i.e., when the paired states become independent from each other. Above about 2.5 T, as seen in the Fig. 3.4(b), the tunnel splitting may lose its meaning.

One can apply a transverse field in addition to the longitudinal field which generates the

[7] Only with applying a transverse field of 3–4 T (i.e., increasing tunnel splitting), the pure tunneling regime was observed below 0.8 K [85].

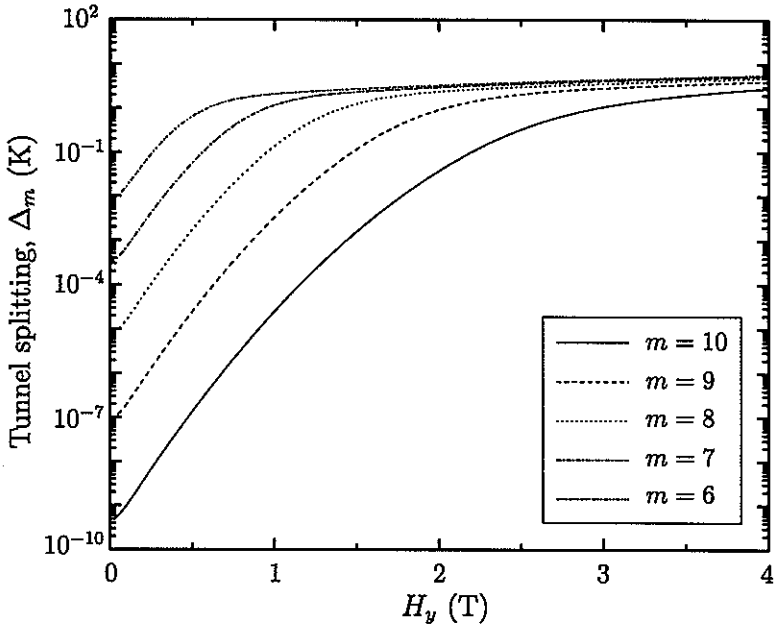

Figure 3.11 Calculated tunnel splitting between the pair of states, $\pm m$ with $m = 10, \cdots, 6$ in a transverse field applied along the medium y axis.

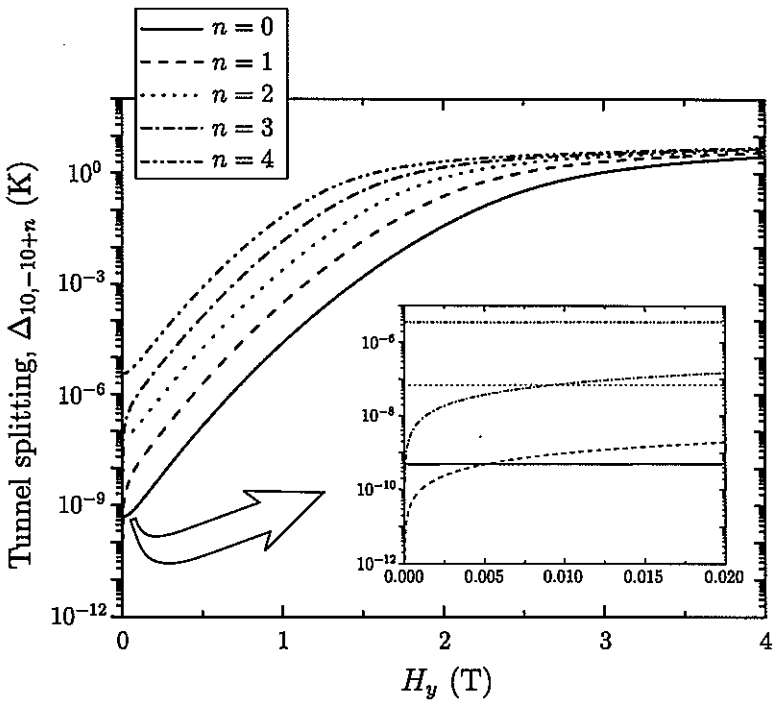

Figure 3.12 Calculated tunnel splitting between $m = +10$ and $m = -10+n$ states, where n is an integer. At very low fields, the parity effect is observed (inset).

energy matching condition at a field given by Eq. (3.25).[8] The calculated tunnel splitting between $m = +10$ and $m = -10 + n$ with an integer n is shown in Fig. 3.12. For very small field, we observe the parity effect (see inset in Fig. 3.12). Except for the low field region, the tunnel splitting increases with increasing n, just like the case with increasing m in zero field (see Fig. 3.11). The parity effect is clearly visible when the field is applied along hard x axis, as shown in Fig. 3.13(b). The parity effect could be associated with the Kramer's theorem if we introduce an effective total spin. At zero transverse field, the $m = +10$ and $m = -10 + n$ states form a *quasi-ground state* corresponding to the effective total spin, $(20 - n)/2$. For odd integer n, the total spin is a half integer so that the ground state must be doubly degenerate.

3.3.3.2 Tunnel splitting with an applied field along hard axis: quantum tunneling oscillation

For H applied along x axis, we see that Δ_m oscillates regularly as a function of the applied field, as shown in Fig. 3.13(a). The first minimum occurs at 0.13 T and the second minimum at 0.4 T, and so on, the separation between minima being 0.27 T. Also the number of minima is determined by m value, that is, 10 for $m = 10$. The unique quantum feature arises from constructive or destructive interference of quantum spin phases of two tunnel paths, which is an analogue of Berry phase [99]. The interest on the *geometrical* phase arises from the fact that it, unlike the *dynamic* phase, is a measurable physical quantity. The quantum oscillation in small magnetic particles has been predicted theoretically [100–102] utilizing the Feynman path integral formalism. For the tunneling between degenerate spin doublet separated by the energy barrier, however, no classical path exists. This problem is detoured by introducing an imaginary time (or Euclidean time) $t = i\tau$. The imaginary-time propagator is given by [103]

$$U_{fi} = \langle f|e^{-\mathcal{H}t/\hbar}|i\rangle = \int \mathcal{D}e^{-\mathcal{S}/\hbar} \tag{3.26}$$

where $|i\rangle$ and $|f\rangle$ represent initial and final state, respectively, $\mathcal{D}$ is defined via the discretised version of the path integral, and $\mathcal{S} = \int d\tau \mathcal{L}$ is the classical action defined through the classical

[8] Actually we used the precise matching field value, $H_z(n) = 0.2153296510645n$. Later, we will show that the precise value is required for the simulation of the quantum phase interference effect.

Lagrangian. In our case, we can assume only two tunneling paths in yz plane, clockwise (path 1) and counterclockwise (path 2). The phase difference for the two paths is deduced to be [101]

$$(\mathcal{S}_1 - \mathcal{S}_2)/\hbar = -iSA_{12}, \tag{3.27}$$

where $\mathcal{S}_1$ and $\mathcal{S}_2$ are the actions for the paths 1 and 2, respectively, S is the total spin, and A_{12} is the area enclosed by the two *instanton* paths. Therefore, if A_{12} equals $n\pi/S$ with an odd integer n, the tunnel splitting is quenched. More precisely, according to Garg [102], the tunnel splitting is quenched whenever[9]

$$H_x = 2\sqrt{2E(|D| + E)}(m - n + 1/2)/\mathrm{g}\mu_B, \tag{3.28}$$

where m runs from 1 to S, and n is an integer up to m, and E and D are the anisotropy constants in Eq. (3.10). Also similar results have been derived by using WKB approximation [104, 105]. Eq. (3.28) explains not only the exact field value for the suppression of the tunnel splitting but also the number of minima for given m, although Eq. (3.28) will break down when the higher order Hamiltonian terms are included.

We can also setup quasi-degenerate paired states such as $m = +10$ and $m = -10 + n$ with integer n in the presence of a longitudinal field, $nD/\mathrm{g}\mu_B \sim 0.22n$. However, our calculation shows that the resonant tunneling condition with a longitudinal field can only occur at $H_z(n) = 0.2153296510645n$. Changing the longitudinal field by the amount of 10^{-8} T, we find that the oscillations disappear completely. It is apparent that the required accuracy is far beyond the ability of any experimental technique, which explains why there must be a broadening mechanism for the tunneling (see subsection 3.3.1.3).

The calculated results for $n = 0 - 4$ are shown in Fig. 3.13(b). The parity effect is clearly shown. As mentioned previously, the parity effect could be viewed as a result of the different character of half-integer spin and integer one. The quenching of the tunnel splitting in zero field for the half-integer spins is easily checked by applying any half-integer m in Eq. (3.28). Also we find that the number of oscillation is consistent with the effective spin description.

[9] Garg's Hamiltonian in the form of $\mathcal{H} = k_1 S_x^2 + k_2 S_z^2$ is different with Eq. (3.10). In this case, k_1 and k_2 in his formula should be rewritten in terms of D and E, i.e., $k_1 = 2E$ and $k_2 = D + E$.

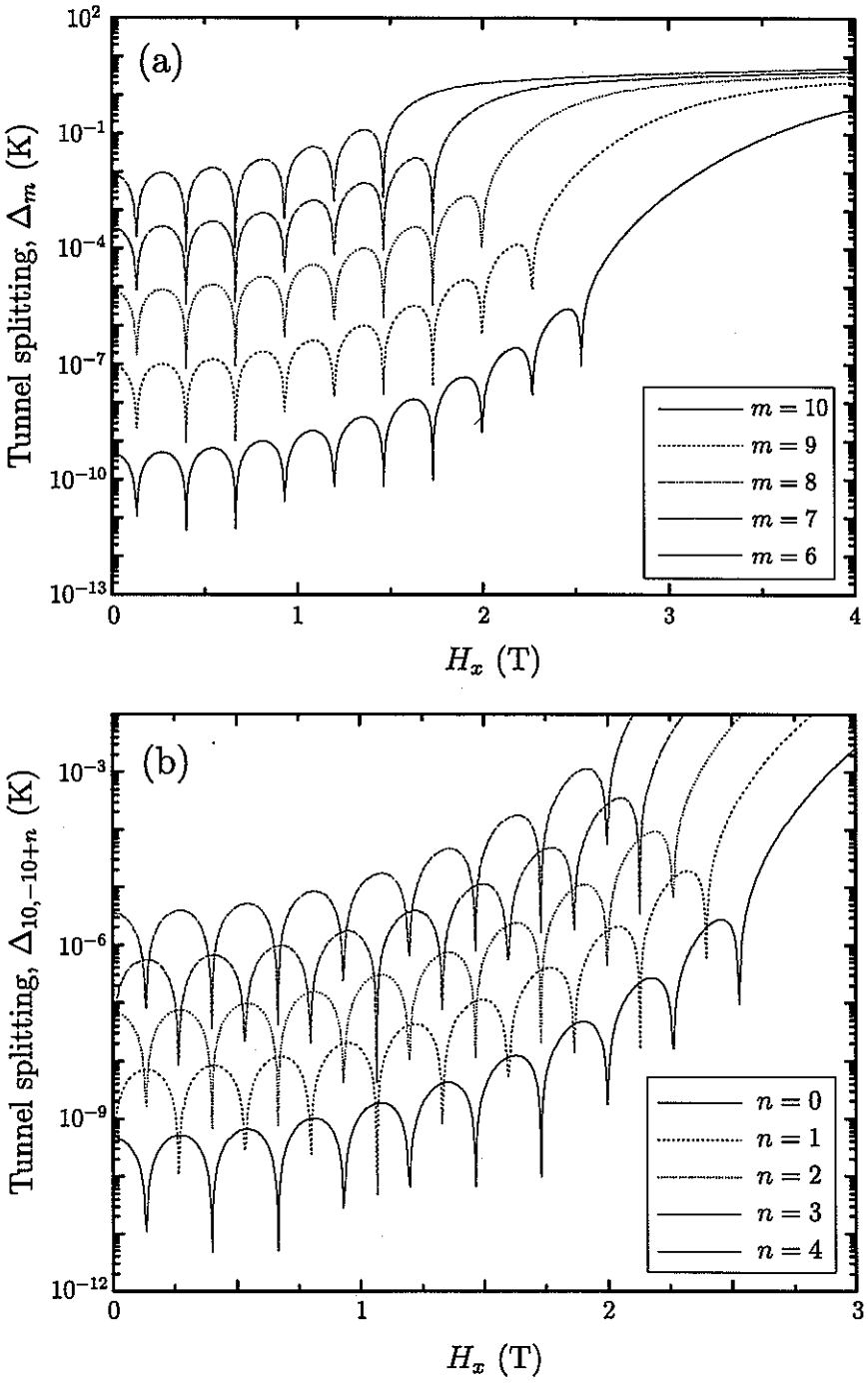

Figure 3.13 (a) Calculated tunnel splitting of the paired states $\pm m$ from $m = 10$ to $m = 6$ for the transverse field applied parallel to x. Δ_m shows an oscillatory behavior. (b) The parity effects calculated for the transition $+10 \leftrightarrow -10 + n$ with $n = 0, 1, 2, 3, 4$ at $\phi = 0$ (hard axis).

The topological phase interference as well as the parity effect have been measured by experiment, for the first time, by Wernsdorfer and Sessoli [30] by the use of the Landau-Zener tunneling probability [106–108],

$$P_{m,m'} = 1 - \exp\left(\frac{\pi\Delta^2_{m,m'}}{2\hbar g\mu_B dH/dt}\right), \tag{3.29}$$

where dH/dt is the constant sweeping rate of the field, and m and m' are the levels which are crossed. With a fixed sweeping rate, the tunnel splitting Δ is extracted from Eq. (3.29). The experimental results, however, revealed quantitative differences with our theoretical calculations. First, energy scale of the tunnel splitting is two orders of magnitude larger than calculated one. Second, the period of oscillation (0.41 T) is substantially larger than the calculated one (0.27 T). Third, there are only 4 quenching fields instead of 10. These disagreements could be elucidated by taking into account the fourth order terms in the spin Hamiltonian. We simulated this situation adding the higher order Hamiltonian to Eq. (3.10),

$$\mathcal{H}' = D_2 S_z^4 + E_2[S_z^2(S_x^2 - S_y^2) + (S_x^2 - S_y^2)S_z^2] + C(S_+^4 + S_-^4), \tag{3.30}$$

where $D_2 = 3.54 \times 10^{-5}$ K, $E_2 = 2.03 \times 10^{-7}$ K, and $C = -3.5 \times 10^{-5}$ K. D_2 and E_2 values are the same as the ones in Ref. [66] but C, which is 8 times larger than the value in Ref. [66] with the opposite sign, has been determined from the best fit to the experiment. Since the C term is most important one with regard to the tunnel splitting, this approach should be acceptable for our purpose. The result is shown in Fig. 3.14, where the experimental data points were taken from Ref. [30]. Our calculated results reproduce the period of oscillation and the correct energy scale in the experiment. But the discrepancy between the theory and the experiment is still not ignorable. It is believed that there is a possibility of *misalignment* effects. Within the single crystal, the anisotropy axes of each molecule may not coincide with those of the other molecule, making a conic distribution of angles. In other words, there is no "unique" anisotropy axes for the crystal, and an external field cannot be applied "along" one of anisotropy axes. We expect that the distribution angle for x and y axes is much larger than the one for easy z axis due to the strength of the crystal field.

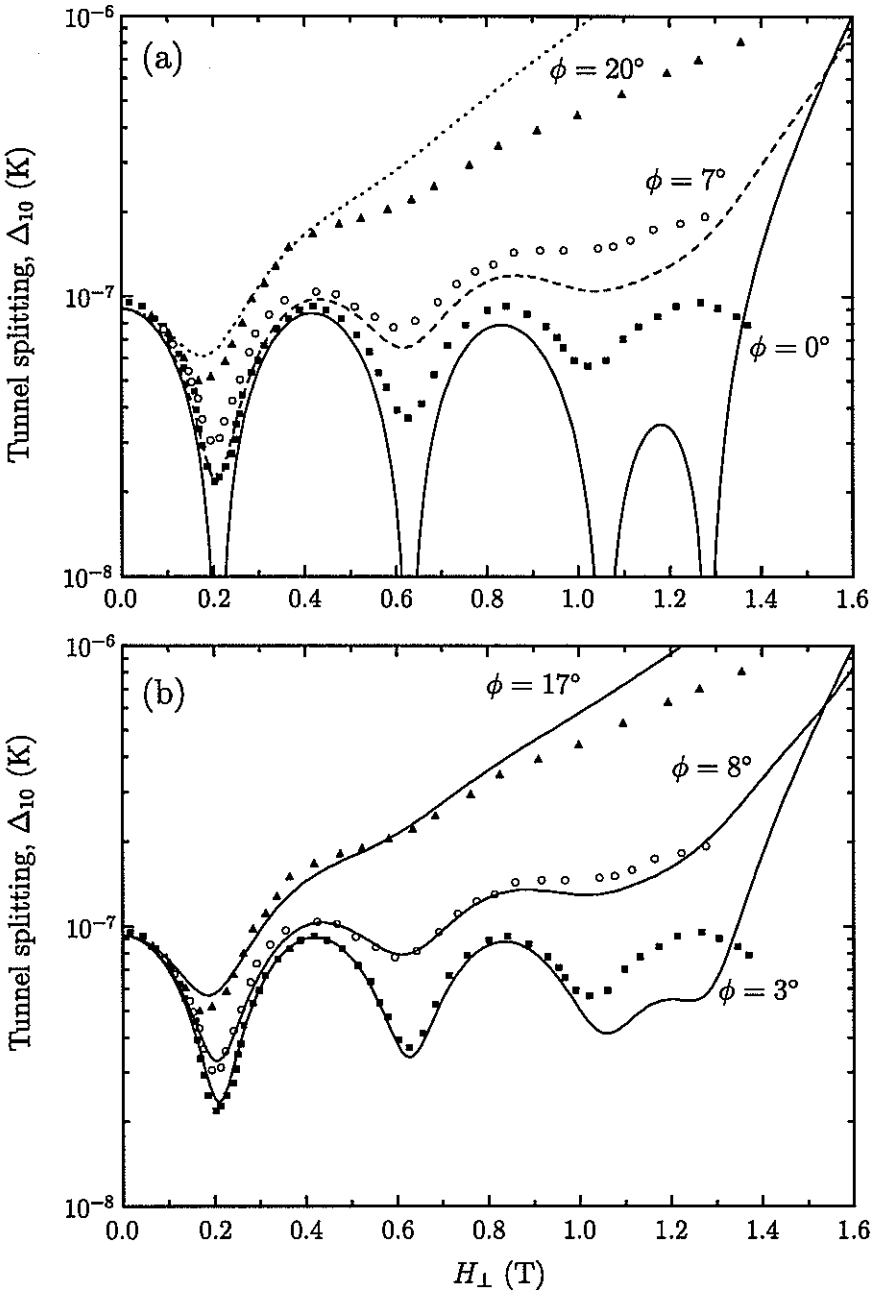

Figure 3.14 Comparison of the experiment with calculated tunnel splitting of $m = 10$ levels taking into account the higher order Hamiltonian [Eq. (3.30)]. (a) The different azimuthal angle ϕ's are the same as the ones in the experiment. (b) We consider the misalignment effect, allowing ϕ to vary up to 3° and applying a tiny longitudinal field, 8×10^{-10} T. The experimental data were taken from Ref. [30].

As a matter of convenience, we assume that the sample is experimentally misaligned by some angle, and expect that the assumption would end up with a similar result as compared to the one obtained by the exact calculations considering all distribution of the molecules. This situation has been simulated allowing the azimuthal angle ϕ to vary within $\pm 3°$. The results are shown in Fig. 3.14(b) for $\phi = 3°, 8°$, and $17°$. We also assumed the longitudinal field component of 8×10^{-10} T for better fit. The theoretical curves fit the experimental data very nicely except the last oscillation when $\phi = 0$. The remained discrepancy may be corrected if we consider the distribution of the anisotropy axes accurately. However, this is sufficient for our purpose, and we stop this discussion here.

Furthermore, the fact that the number of minima is 4 agrees with the experiment. At first sight, this result is rather surprising because it arises from the weak fourth order anisotropy term, $C(S_+^4 + S_-^4)$. In the presence of the fourth order anisotropy, Eq. (3.28) is no longer true, and the number of oscillations is not determined by m. It is because the fourth order Hamiltonian term can couple $m = \pm 10$ states by 5 applications, while the second order term by 10. This fact is associated with the possible number of the area enclosed by the tunneling paths that quenches the tunnel splitting. That is, the number of minima depends directly on the symmetry of the anisotropy [92]. As an example, let us suppose $E = 0$ and $C \neq 0$. There is no oscillation because x axis is no longer hard axis. For $\phi = 45°$ (this is new hard axis), there appear 5 oscillations (as it is the case for Mn12ac). This is due to the fact that with increasing H_x, the allowed states which can be coupled by the fourth order anisotropy term are $S_z = \pm 10, \pm 8, \pm 6, \pm 4$, and ± 2. If both the second and the fourth order terms coexist, the number of minima depends solely on the relative strength of the anisotropy constants due to interference between them. Fig. 3.15(a) reflects the interference effect. With increasing C, the period increases, while the number of minima decreases. If $C/E > 10^{-2}$, there is no more oscillation. Thus in order to observe the phase effect, C should fulfill the condition, $C/E < 10^{-2}$. It is noticed that the number of minima is a multiple of an integer.[10] We emphasize that C must be negative for this argument to hold. For positive C, the behavior is

[10]This result is in agreement with Ref. [109, 110]. The authors investigate the role of C by introducing "boundary jump instantons" which interfere with the conventional "continuous" instantons.

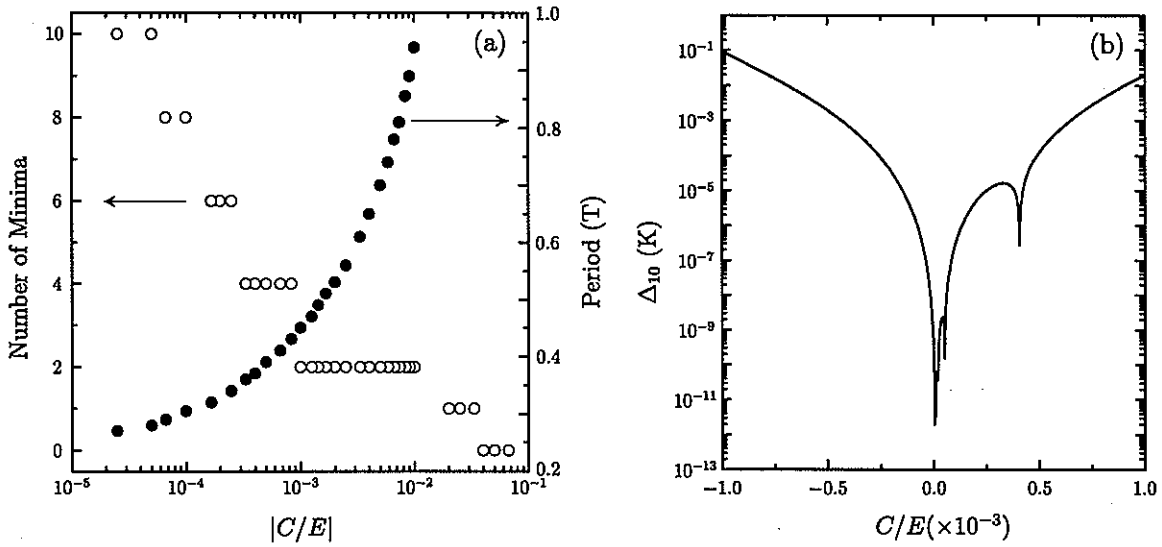

Figure 3.15 Dependence of the quantum phase effect on the fourth order anisotropy C. (a) The period increases and the number of minima decreases with increasing C. Note that C is negative and $E = 0.047$ K is the second order anisotropy. (b) Tunnel splitting Δ_{10} in zero field is asymmetric around $C = 0$. The argument made in (a) is no longer applicable for $C > 0$.

complex. As we can see in Fig. 3.15(b), the tunnel splitting Δ_{10} in zero field shows a different behavior depending on the sign of C. This is because, for $C > 0$, Δ_{10} at zero field is not fixed to maximum but the parity changes smoothly with increasing C, resulting in oscillatory behavior as shown in Fig. 3.15(b). In other words, the "wave" of the regular quenching of the tunnel splitting moves to the left. As a matter of fact, the period cannot be defined in this case because the separation between the minima increases with increasing field for a given positive C value.

3.3.3.3 QTM in transverse magnetization

We go back now to the theoretical results shown in Fig. 3.6 and in particular to the peak which appears in the curve of $\partial M/\partial H$ vs H. In the following we want to analyze the origin of the peak in $\partial M/\partial H$ by using a somewhat different approach from Ref. [71]. In Fig. 3.6, it is noticed that

1. The peak smears out and moves toward lower fields gradually as T is increased,

2. At low field, $\partial M/\partial H$ is smaller at low temperature than at high temperature, and becomes temperature independent at sufficiently low temperature (< 0.5 K),

3. After the peak, both M and $\partial M/\partial H$ follow the *normal* behavior as in the case of H applied along easy axis.

At sufficiently low temperature, only the lowest energy states $m = \pm 10$ would be occupied. When a transverse field is applied, the transverse magnetization can be written as:

$$\begin{aligned} M_\perp &= \frac{N}{Z}\left(-\frac{\partial E_+}{\partial H}e^{-E_+/kT} - \frac{\partial E_-}{\partial H}e^{-E_-/kT}\right) \\ &= N\left(-\frac{\partial E_-}{\partial H} - \frac{\partial \Delta}{\partial H}p_+\right), \end{aligned} \tag{3.31}$$

where $E_\pm$ is the energy for ± 10 states, and the probabilities of occupation of the two states are defined by $p_\pm \equiv \exp(-E_\pm/kT)/Z$. At low field, $\partial\Delta/\partial H$ is so small that Eq. (3.31) is almost temperature independent. The peak of $\partial M/\partial H$ is clearly due to the change of $-\partial E_-/\partial H$ arising from the increase of the splitting of the energy levels. We will define a cross over field H_c as the field at which the peak of $\partial M/\partial H$ is located. Since $-\partial E_-/\partial H \cong -\partial E_+/\partial H$ at $H < H_c$, we may interpret that the molecules occupying equally the quasi-degenerate magnetic levels at $H < H_c$ collapse rapidly toward the lowest level at $H > H_c$. We notice that the peak itself does not become T-independent even at very low T. The reason is that the second term in Eq. (3.31) becomes non-negligible at fields close to H_c because $\partial\Delta/\partial H$, which is positive, starts to increase rapidly. However, it becomes T-independent again at the fields much higher than H_c because p_+ decreases exponentially with increasing field.

With increasing temperature, the higher energy levels will be occupied. For simplicity, let us consider an intermediate temperature region in which the first excited doublet ($m = \pm 9$) could be occupied. Then, the transverse magnetization is written as

$$M_\perp = N\left(-\frac{\partial E_1}{\partial H} - \frac{\partial \Delta_{13}}{\partial H}(p_3 + p_4) - \frac{\partial \Delta_{12}}{\partial H}p_2 - \frac{\partial \Delta_{34}}{\partial H}p_4\right), \tag{3.32}$$

where we denote each state by a number in such a way that state 1 has the lowest energy and correspondingly p_1 is the probability of occupation of the state 1. The first and second

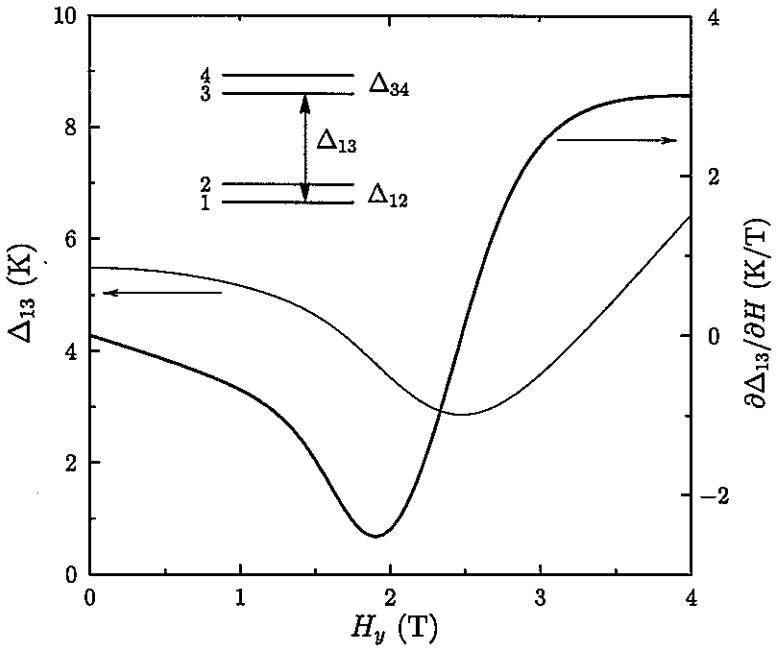

Figure 3.16 Energy difference between states 1 and 3 and its derivative in the transverse field along medium y axis. Schematic diagram for the levels is shown in inset.

terms are the dominant ones as compared with the other two terms. We note that $\partial\Delta_{13}/\partial H$ is negative at low field (see Fig. 3.16) so that the magnetization at high T is larger than that at low T at a given low field. After the peak of $\partial M/\partial H$ i.e., at fields above H_c, $\partial\Delta_{13}/\partial H$ becomes positive and keeps increasing, which results in the "normal" field dependence of both M and $\partial M/\partial H$ as in the case of a longitudinal field, as it is evidenced in Fig. 3.6.

The fact that the peak moves toward lower fields and is broadened by increasing T indicates that the splitting of the levels for smaller m states ($\pm 9, \pm 8, \ldots$) affects the total magnetization M progressively. Note that H_c decreases with decreasing m, as shown in Fig. 3.4. Furthermore, the fact that the peak is persistent only in a specific range of temperatures (at 8 K the peak disappears completely, as shown in Fig. 3.6) suggests that there exists a crossover temperature, above which the peak of $\partial M/\partial H$ disappears.

Fig. 3.17 shows the temperature dependence of M and $\partial M/\partial H$ calculated at 0.1 T. Indeed, below about 0.6 K both M and $\partial M/\partial H$ become T-independent regardless of the field direction. In order to define different regions of spin dynamics in the form of a phase diagram we define

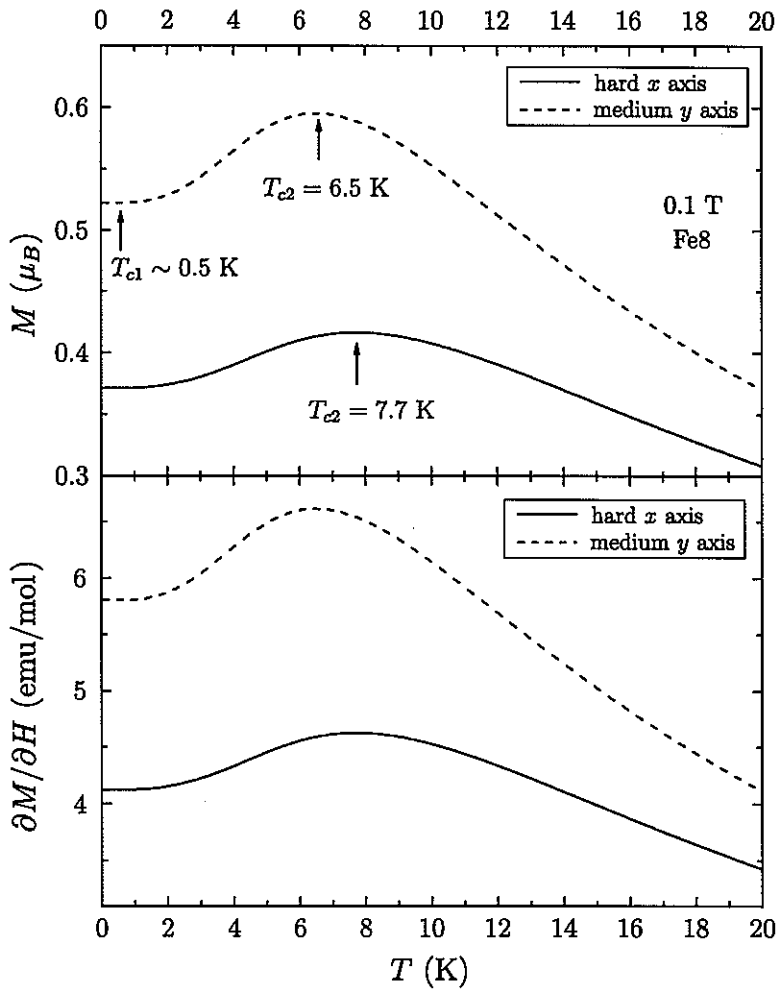

Figure 3.17 Magnetization and magnetic susceptibility vs T at 0.1 T. There appears a broad but clear maximum of both M and $\partial M/\partial H$.

two crossover temperatures T_{c1} and T_{c2}. T_{c1} is determined from the temperature above which M differs by the amount of 0.001% of M. T_{c2} is defined as the temperature at which the broad maximum occurs in $M(T)$ and $\partial M(T)/\partial H$ (see Fig. 3.17).

Here, we propose a new interpretation of the crossover temperatures T_{c1} and T_{c2} defined above. First, the temperature independence of M (or $\partial M/\partial H$) below T_{c1} at low fields is a required, although probably not sufficient, condition for pure quantum tunneling regime, since it is obvious that the T-independence of M cannot occur unless most of the molecules occupy the ground states. Second, the presence of the peak of $\partial M/\partial H$ at a given $T < T_{c2}$ could be thought as an indication of the thermally assisted tunneling regime, since the peak means that

only the energy levels far below the top of the energy barrier could be occupied. Above T_{c2}, the tunneling will not essentially contribute to the relaxation of the magnetization since the thermal relaxation over the top of the energy barrier becomes very fast. Therefore, like the preceding argument about pure tunneling regime, we argue that the peak of $\partial M/\partial H$ is one of the required condition for the thermal-assisted QTM.

Although above argument cannot be established at the moment, we performed calculations of the field dependence of the crossover temperatures. In Fig. 3.18(a), the field dependence of T_{c1} and T_{c2} in Fe8 is shown. The diagram, which looks like a phase diagram, shows very nice picture of three distinct regions. We may classify the regions into pure quantum tunneling region when $T < T_{c1}$, thermal-assisted tunneling region when $T_{c1} < T < T_{c2}$, and pure thermal relaxation region when $T > T_{c2}$. For the comparison, also we calculated the magnetization of Mn12ac in the same way done in Fe8, and the result is shown in Fig. 3.18(b). As we can see, for Mn12ac, the diagram is much simpler due to the absence of the second order in-plain anisotropy E, and the crossover temperatures are much higher than those in Fe8 due to the large axial anisotropy $D \sim -0.6$ K [111]. $T_{c1} \sim 0.6$ K of Fe8 is in good agreement with the experimental result (~ 0.4 K). Unfortunately, the experimental T_{c1} in Mn12ac is not exactly known because the relaxation time of the magnetization is extremely long (about two months at 2 K). However, $T_{c1} \sim 1.2$ K agrees well with the fact that a pure quantum tunneling regime is achieved below 0.8 K in the presence of a transverse field 3–4 T [85]. It is clear that T_{c1} and T_{c2} are essentially determined by the height of the energy barrier (i.e., by the magnitude of D value).

As discussed above, T_{c1} and T_{c2} in the diagram should be regarded as a rough estimation for the possible tunneling regime for given magnetic anisotropy parameters. Nevertheless the theoretical diagram can be a good guidance for the actual experiment, and be useful for the analysis of the experimental results. The experimental verification of the "phase diagram" seems possible through the precise measurements of the magnetization on the single crystal. However, in order to measure T_{c1}, the alignment of the sample should be exact. In fact, even tiny misalignment of the sample will destroy the otherwise temperature independent region,

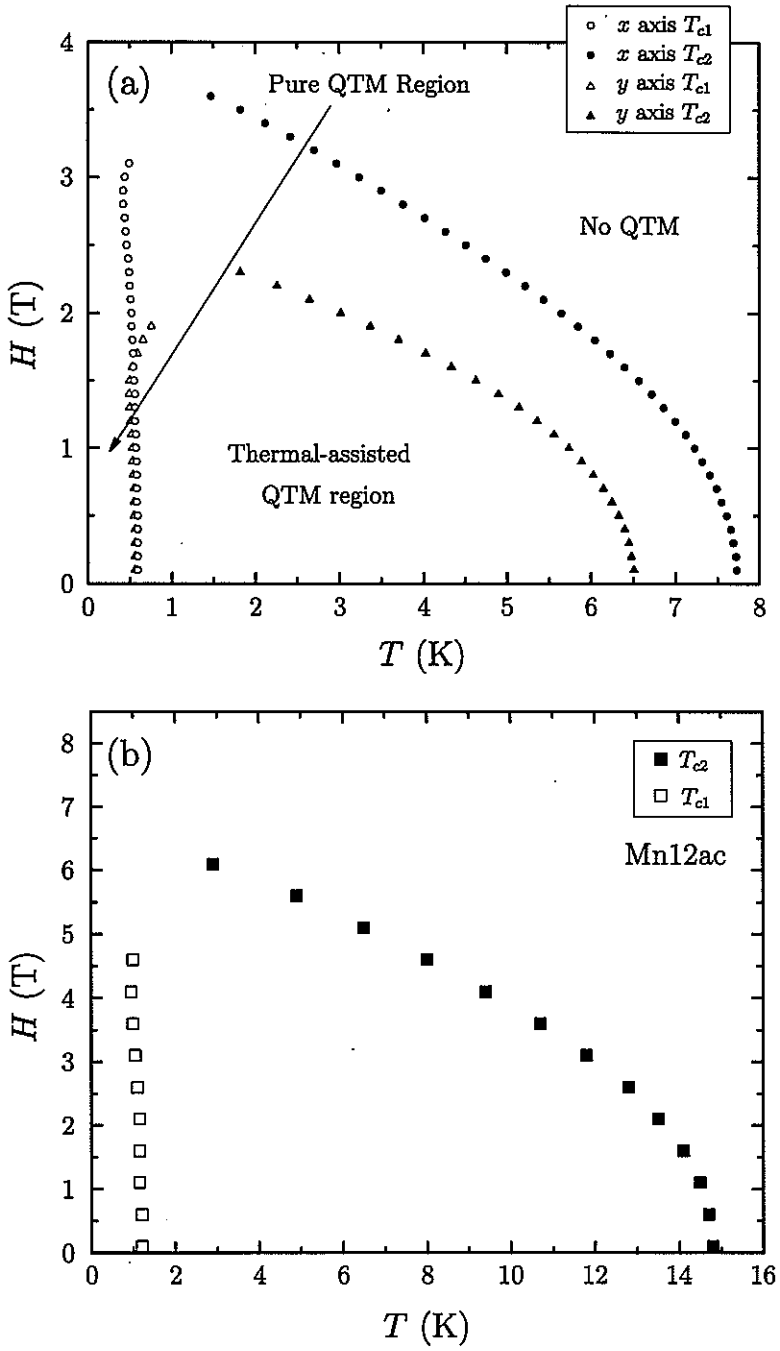

Figure 3.18 The relation between H and the crossover temperatures T_{c1} and T_{c2} obtained from the calculated transverse magnetization in Fe8 (a) and Mn12ac (b). T_{c1} for both clusters is almost H-independent up to a reasonable field, and is consistent with the experimental observation ($\sim$ 0.4 K for Fe8 and $\sim$ 0.8 K for Mn12ac).

as it has been simulated by introducing small amount of the z field component. Indeed, the experimental result shows that M increases at very low temperature rather than becoming T-independent after the broad maximum (see Fig. 3.7). However, T_{c2} will still be measurable as long as the misalignment is small, say up to 5°.

CHAPTER 4 ^{57}Fe NMR and relaxation in isotopically enriched Fe8

In this chapter, we discuss ^{57}Fe NMR measurements performed in oriented powder and single crystal of enriched ^{57}Fe8 molecular cluster in the temperature range 0.05–1.7 K in zero and external fields for both transverse and longitudinal orientation of H with respect to the anisotropy axis. The ^{57}Fe NMR spectrum is analyzed in terms of a major contribution due to the hyperfine interaction arising from core polarization. The measured temperature dependence of the resonance frequency is explained well by calculating the local average magnetic moment of the Fe^{3+} ion with a simple model which incorporates the effects of thermal fluctuations. Nuclear spin-lattice relaxation rate ($1/T_1$) and spin-spin relaxation rate ($1/T_2$) were investigated via temperature and field dependences. The obtained results are analyzed in terms of both intrawell thermal fluctuations of the hyperfine fields due to spin-phonon interaction, and interwell fluctuations due to phonon assisted quantum tunneling of the magnetization. It is shown that in zero external field and at low T the ^{57}Fe $1/T_1$ is dominated by a strong collision mechanism due to the fact that phonon assisted tunneling transitions generate a sudden reversal of the local quantization field at the nuclear site. The data could be explained satisfactorily by assuming that the ^{57}Fe $1/T_1$ measures directly the effective phonon assisted tunneling rate. However, in order to fit the data we had to assume a larger in-plane anisotropy than previously reported, resulting in a much bigger tunneling splitting in zero field. A comparison with published data of ^{55}Mn in Mn12 indicates that a similar tunneling driven relaxation mechanism applies also in Mn12. Finally the H and T dependence of ^{57}Fe $1/T_2$ is well explained simply in terms of thermal fluctuations of the magnetization without any tunneling contribution. At very low T the $1/T_2$ approaches a limiting value which can be explained in terms of the dipolar interaction between proton and ^{57}Fe nuclei in the quasi static regime.

4.1 Introduction

Single molecule magnets (SMMs) are magnetic systems formed by a cluster of transition metal ions within large organic molecules [2, 112]. SMMs are characterized by nearly identical and magnetically isolated molecules with negligible intermolecular exchange interactions, which allows the investigation of nanomagnetism from the macroscopic measurement of the bulk sample. Recently, SMMs have been paid much attention not only for the fundamental physical properties but also for the potential applications in quantum computing and data storage [33]. Among the single molecule magnets, Mn12ac and Fe8 clusters [26, 95], which have a high total ground state spin ($S = 10$), are of particular interest due to the superparamagnetic behavior and the quantum tunneling of the magnetization (QTM) observed at low temperature [28, 29, 113] due to the large uniaxial anisotropy.

The octanuclear Fe^{3+} cluster [25] (Fe8) is a particularly good candidate for the study of quantum effects since it couples an uniaxial anisotropy leading to an energy barrier [95] of $\sim$ 25 K to a non negligible in-plane anisotropy. The latter is crucial in enhancing the tunneling splitting of the pairwise degenerate magnetic quantum states. In fact, Fe8 shows pure quantum regime below 0.4 K and periodic oscillations of the tunnel splitting interpreted in terms of Berry phase [30, 81, 99]. Moreover, it was found that the enrichment of ^{57}Fe isotope in Fe8 shortens the relaxation time demonstrating that the hyperfine field plays a key part in QTM [82]. Together with intensive theoretical investigations [78, 80, 94, 114, 115]. QTM in Fe8 has been revealed by various techniques such as magnetization measurements [30, 81]. ac-susceptibility [95, 96], specific heat measurement [97, 116], high-frequency resonant experiments [117], circularly polarized microwave technique [118], and nuclear magnetic resonance [43, 119].

Nuclear magnetic resonance (NMR) has proved to be a powerful tool to investigate the local properties of magnetic systems because the nuclear spin is very sensitive to local fields and thus provides valuable information on spin dynamics. Several proton NMR studies on Fe8 have been already performed yielding information about hyperfine interaction, fluctuations of the local moments of Fe^{3+} ions [57], and tunneling effects [43, 70, 119]. In proton NMR,

however, we can obtain only indirect information due to an averaging effect arising from the wide distribution of protons in each molecule and the weak hyperfine coupling between Fe moments and protons.

^{57}Fe is, in principle, a much better than proton since it couples directly to the magnetic electrons of the Fe^{3+} ions with a strong hyperfine field which allows the investigation of ^{57}Fe NMR in zero external field. The only drawback is that the strong coupling makes the NMR signal detectable only in a narrow temperature range. Previous ^{57}Fe NMR studies have yielded direct information on the local magnetic structure of the ground state and the hyperfine interactions [40, 41]. In addition to the static effects mentioned above, ^{57}Fe NMR can provide precious information about the dynamic magnetic properties, including the tunneling effect, through the measurements of the relaxation rates as a function of temperature and external field, and by the temperature dependence of the resonance frequency in zero field, which are the subjects of the present investigation.

In this chapter, we report ^{57}Fe NMR measurements in both a sample of oriented powder and a single crystal both enriched in the ^{57}Fe isotope. In Sec. 4.2, the sample properties and some experimental details are illustrated. After presenting the experimental results in Sec. 4.3, the hyperfine interactions and static magnetic properties are analyzed in Sec. 4.4 with emphasis on the temperature dependence of the nuclear resonance frequency in zero field. In Sec. 4.5 we discuss and deduce theoretical spin dynamics models for the nuclear relaxation rates in the low temperature region. Detailed comparison of the data of the relaxation rates with the theoretical models proposed in Sec. 4.5 are reported in Sec. 4.6. Also the relaxation rates of ^{55}Mn are compared with those of ^{57}Fe. In Sec. 4.7, our experimental results and theoretical analysis are summarized.

4.2 Sample properties and experimental details

The formula of the molecular cluster is $[Fe_8(tacn)_6O_2(OH)_{12}]^{8+}[Br_8 \cdot 9H_2O]^{8-}$ (in short Fe8) where tacn is the organic ligand 1,4,7-triazacyclonane and the ionic charge 8+ of the cation is compensated by seven bounded Br^- ions and one Br^- counterion. Fe8 consists of eight Fe^{3+}

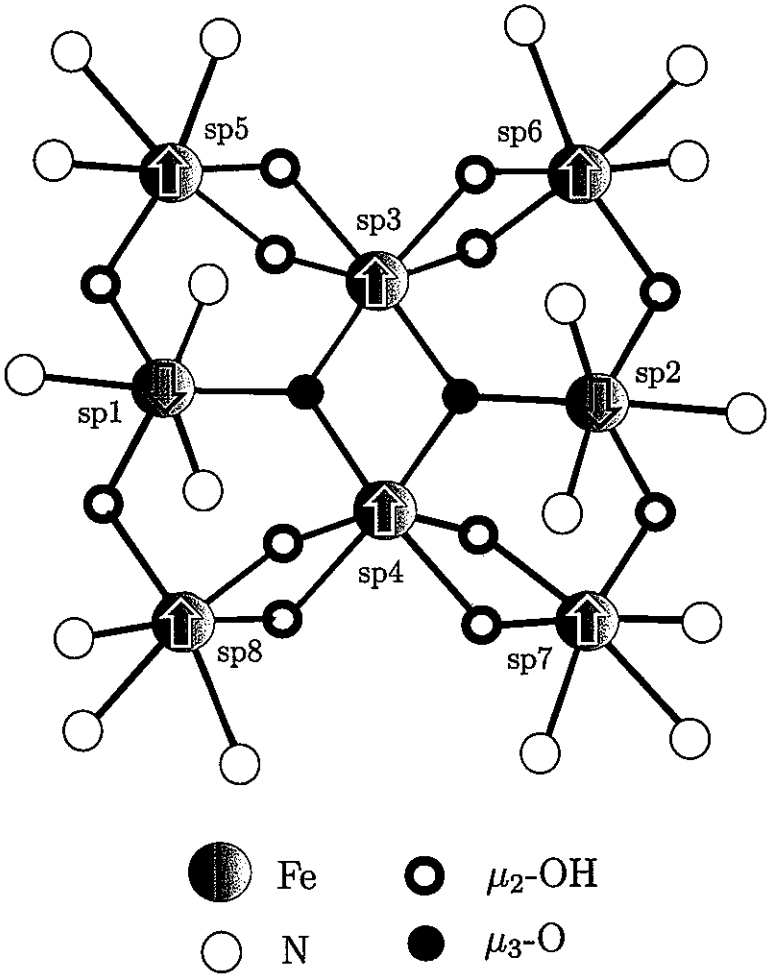

Figure 4.1 Schematic diagram of Fe8 molecular cluster. The arrows represent ionic spin direction of Fe^{3+} ion with $s = 5/2$ in $S = 10$ ground state.

ions ($s = 5/2$) where the Fe ions are coupled together by twelve μ_3-oxo and μ_2-hydroxo bridges through different exchange pathways resulting in well-known butterfly configuration. The magnetic properties of Fe8 at low temperatures are characterized by a total spin of $S = 10$ for each molecule resulting from competing nearest neighbor antiferromagnetic interactions between the Fe^{3+} ions [65].

The $S = 10$ magnetic ground state of the Fe8 molecular cluster can be described by a total spin model Hamiltonian,

$$\mathcal{H} = DS_z^2 + E(S_x^2 - S_y^2) + g\mu_B \mathbf{S} \cdot \mathbf{H}, \tag{4.1}$$

where S_x, S_y and S_z are the three components of the spin operator, D and E are the axial and the rhombic anisotropy parameter, respectively, μ_B is the Bohr magneton, and the last term of the Hamiltonian describes the Zeeman energy associated with an applied field H.

The crystal structure of Fe8 is shown in Fig. 4.1. The arrows represent the spin structure of Fe^{3+} ions in the ground state $S = 10$. In order to synthesize the ^{57}Fe-enriched Fe8 cluster, 95-% enriched ^{57}Fe foil (53.3 mg, 0.936 mmol) was carefully dissolved in 400 mL of a 3:1 (v/v) mixture of concentrated HCl and HNO_3 in a Kjeldahl flask. The solution was boiled and HCl added dropwise to keep the volume constant until evolution of brown NO_2 fumes ceased. To the cool concentrated solution excess thionyl chloride was added dropwise (CAUTION: vigorous evolution of SO_2 and HCl!) and the unreacted portion was distilled off under nitrogen. The black lustrous $FeCl_3$ residue was dissolved in methanol (4 mL) and treated with a solution of tacn (112 mg, 0.867 mmol) in methanol (1 mL) with stirring. Yellow [^{57}Fe(tacn)Cl_3] was collected by filtration, washed with ethanol (1.5 mL) and dried under vacuum (194 mg, 76-% yield). The solid was dissolved in 15 mL of water containing 1.5 mL of pyridine and the solution was stirred for 1 h before addition of NaBr (3.9 g). After additional 10′ stirring, any undissolved material was removed by centrifugation and the clear solution was left undisturbed in a dessiccator at reduced pressure (300–350 mmHg) over P_2O_5 for 2–3 weeks. Crystalline ^{57}Fe8 (126 mg, 67-% yield) was collected by filtration and dried by N_2 before measurement. The oriented-powder sample of Fe8 has been prepared by mixing the powdered material with epoxy (EpoTech 301) and letting it to set in a magnetic field of 7.2 T at room temperature

for 12 hours. The sample filling factor is about 20–30 % out of the volume of a cylinder with 5 mm diameter and 20 mm length. Orienting the powder sample results in a better signal to noise ratio and a narrow signal even in zero magnetic field due to the orientation of the grains with respect to the radio frequency magnetic field. In collaboration with Y. Furukawa we also succeeded in making a single crystal of ^{57}Fe8 [$\sim 3 \times 2 \times 1(\mathrm{mm}^3)$] which was used to investigate the effect of a field perpendicular to the magnetic easy axis and the relaxation measurements at low temperatures.

The ^{57}Fe NMR measurements were performed using TecMag Fourier Transform (FT) pulse spectrometer. A $(\pi/2 - \pi)$ pulse sequence (Hahn echo) has been used for the measurements with 1.5–3 μs $\pi/2$ pulse length and 8–12 μs separation between pulses depending on the spectrometer and experimental conditions. The NMR line was saturated with the comb pulse train with 10 pulses for the measurement of T_1 and the obtained recovery data with variable delays were fitted to the single exponential recovery law. The experiment has been carried out in the temperature range of 0.05—1.7 K by using both a closed cycle ^{3}He cryostat in Ames and a ^{3}He–^{4}He dilution refrigerator cryostat in Sapporo, Japan.

4.3 Experimental results

4.3.1 ^{57}Fe NMR spectrum

The zero-field ^{57}Fe NMR spectra in Fe8 at 1.5 K is shown in Fig. 4.2(b). A fine structure of the spectra was observed from the narrow NMR lines, namely, a quadruplet at higher frequency, a doublet at intermediate frequency, and a second doublet at lower frequency. Hereafter, we refer to each line as sp1—sp8 from low frequency to high frequency and in Fig. 4.1 the Fe^{3+} ion site associated with each NMR line is labeled accordingly. The experimental results in zero field are summarized in Tab. 4.1. When an external field is applied along the easy axis z of the oriented powder as shown in Figs. 4.2(a) and 4.4(a), the values of the resonance frequencies of the different lines shift as expected from the model for the internal structure of the Fe8 magnetic ground state [65]. For the transverse external field, the shift is very small at low fields while the linewidth of each line is much broader as shown in Fig. 4.2(c).

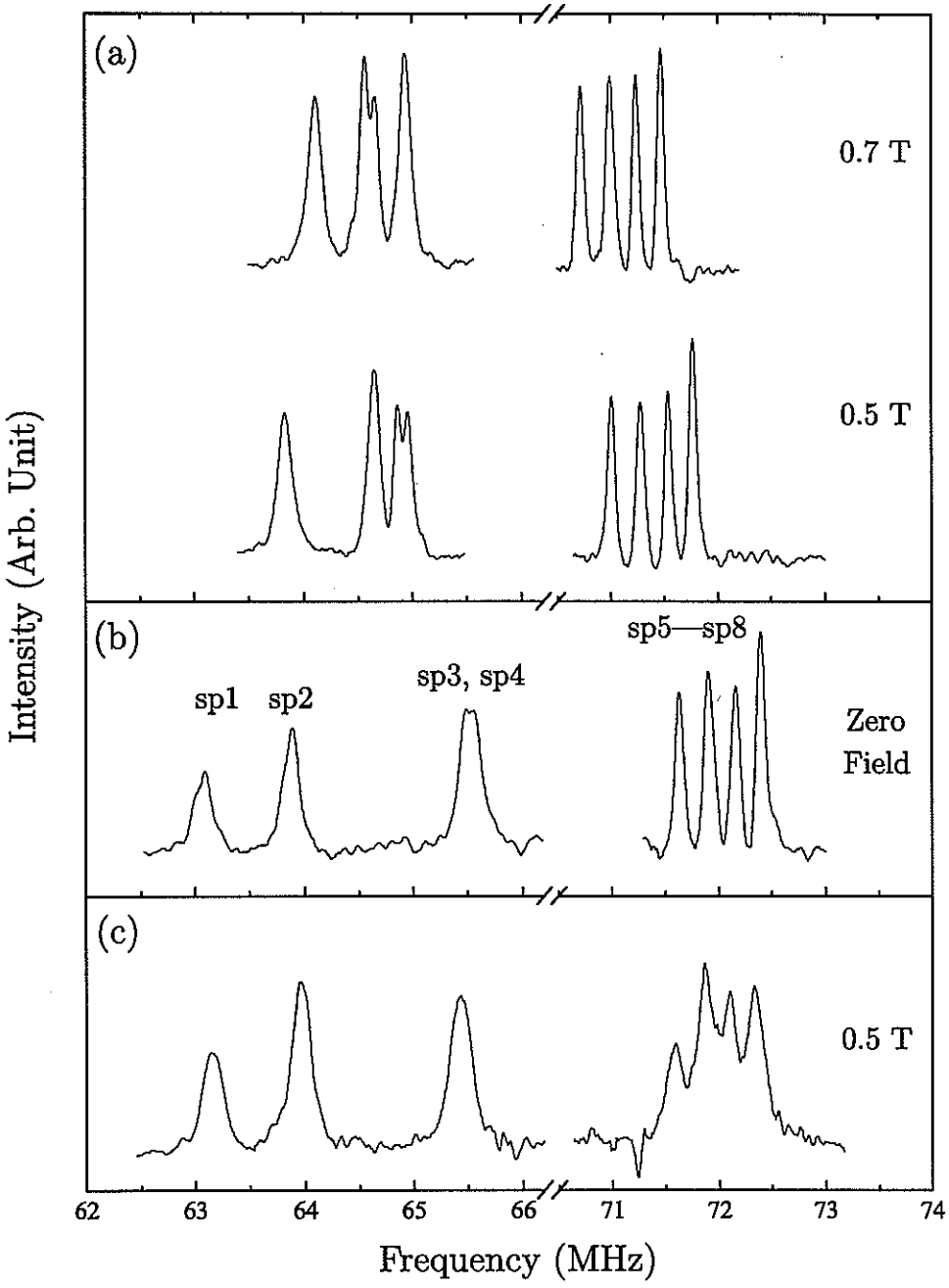

Figure 4.2 The ^{57}Fe NMR spectra and the field dependence in the case of: (a) $H \parallel z$ (b) zero field (c) $H \perp z$. Each line is labeled with sp1—sp8 (see Tab. 4.1).

nuclear site	Frequency (MHz)	H_{eff} (T)
sp1	63.09	45.86
sp2	63.89	46.44
sp3	65.46	47.58
sp4	65.55	47.65
sp5	71.63	52.07
sp6	71.90	52.26
sp7	72.16	52.45
sp8	72.39	52.62

Table 4.1 NMR resonance frequencies and corresponding effective local fields obtained at 1.5 K in zero field.

Fig. 4.4(b) shows the transverse field (along the medium y axis) dependence of the resonance frequencies measured in single crystal. The measurements of the temperature dependence of the resonance frequency $\nu(T)$ and of the ^{57}Fe nuclear spin-lattice relaxation rate reported in this chapter refer only to the line sp8 in the spectrum (see Fig. 4.2). This is sufficient for the purpose of studying the relative variations of the hyperfine fields and for the study of the spin dynamics. For confirmation $1/T_1$ has been measured at 1.5 K for each the eight NMR lines in the ^{57}Fe spectrum and the results were found to be within 10% error.

The temperature dependence of the resonance frequency, $\nu(T)$, in zero field in the temperature range 0.5—1.7 K is shown in Fig. 4.3. Above 1.7 K, the signal is not detectable due to the very short nuclear spin-spin relaxation time, T_2, as explained in details in next section. The nuclear Larmor frequency decreases gradually as the temperature increases and it drops rapidly above 1.5 K when the signal becomes undetectable. The behavior of the temperature dependence of $\nu(T)$ in Fig. 4.3 can be ascribed to the reduction of the average spin moment, $\langle S \rangle$, due to the thermal fluctuations of the magnetic sublevels. The limiting value of $\nu(T)$ as $T \to 0$ corresponds to the hyperfine field when the Fe8 molecules occupy the $m = \pm 10$ ground state.

4.3.2 Nuclear relaxation rates

The measurements of relaxation rates of ^{57}Fe were performed in the field range 0–1 T at 1.35 K for the field dependences, and in the temperature range 0.05–1.7 K at zero field for the

temperature dependence. When a longitudinal field is applied, a fast drop of $1/T_1$ appears at very low fields, while for higher fields $1/T_1$ decreases monotonically with increasing field at a much slower rate as shown in Fig. 4.5. On the other hand, as it is shown in Fig. 4.6, $1/T_1$ increases rapidly at low fields and more slowly at higher fields in an transverse field. In the field range 1—2.5 T, the weak ^{57}Fe NMR signal cannot be measured since it overlaps with the much stronger signal from ^{1}H NMR. Due to the strength of the proton signal and its considerable width, the field range of overlap is very wide. The longitudinal and transverse field dependences of $1/T_2$ are shown in Fig. 4.9. The temperature dependence of $1/T_1$ in zero field is shown in Fig. 4.8. $1/T_1$ shows fast decrease with decreasing temperature as it is expected due to the reduction of the thermal fluctuations of the hyperfine fields.

The temperature dependence of nuclear spin-spin relaxation rate ($1/T_2$) is very similar to one of $1/T_1$ although the magnitudes of the two relaxation rates differ by more than three orders of magnitude as shown in Fig. 4.10. When T is about 1.7 K the value of $1/T_2$ is about 10^5 s^{-1}, which is close to the limit of signal detectability in our spectrometer explaining the disappearance of the signal above 1.7 K. The measured T_2 is much shorter than the value expected for nuclear dipolar interaction in the intermediate temperature range 1–1.7 K. This circumstance together with the strong temperature dependence indicates that $1/T_2$ is driven by the slow dynamics of a strong hyperfine interaction above 1 K.

4.4 Hyperfine interactions and static magnetic properties

4.4.1 Hyperfine interactions

The hyperfine field at the Fe^{3+} nuclear sites arises mainly from core polarization of inner s electrons due to $3d$-electrons. For a free Fe^{3+} ion, the theoretical value of core polarization field χ per unpaired d-electron is -3.00 a.u. (1 a.u. $= 4.21$ T [120]). Then we get $H_{\text{core}}(Fe^{3+}) = 5 \times \chi = -63.15$ T. Experimentally, the maximum hyperfine field found for Fe^{3+} in a solid had been reported to be 62.2 T in the antiferromagnetic ionic compound FeF_3 using Mössbauer effect [121]. Thus it is reasonable to assume the value of about 62 T for the core polarization hyperfine interaction by the half-filled $3d$ shell in a pure ionic configuration. Since the measured

effective fields are smaller than the theoretical value (see Table. 4.1), one deduces that there is strong reduction of the local hyperfine field at the nuclear sites. The reduction can arise from positive contributions to the total hyperfine field and/or to a delocalization of the $3d$ electron due to covalent bonding. The dipolar hyperfine field is normally zero in orbital singlet state like $3d^5$ configuration due to quenching of the orbital angular momentum [122]. But if Fe^{3+} ions in Fe8 do not have pure $3d^5$ configuration, the dipolar term could be non-negligible. One can make a qualitative estimate the dipolar contribution from quadrupole splitting, Δ_Q, in Mössbauer spectroscopy using the fact that Δ_Q arises from an aspherical distribution of electrons in the valence orbitals and an aspherical charge distribution in the ligand sphere and/or lattice surroundings with symmetry lower than cubic [123]. The small values of Δ_Q 0.13, -0.11 and 0.057 mm/s, respectively, in Ref. [124] leads to the conclusion that the dipolar term would be too small to contribute to the main reduction of the local hyperfine fields but could contribute to the fine splitting of the lines in each Fe group. Therefore, the reduction of the local fields is attributed to the covalent bonds of Fe^{3+} ions with neighboring ligands. Since the covalency can result in both delocalization of $3d$-electrons and $4s$ hybridization, one can describe the configuration of the magnetic electron in the covalent bond as $3d^{5-x}4s^y$. From the comparison of isomer shift values in Mössbauer spectroscopy [124] to the relation between isomer shift and partially occupied $4s$ orbitals by Walker *et al.* [125] we estimated $y \leq 0.05$. If we consider only the delocalization of $3d$ electrons, we get $x = 0.75$ for sp1 and sp2, 1.16 sp3 and sp4, and 1.3 for sp5–sp8 from the comparison of the experimental hyperfine field and the theoretical value of 62 T. The above values for x should be viewed as upper limits since part of the reduction of the negative core polarization field can arise from the positive contact hyperfine field due to the $4s$ hybridization y. In fact since the hyperfine field due to a $4s$ electron in a neutral Fe atom is estimated to be 380 T [126], even a small admixture y of $4s$ character in the wave function can generate a sizable contact hyperfine contribution to the internal field, resulting in a local internal field in agreement with experiments even for a Fe^{3+} local moment close to the localized $3d^5$ configuration. For example, if we assume tentatively spin moments of $5\mu_B$ for all Fe site, the value of y is estimated to be 0.01,0.009, and 0.006 for

the lateral, central, and apical sites, respectively.

It is noted that even by taking the upper limit values for x, our estimation for the $3d$ delocalization are still smaller than the values calculated with density functional theory (DFT) calculations [127] or obtained from polarized neutron diffraction (PND) measurements [62]. For example, in DFT studies, the authors calculated local spin moments in each Fe group to be $3.9\mu_B$ for lateral sites, $-3.6\mu_B$ for central sites and $3.8\mu_B$ for apical sites to be compared with $5\mu_B$ for a localized $3d$ configuration. The magnitude and the direction of the spin moment are in qualitative agreement with our NMR results. However, our analysis in NMR spectrum shows that the spin moment of central sites should be smaller than that of apical sites again assuming the same hyperfine coupling constant. Furthermore, the difference of the magnitude of the local moment between lateral sites and central sites as inferred from the position of the resonance lines in the spectrum (see Fig. 4.2 and Table. 4.1) is much larger than the reported value. Also the large differences of the spin moments within the same group reported in PND results [62] are not consistent with NMR results.

The detection of eight different lines leads to a conclusion that there are eight inequivalent Fe^{3+} ions. The splittings among NMR lines in each Fe group are less than 300 kHz (i.e., $\leq$0.2 T). The fine structure of the NMR spectrum which gives rise to the splitting for each of the three main groups of Fe ions suggests that environments for the Fe ions are slightly different for the different ions within the same group. Since the spin density and/or the character of the wave function must depend on the bond angles and the distances in the superexchange bridges, the fine structure of the NMR spectrum could be attributed to small differences in the covalent bonds for the different ions within the same group.

4.4.2 Reduction of the hyperfine field due to thermal fluctuations

As seen in the previous subsection the dominant contribution to the hyperfine field originates from contact interaction via a core polarization mechanism. Therefore we can assume that the resonance frequency is simply proportional to the average local spin moment in the Fe^{3+} ion, i.e. $\nu = A\langle s \rangle$. The reduction of the resonance frequency can arise either from a

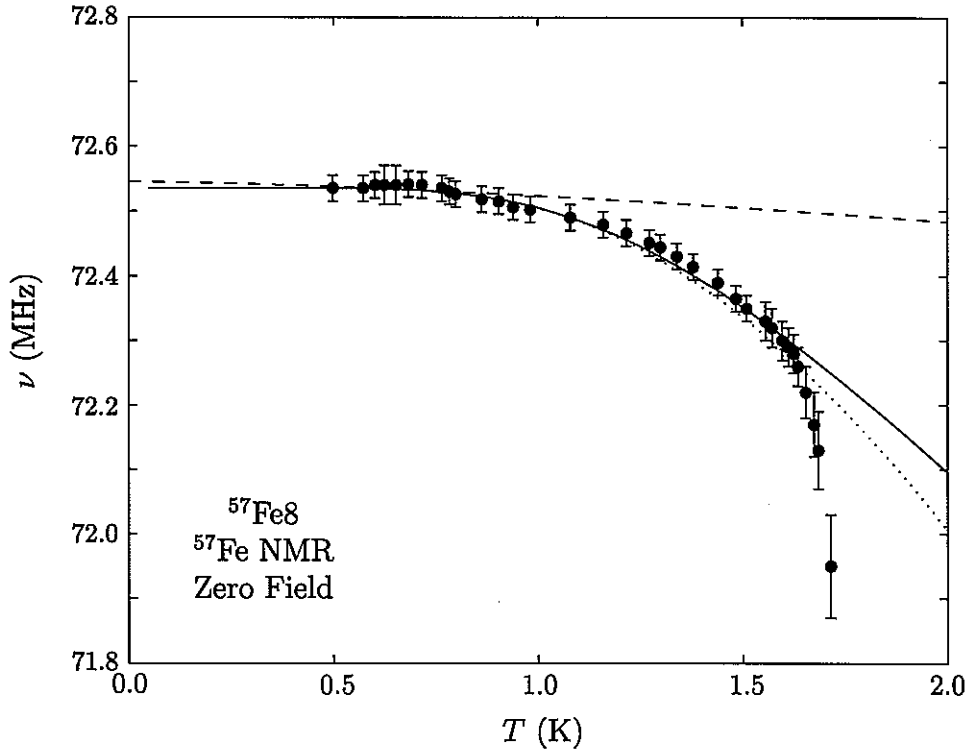

Figure 4.3 Temperature dependence of resonance frequency of sp8 NMR line. Theoretical curves were obtained from Eq. (4.2) considering the two lowest levels (solid line) and all levels up to $m = \pm 5$ (dotted line). Bloch $T^{3/2}$ law (dashed line) is drawn for the comparison.

decrease with temperature of the hyperfine coupling constant A or from a reduction of the average spin moment due to thermal fluctuations. Since the temperature dependence of A is negligible at low temperature the reduction of the hyperfine field is a direct measure of the reduction of the local magnetization. We assume that the average local spin moment $\langle s \rangle$ is proportional to the average total moment $\langle S \rangle$ of the molecule. Thus, we express $\nu(T)$ as a statistical average of the total magnetic moment of the molecule on the basis that the average total moment is reduced by thermal excitations from the magnetic ground state $m = \pm 10$ to excited states:

$$\begin{aligned} \frac{\nu(T)}{\nu(0)} &= \frac{\langle S \rangle}{\langle S \rangle_{T=0}} \\ &= \frac{1}{\langle S \rangle_{T=0}} \left(\frac{\sum_m |m| \exp\left(-E_m/T\right)}{Z} \right), \end{aligned} \tag{4.2}$$

where E_m is the energy of mth sublevel of $S = 10$ and Z partition function. We assume that the magnitude of spin moment of a mth state corresponds to the value projected into quantization axis e.g., 0.9 for $m = \pm 9$ state. Although this approach is based on a semiclassical picture of the spin, it provides a very successful theoretical curve. The result is shown in Fig. 4.3. The theoretical curve, however, depends strongly on the choice of D and E values in the Hamiltonian, Eq. (4.1). So far the values of D -0.295, -0.276 and -0.293 K, and E 0.055, 0.035 and 0.047 K have been reported by EPR [64], magnetization measurements [70], and neutron spectroscopy [66], respectively. In our calculation, the best agreement is found for the choice of the parameters reported in Ref. [66] ($D = -0.293$ K and $E = 0.047$ K). In this thesis, these values of D and E are used in all theoretical calculations.

The three curves in Fig. 4.3 were obtained considering (i) Bloch $T^{3/2}$ law [128] (dashed line), (ii) Eq. (4.2) with only two lowest sublevels ($m = \pm 10$ and $m = \pm 9$) (solid line), (iii) Eq. (4.2) with all levels up to $m = \pm 5$ (dotted line).[1] As expected, the Bloch $T^{3/2}$ law based on spin wave theory does not apply to nanosize molecular magnets.[2] The agreement with the cases (ii) and (iii) is quite good with the exception of the last higher temperature three points. Those points are affected by a large error because the signal becomes very weak due to the shortening of T_2 (see next section). Thus it cannot be established for sure if the resonance frequency starts to drop rapidly at $T > 1.6$ K. The drop could indeed take place if higher order states are included for higher temperature.

4.4.3 Determination of the local spin arrangement in the ground state

As we can see in Figs. 4.2(a) and 4.4(a), with increasing the parallel field, the resonance lines sp1 and sp2 shift to a higher frequency, while sp3–sp8 shift to a lower frequency. The slope of the parallel field dependence of the resonance frequency is $\sim |1.37|$ MHz/T for each peak, which coincides with the gyromagnetic ratio γ_n of the ^{57}Fe nucleus. As the resonance

[1] As discussed in Chapter 3, the levels of $|m| < 5$ are strongly admixed, and thus the quantum number m loses any physical significance [67]. Conversely, this fact implies that the height of the energy barrier is not well defined.

[2] A theoretical approach to apply the *modified* spin wave theory has been attempted in Ref. [129]. However, the application of the theory to Fe8 will be difficult due to complicated internal magnetic structure of Fe8 cluster.

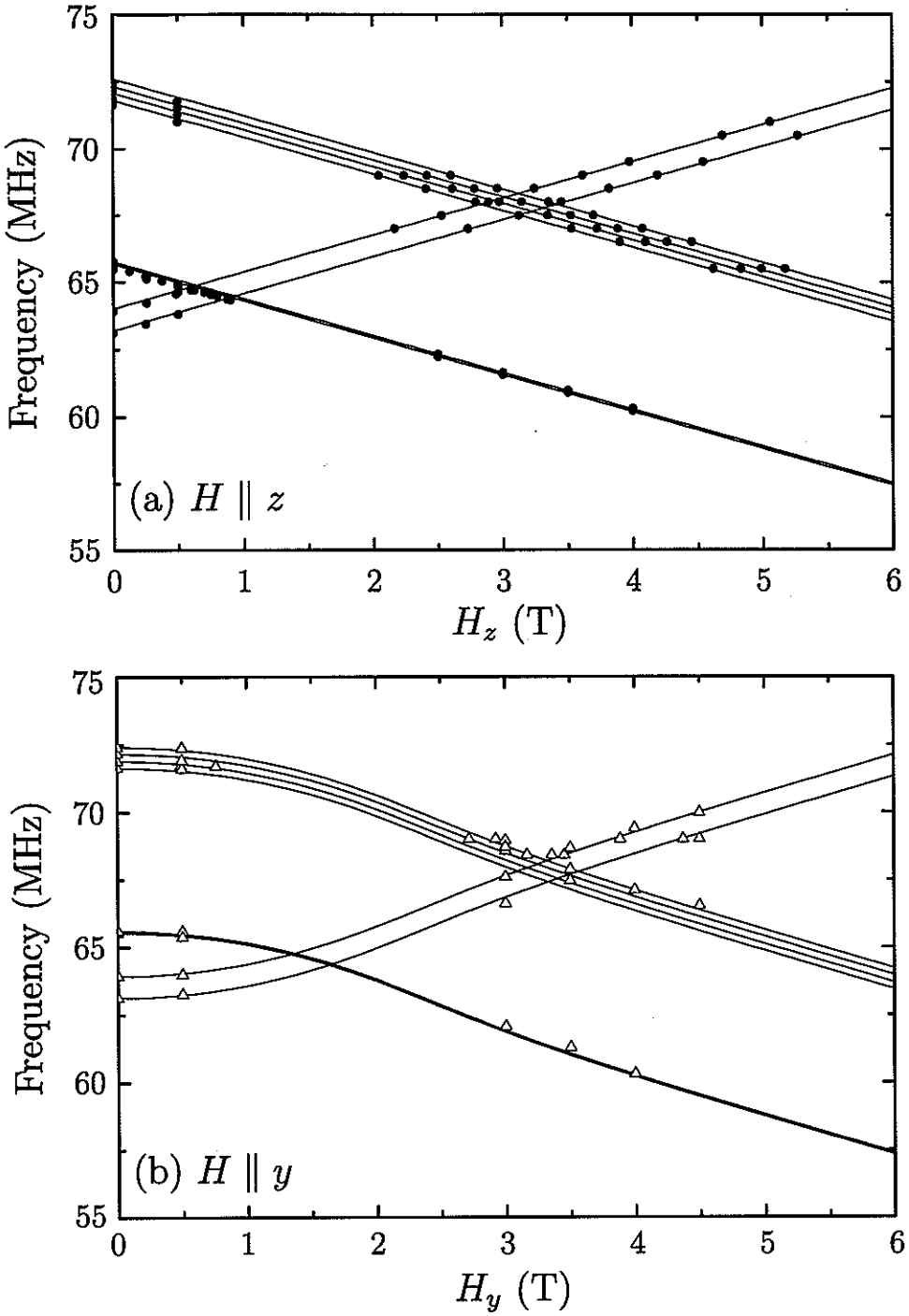

Figure 4.4 Field dependence of the resonance frequency for each peak measured at $T = 1.5$ K. (a) $H \parallel z$ (easy axis): the solid lines are determined by the gyromagnetic ratio γ_n of the ^{57}Fe nucleus (b) $H \parallel y$ (medium axis): the solid curves represent the calculated results according to Eq. (4.3).

frequency is proportional to the vector sum of the internal field ($\mathbf{H}_{\text{int}}$) and external field ($\mathbf{H}_{\text{ext}}$), $\nu = \gamma_n|\mathbf{H}_{\text{int}} + \mathbf{H}_{\text{ext}}|$, this result indicates that the direction of the internal field at the Fe sites for sp3 and sp4 is opposite to that for the other peaks. Since, as discussed in previous section, the internal field at the nuclear site is dominated by core polarization, H_{int} is negative and the direction of the internal field at nuclear sites is opposite to that of the Fe spin moment. Therefore we conclude that the spin direction of Fe ions for sp1 and sp2 is antiparallel to the external field, while that of Fe ions for sp3–sp8 is parallel to the external field.

The observed spectra can be classified into three groups: the first is sp1 and sp2, the second is sp3 and sp4, and the third is sp5–sp8. It is reasonable to assign the third group with four peaks (sp5–sp8) to the four Fe^{3+} ions located at the lateral sites with nearly the same environment in the cluster. As for the site assignment of the other peaks, one notes that in the coupling scheme depicted in Fig. 3.1(a) the exchange constant $J_1 = -52.5$ K is larger than $J_4 = -22.5$ K. As a consequence, the spin direction of Fe ions at the central sites must be opposite to that of Fe ions at the lateral sites and be parallel to that at the apical sites. Therefore, the first group of two lines sp1 and sp2 should be associated with the two Fe ions with spin direction antiparallel to that of the lateral sites. By exclusion, the second group sp3 and sp4 is ascribed to the two Fe ions at the apical sites. Therefore we conclude that the spin direction of Fe ions for the central sites is antiparallel to the external field, while that of Fe ions for the apical and lateral sites is parallel to the external fields. This is a direct confirmation of the spin structure for inner magnetic structure of the cluster as shown in Fig. 4.1.

In order to elucidate the changes of the local Fe^{3+} spin configuration in the superparamagnetic state under application of a transverse field along the medium (y) axis which is perpendicular to the easy axis, we have measured ^{57}Fe NMR spectrum in transverse field using the single crystal. Figs. 4.2(c) and 4.4(b) show the magnetic field dependence of the resonance frequencies for each peak. As described above, the resonance frequency is proportional to the effective internal field at the nuclear site, which is the vector sum of H_{int} due to Fe spin moments and H_{ext} due to the external field: $|\mathbf{H}_{\text{eff}}| = |\mathbf{H}_{\text{int}} + \mathbf{H}_{\text{ext}}|$. The opposite field dependence observed in Fig. 4.4(b) of $|H_{\text{eff}}|$ for the central sites with respect to the lateral and apical sites

indicates that the projection along the external field of the spin moments of Fe^{3+} ions at the central sites is of opposite sign with respect to that of Fe^{3+} ions at the apical and lateral sites. This leads to the conclusion that the individual spin moments of all Fe ions do not cant independently along the direction of the transverse field but rotate rigidly maintaining the same relative spin configuration.

In order to analyze the experimental results quantitatively, we have calculated the transverse field dependence of $|H_{\rm eff}|$, following a method used for the analysis of transverse field dependence of ^{55}Mn NMR spectrum in Mn12 cluster [59]. As pointed out in Ref. [59], in the presence of a transverse field, the direction of the internal local field, $|\mathbf{H}_{\rm int}|$, is canted from the easy axis [1, 59] by $\theta = \sin^{-1}(M_\perp/M_s)$, where $M_\perp$ is the transverse magnetization and M_s is the saturation magnetization of the $S = 10$ ground state. The length of the effective magnetic field is given by

$$|\mathbf{H}_{\rm eff}| = |\mathbf{H}_{\rm int} + \mathbf{H}_{\rm ext}| = \sqrt{H_{\rm int}^2 + H_{\rm ext}^2 + 2H_{\rm int}H_{\rm ext}\sin\theta}, \tag{4.3}$$

where the sign of $H_{\rm int}$ is taken to be positive for Fe ions at the central sites and negative for Fe ions for the apical and lateral sites, respectively. The agreement of the calculated field dependence of the resonance frequencies for each site with the experimental results shown in Fig. 4.4(b) is excellent. We thus confirmed from the microscopic point of view that the local ferrimagnetic spin configuration of the Fe8 cluster in its $S = 10$ ground state is not modified by the transverse magnetic field up to fields of at least 5 T.

4.5 Spin dynamics

4.5.1 Nuclear relaxation due to thermal fluctuations

In the case of a system of nuclear spins acted upon by strong randomly fluctuating local fields arising from the hyperfine interaction of the nuclei with the electronic spins, $1/T_1$ and $1/T_2$ can be simply expressed in a semi-classical approach in terms of the correlation function of a randomly time dependent perturbation term $\mathcal{H}_1$ in the Hamiltonian representing the

nuclear-electron coupled system [46, 49],

$$\frac{1}{T_1} = \mathcal{J}_\perp(\omega_L) = \frac{2}{\hbar^2}\int_{-\infty}^{+\infty}\langle \mathcal{H}_1^\perp(t)\mathcal{H}_1^\perp(0)\rangle e^{-i\omega_L t}dt, \tag{4.4}$$

$$\begin{aligned}\frac{1}{T_2} &= \mathcal{J}_z(0) + \frac{1}{2T_1} \\ &= \frac{2}{\hbar^2}\int_{-\infty}^{+\infty}\langle \mathcal{H}_1^z(t)\mathcal{H}_1^z(0)\rangle dt + \frac{1}{2T_1},\end{aligned} \tag{4.5}$$

where ω_L is the nuclear Larmor frequency and $\mathcal{J}_\alpha(\omega)$ are spectral densities of longitudinal ($\alpha = z$) and transverse ($\alpha = \perp$) components of the fluctuating local field. It is noted that Eqs. (4.4) and (4.5) are valid in the weak collision limit in which one assumes that the correlation time is much shorter than the relaxation time so that many elementary processes of fluctuations are required to induce a transition in the stationary nuclear Zeeman energy levels. In Eq. (4.5), we neglect the contribution due to rigid lattice nuclear dipolar interaction and we assume the fast motion regime i.e., the fluctuations of the local hyperfine field are fast with respect to the interaction frequency itself [46]. Since each ^{57}Fe nucleus is dominated by the contact hyperfine interaction with the ionic spin of the Fe^{3+} ion to which the nucleus belongs, one has

$$\begin{aligned}\mathcal{H}_1 &= A\mathbf{I}\cdot\mathbf{S} = A\left(I_z S_z + 1/2(I_+ S_+ + I_- S_-)\right) \\ &= \gamma_N\hbar\left(I_z H_z + I_\perp H_\perp\right),\end{aligned} \tag{4.6}$$

where we have introduced the local effective hyperfine field H_α ($\alpha = z, \perp$) and γ_N is the nuclear gyromagnetic ratio. Under the assumption of an exponential decay of the correlation function $G(t)$, one has from Eqs. (4.4)–(4.6)

$$\frac{1}{T_1} = \gamma_N^2\langle\Delta H_\perp^2\rangle\frac{\tau_c}{1+\omega_L^2\tau_c^2}, \tag{4.7}$$

$$\frac{1}{T_2} = \gamma_N^2\langle\Delta H_z^2\rangle\tau_c, \tag{4.8}$$

where $\langle\Delta H_\perp^2\rangle = A^2\langle S_\perp^2\rangle$ and $\langle\Delta H_z^2\rangle = A^2\langle S_z^2\rangle$ and we neglected the second term in Eq. (4.5) since $T_2 \ll T_1$.

In the low temperature region, the fluctuations of the local hyperfine field are due to the transitions among the low lying m magnetic states. For temperatures below 2 K where

our measurements were performed, one can make the assumption that the fluctuating field is due to random jumps between two values of the hyperfine field [46, 130] correspondingly to the $m = \pm 10$ and $m = \pm 9$ states as shown by Goto *et al.* in Mn12 [131]. In this model one can assume a two-state pulse fluctuation with the magnitude h_α of the random field jumps and lifetimes τ_0 and τ_1, respectively for the two states. The average fluctuating field between the two field values $H_1 = \tau_0 h_\alpha/(\tau_0 + \tau_1)$ and $H_2 = -\tau_1 h_\alpha/(\tau_0 + \tau_1)$ can be written as $\langle \Delta H_\alpha(t) \rangle = \tau_1 h_\alpha/(\tau_0 + \tau_1)$.

Utilizing the detailed balance condition for the transition probabilities and some algebra (see Appendix B), one can derive $\langle \Delta H_\alpha^2 \rangle$ and τ_c to be used in Eqs. (4.7) and (4.8),

$$\langle \Delta H_\alpha^2 \rangle = \frac{\tau_0 \tau_1}{(\tau_0 + \tau_1)^2} h_\alpha^2 \approx \frac{\tau_1}{\tau_0} h_\alpha^2, \tag{4.9}$$

$$\tau_c = \frac{\tau_0 \tau_1}{\tau_0 + \tau_1} \approx \tau_1, \tag{4.10}$$

where we used the fact that $\tau_0 = \tau_{-10} \gg \tau_1 = \tau_{-9}$. The lifetimes $\tau_0 = \tau_{-10}$ and $\tau_1 = \tau_{-9}$ can be obtained from the spin-phonon transition probabilities [90],

$$\frac{1}{\tau_m} = W_{m \to m+1} + W_{m \to m-1}, \tag{4.11}$$

with

$$W_{m \to m \pm 1} = C s_{\pm 1} \frac{(E_{m \pm 1} - E_m)^3}{\exp[(E_{m \pm 1} - E_m)/T] - 1},$$

where $s_{\pm 1} = (s \mp m)(s \pm m + 1)(2m \pm 1)^2$ and the spin-phonon coupling parameter will be assumed to be the same as derived from proton relaxation in Fe8 [57].

Finally, the forms of $1/T_1$ and $1/T_2$ are simplified leaving only one fitting parameter,

$$\left(\frac{1}{T_1}\right)_{\text{sp}} = \frac{(\gamma_N h_\perp)^2}{\tau_0} \frac{\tau_1^2}{1 + \omega_L^2 \tau_1^2}, \tag{4.12}$$

$$\left(\frac{1}{T_2}\right)_{\text{sp}} = (\gamma_N h_z)^2 \frac{\tau_1^2}{\tau_0}. \tag{4.13}$$

In this simple model both $1/T_1$ and $1/T_2$ are determined by lifetimes of two lowest mth magnetic levels and by the amplitude of fluctuating field, h_α.

A more general formula for $1/T_2$ had been obtained by Kohmoto *et al.* [130] using a non-linear theory of phase relaxation in the pulse fluctuating field instead of using the correlation

function. We just present the result of the theory without derivation:

$$\frac{1}{T_2} = \frac{1}{\tau_0}\frac{(\gamma_N h_z \tau_1)^2}{1+(\gamma_N h_z \tau_1)^2}. \tag{4.14}$$

In the regime of $(\gamma_N h_z \tau_1)^2 \ll 1$ (fast motion i.e., weak collision limit) the above formula becomes equivalent to Eq. (4.13). While, in the regime of $(\gamma_N h_z \tau_1)^2 \gg 1$ (slow motion i.e., strong collision limit), it leads to:

$$\frac{1}{T_2} = \frac{1}{\tau_0}. \tag{4.15}$$

4.5.2 Nuclear relaxation due to quantum tunneling

The relation between the sublevel broadening δ, which reflects the coupling to the environment such as dipolar and static hyperfine field, and tunnel splitting Δ is very important for the observation of the quantum tunneling of magnetization (QTM) phenomenon. If $\Delta \gg \delta$, a coherent tunneling may occur. If Δ is comparable to δ, the coherent tunneling is suppressed by the decoherence caused by δ but an incoherent tunneling takes place. For the condition of $\Delta \ll \delta$, only phonon-assisted tunneling is possible. For Fe8 cluster, we expect that, if it is observable, the phonon-assisted tunneling will be responsible for the additional nuclear relaxation rates at low fields because $\Delta \sim 10^{-7}$ K from the experiment [30] is much smaller than the value $\delta \sim 10^{-2}$ K, which is inferred from the typical intermolecular dipolar fields [63].

In the previous investigation of the tunneling effect on nuclear spin-lattice relaxation in Fe8 the proton NMR was used as a probe [43]. Since the hyperfine field change at the proton site as a result of a tunneling transition is small compared to the Zeeman energy, a perturbative weak collision approach is still applicable. Thus the proton $1/T_1$ was explained successfully using the expression:

$$\left(\frac{1}{T_1}\right)_T \text{ or } \left(\frac{1}{T_2}\right)_T = A_\alpha^2 \frac{\Gamma}{\Gamma^2+\omega_L^2}, \tag{4.16}$$

where A_α ($\alpha = z$ or $\perp$) is the average fluctuating hyperfine field due to the magnetization reversal when a tunneling transition occurs, ω_L is the nuclear Larmor frequency, and Γ is the phonon assisted tunneling probability [88, 90, 93],

$$\Gamma = \sum_m \frac{\Delta_m^2 W_m}{W_m^2 + (\xi + \Delta E_{m,-m})^2} \exp(-E_m/T), \tag{4.17}$$

where Δ_m is the tunnel splitting for $S_z = m$, W_m a level broadening parameter, ξ is the longitudinal component of the bias field, E_m the energy of level m, and $\Delta E_{m,-m}$ the energy difference between $\pm m$ levels due to an external longitudinal field. Here we use the concept of "effective" tunneling probability between all degenerate sublevels instead of using separate Γ_m, in which case Eq. (4.16) should be rewritten as the summation of different contributions for each m, as was adopted in Ref. [43]. On the other hand, in the case of ^{57}Fe NMR in zero external field and in low fields the change of local hyperfine field cannot be treated as a perturbation. In fact a tunneling transition between pairwise degenerate states $\pm m$ results in the rapid inversion of the local field which is the quantization field for the ^{57}Fe nuclei. This situation is analogous to the quadrupole relaxation generated by a sudden change of the quantization axis as a result of a molecular reorientation [132]. In this case a sudden approximation strong collision approach should be utilized. When the jumps between equilibrium positions accompanied by changes in the Hamiltonian are fast as for a tunneling transition one finds approximately[3]

$$\left(\frac{1}{T_1}\right)_T \text{ or } \left(\frac{1}{T_2}\right)_T = c(2\Gamma), \tag{4.18}$$

where c is a constant of the order of one, i.e., the nuclear relaxation transition probability is the same as the tunneling probability (see Appendix C). Note that for the case of $1/T_2$ Eq. (4.18) is indeed the same as Eq. (4.15) in the slow motion limit. Also the strong collision result [Eq. (4.18)] can be formally derived from Eq. (4.16) in the limit of slow motion ($\Gamma \ll \omega_L$) when $A \approx \omega_L$.

4.6 Analysis of the experimental results for nuclear relaxation rates

4.6.1 Spin-lattice relaxation rate $(1/T_1)$

4.6.1.1 Longitudinal field dependence

The longitudinal field dependence of $1/T_1$ is shown in Fig. 4.5. The relevant feature here is the fast decrease of $1/T_1$ up to $H_z = 0.1$ T. If one fits the data with Eq. (4.12) in terms of

[3] A simple case of strong collision due to a rapid inversion of a magnetic field has been illustrated by Abragam [45] pp. 477–479.

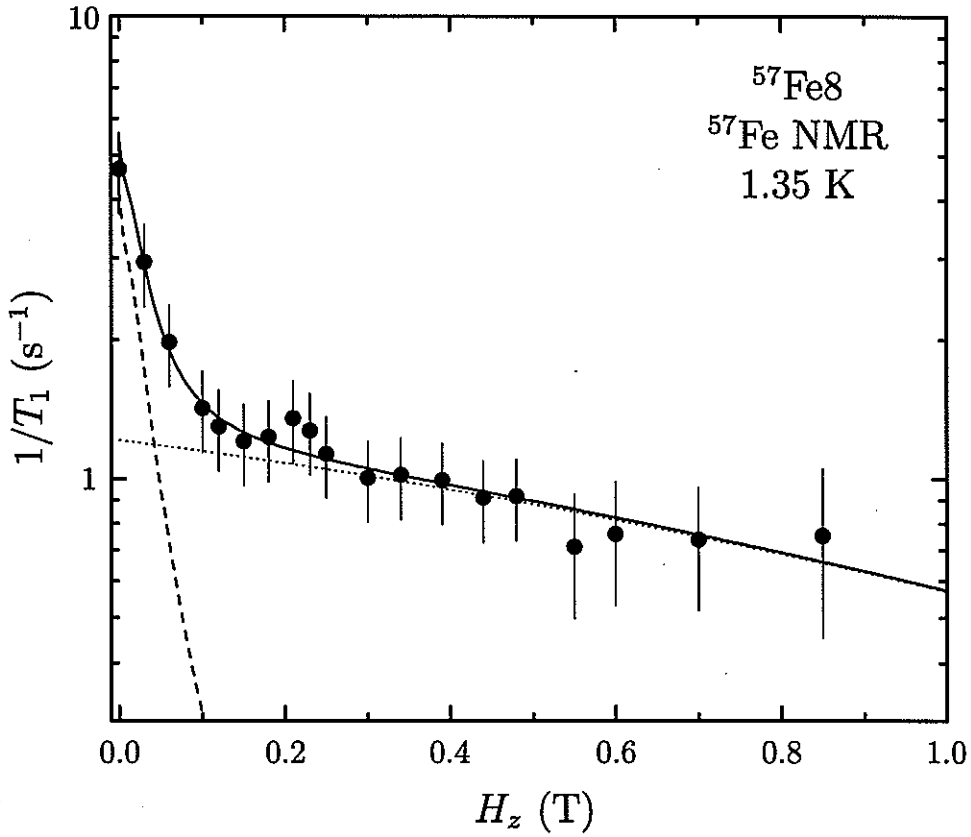

Figure 4.5 Longitudinal field dependence of $1/T_1$. Dotted line is from Eq. (4.12), dashed line from Eq. (4.18) with the appropriate parameters (see text), and solid line is the sum of the two contributions. Small enhancement at 0.22 T is attributed to the transitions of the magnetization between $m = +10 - n$ and $m = -9 + n$ where $n = 0, 1, 2 \cdots$.

the thermal fluctuations of the magnetization one obtains a good fit only at fields higher than 0.2 T by choosing $\gamma_N h_\perp = 2.73 \times 10^5$ (rad Hz) in Eq. (4.12) (see Fig. 4.5). The additional contribution to $1/T_1$ at $H_z \to 0$ is strongly suggestive of a direct contribution due to phonon-assisted tunneling. In fact such a contribution, described by Eq. (4.18), would be effective only at $H_z = 0$ and at the first level crossing ($H_z = 0.22$ T) where a small maximum can be observed in Fig. 4.5. Outside these field values the tunneling probability in Eq. (4.17) drops off rapidly due to the breaking of the pairwise degeneracy of the m states [see term $\Delta E_{m,-m}$ in Eq. (4.17)].

Unfortunately, it appears that the calculated tunnel splitting values obtained by the di-

agonalization of Eq. (4.1) are too small to give sizeable contribution to the relaxation rates at zero and low fields. However, the fact that the experimental value [30] $\Delta_{10} \sim 10^{-7}$ K is three orders larger than the calculated value implies that the higher order Hamiltonian terms play an important role in determining Δ_m. Thus we recalculated Δ_m adding the fourth order Hamiltonian to Eq. (4.1),

$$\begin{aligned}\mathcal{H}' = & D_2 S_z^4 + E_2[S_z^2(S_x^2 - S_y^2) + (S_x^2 - S_y^2)S_z^2] \\ & + C(S_+^4 + S_-^4),\end{aligned} \tag{4.19}$$

with the parameters, $D_2 = 3.54 \times 10^{-5}$ K, $E_2 = 2.03 \times 10^{-7}$ K, and $C = 4.3 \times 10^{-6}$ K from Ref. [66]. We find that the modified Hamiltonian gives rise to still small Δ_m values. Since the fourth order transverse term, $C(S_+^4 + S_-^4)$, is most important with regard to the tunnel splitting we adjusted C value in order to reproduce a correct order of magnitude of the measured ground state tunnel splitting $\Delta_{10} \sim 10^{-7}$ K [30, 81]. Choosing $C = -2.7 \times 10^{-5}$, which is a factor of 6 larger, with the opposite sign, than the value reported in Ref. [66], one obtains $\Delta_{10} = 4.5 \times 10^{-8}$, $\Delta_9 = 3.6 \times 10^{-6}$, and $\Delta_8 = 1.3 \times 10^{-4}$ K. It should be pointed out that the exact values of Δ_m with lower m could be very different because the other higher order terms are strongly correlated with each other, and so affect relative values between Δ_m as well as absolute values of Δ_m. Moreover, this fact is not relevant in our analysis as long as Δ_m values are within a reasonable order of magnitude because the most important physical quantity in our analysis is the effective tunneling probability Γ, which could always be reproduced by small adjustment of the broadening parameter W_m. It is noted that the large tunneling splitting required to explain our data in ^{57}Fe enriched Fe8 is consistent with the observation that the isotopic substitution increases the tunneling rate [82].

With the values of Δ_m calculated above inserted in Eq. (4.17) and Eq. (4.18), one explains well the extra contribution found in the H_z dependence of $1/T_1$ with the choice of the parameters, $W_{10} = 2.5 \times 10^8$, $W_9 = 7 \times 10^9$, $W_8 = 9 \times 10^{10}$, $\xi = 4.4 \times 10^9$ (rad Hz), and $c = 1$ (see Fig. 4.5). Note that the parameter ξ, which was fixed in order to restrict the number of free parameters, corresponds to about 0.05 T (~ 0.033 K), which is a correct order of magnitude for the intermolecular dipolar fields [77].

The T and H dependences of Γ calculated from the parameters given above are shown in Fig. 4.11. The remarkable finding is that in this temperature range the low field value of the ^{57}Fe relaxation rate $1/T_1$ gives directly the phonon-assisted tunneling rate as a result of the strong collision mechanism.

Another interesting feature in Fig. 4.5 is the small enhancement of $1/T_1$ found at about 0.22 T. The enhancement could be attributed to QTM between $m = +10-n$ and $m = -9+n$ states, where $n = 0, 1, 2\cdots$, with the knowledge of the fact that level crossings are expected to occur at $0.22n'$ T, where n' is an integer. The enhancement of $1/T_1$ at 0.22 T is consistent with the stepped hysteresis found in magnetization measurements [30] and the similar enhancement effect in ac-susceptibility measurement [116].

4.6.1.2 Transverse field dependence

The transverse field dependence of $1/T_1$ is shown in Fig. 4.6. Contrary to the case of the H_z dependence, $1/T_1$ increases rapidly with increasing $H_\perp$. The spin-phonon contribution calculated by Eq. (4.12) appears to be very long compared to the experimental data, and weakly field dependent (dashed line in Fig. 4.6). Thus we may think that QTM is responsible for the fast increase of $1/T_1$ because Δ_m is expected to increase exponentially in an applied transverse field as calculated from the model Hamiltonian. However, the tunneling contribution given by Eq. (4.16) with the same parameters used in the H_z dependence of $1/T_1$ increases too fast leading to the wrong fit of the data above 0.2 T (dashed line in Fig. 4.6).

One may ask why the tunneling contribution predicted by the theory cannot be detected in the experiments. The answer could be given by the consideration of the fact that our sample is aligned powder so that it would be difficult to estimate the transverse field dependence of Δ_m due to the distribution of molecules in xy-plane, and/or a small misalignment of the sample may greatly reduce the tunneling contribution. We argue that the tunneling effect on the relaxation rate $1/T_1$ can be quenched by the presence of a small longitudinal component of the field. In fact, it was found, by proton NMR in Fe8 single crystal, that the tilting of 5° between the applied field and the xy plane eliminates the tunneling effects [43]. In our measurements,

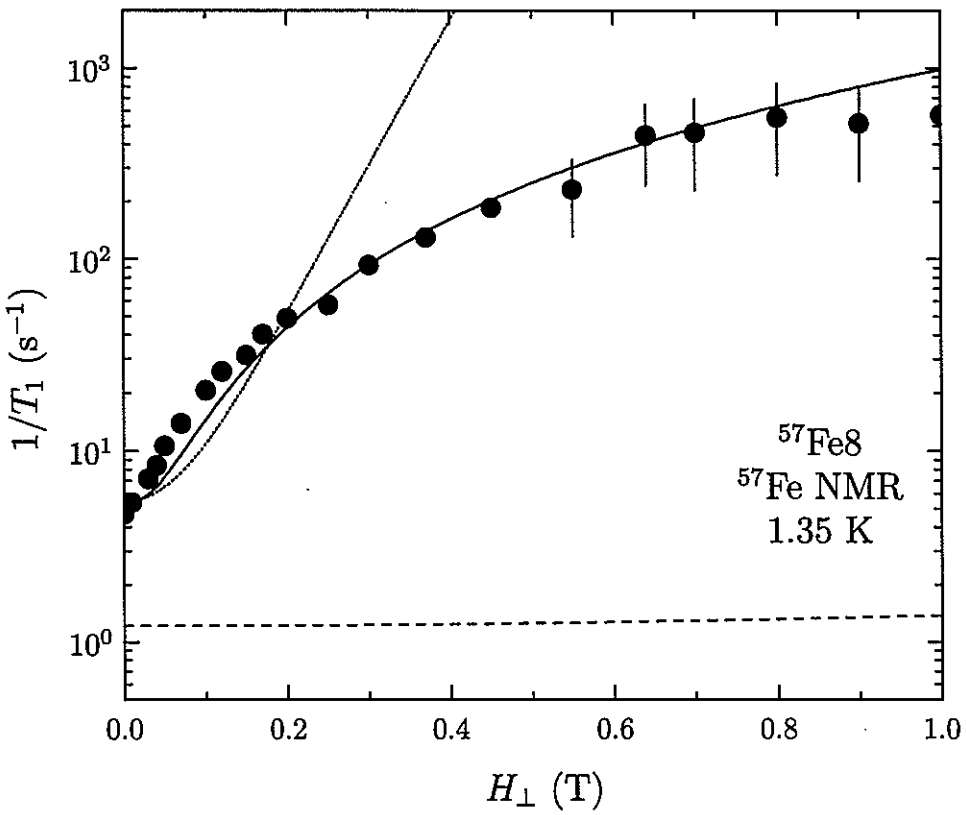

Figure 4.6 Transverse field dependence of $1/T_1$. Dashed line represents spin-phonon contribution only [Eq. (4.12)], dotted line is the result of the calculation of the tunneling contribution without misalignment of the sample, and solid line is from the canting effect together with weak contributions from the thermal and the tunneling fluctuations. [Eq. (4.20)].

the possibility of the misalignment of the sample at least up to 5° should be taken into account. If so, it would be difficult to observe the increase of $1/T_1$ due to the tunneling contribution. In order to verify this argument, we simulated the situation in which the sample is misaligned by 3° off xy plane on the assumption of the azimuthal angle $\phi = 45°$. As it is clearly seen in Fig. 4.7, the degeneracies between $\pm m$ level pairs at zero field, which are preserved without tiling angle [Fig. 4.7(a)], are removed immediately by applying the transverse field for the misalignment of 3° [Fig. 4.7(b)]. It means that the energy difference between $\pm m$ levels cannot be treated as the tunnel splitting because $\pm m$ levels are no longer degenerate states in the tilted "transverse" field. It should be emphasized that this situation is also true for a tiny

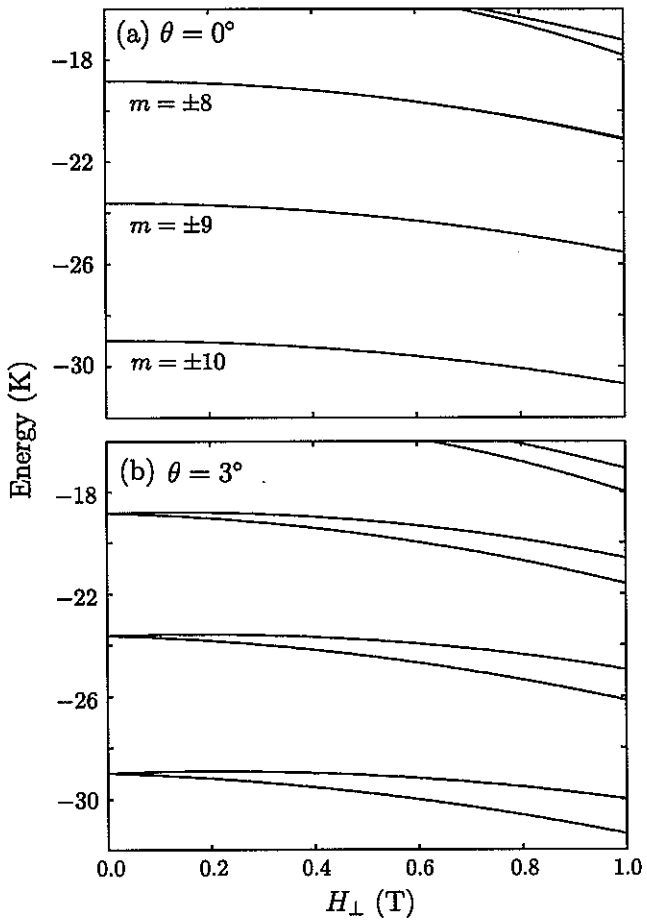

Figure 4.7 Energy level diagrams of three lowest $\pm m$ pairs in an applied transverse field (a) with no tilting (b) with a tilting angle, $\theta = 3°$. It is evident that a small misalignment of the sample off xy plane removes the degeneracy of $\pm m$ sublevels.

misalignment, for example 0.5°. Therefore, the predicted fast increase of Δ_m with a transverse field does not take place in presence of an even small misalignment of the sample.

When a transverse external field is applied, however, we should consider "canting effect", as discussed in Sec. 4.4. The transverse components of the fluctuation of the local field generated by canting of the magnetization could be very efficient for the spin-lattice relaxation process. Consequently $1/T_1$ due to canting effect should be added to the spin-phonon and the tunneling contributions,

$$\frac{1}{T_1} = \left(\frac{1}{T_1}\right)_{\text{cant}} + \left(\frac{1}{T_1}\right)_{\text{sp}} + \left(\frac{1}{T_1}\right)_{T}. \tag{4.20}$$

Here we assume that $(1/T_1)_{\text{cant}}$ can be obtained replacing $\gamma_N h_\perp$ in Eq. (4.12) with $\alpha \sin\Theta$ where Θ is the angle between $\mathbf{H}_{\text{eff}}$ and $\mathbf{H}_{\text{int}}$ and $\alpha = 4.1 \times 10^8$ (rad Hz) has been chosen in order to fit the data. The agreement between the data and the theory, as it is shown as solid line in Fig. 4.6, is very good except the small deviations at low fields. Therefore, for the $H_\perp$ dependence of $1/T_1$, $(1/T_1)_{\text{cant}} \gg (1/T_1)_{\text{sp}} + (1/T_1)_T$.

4.6.1.3 Temperature dependence

Fig. 4.8 shows the temperature dependence of $1/T_1$ in zero field. The spin-phonon contribution, which is represented by dotted line in Fig. 4.8, was calculated from Eq. (4.12) with the same parameter $\gamma_N h_\perp = 2.73 \times 10^5$ (rad Hz) as obtained from the analysis of H_z dependence of $1/T_1$. It is clear that the data cannot be explained with the spin-phonon contribution alone. Thus we consider the tunneling contribution. In calculating the tunneling contribution to $1/T_1$ from Eq. (4.17) and Eq. (4.18) we must include the contribution of the tunneling between the $m = \pm 8$ states since, although the Boltzmann population of these higher states is low at low T, the tunneling splitting Δ_m in Eq. (4.17) increases dramatically with decreasing m value. This is not the case in Eq. (4.12) where only the contribution from the first two sets of levels $m = \pm 10$ and $m = \pm 9$ need to be considered.

The additional contribution from the tunneling calculated from Eq. (4.18) was added to Eq. (4.12), and the obtained theoretical curve, represented by solid curve in Fig. 4.8, is in excellent agreement with the experimental data.

4.6.2 Spin-spin relaxation rate $(1/T_2)$

4.6.2.1 Field dependences

The longitudinal and transverse field dependences of $1/T_2$ are shown in Fig. 4.9. In the longitudinal field, $1/T_2$ decreases at a moderate rate with increasing H_z, while it is almost constant in the transverse field. $1/T_2$ in both directions can be fitted by Eq. (4.13) with $\gamma_N h_z = 2 \times 10^7$ (rad Hz). The tunneling contribution calculated from Eq. (4.18) is negligible so that the spin-phonon contribution is dominant for $1/T_2$. Also it turns out that the canting

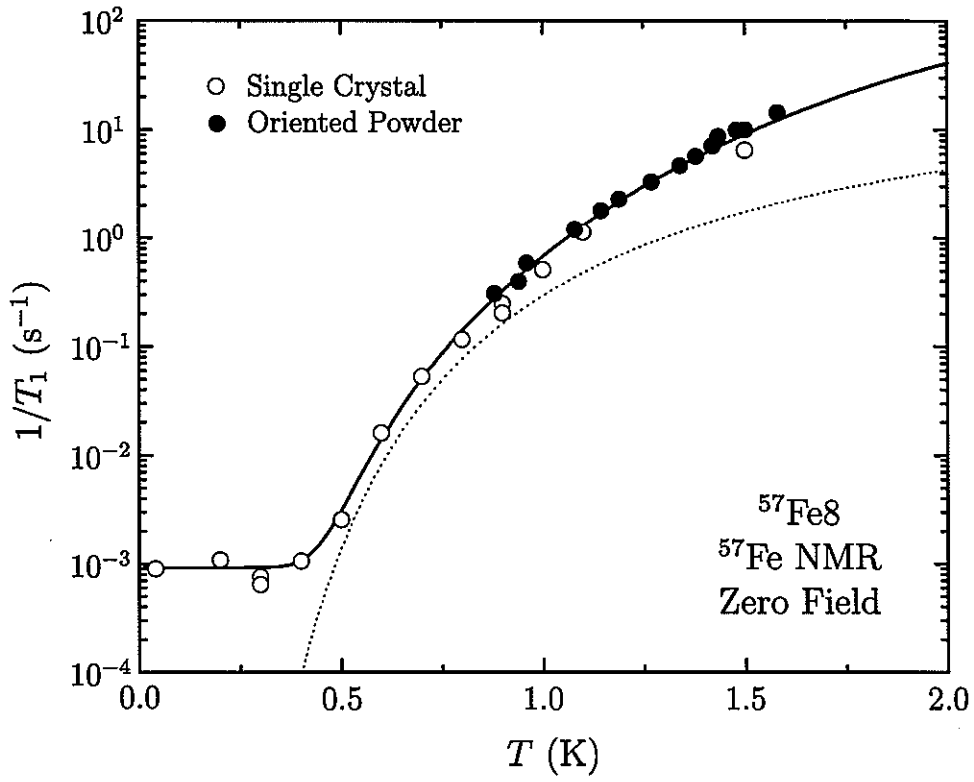

Figure 4.8 Temperature dependence of $1/T_1$. Theoretical curves are given by Eq. (4.12) (dotted line) and the additional contribution is fitted well by adding Eq. (4.18) to Eq. (4.12) (solid line) with the appropriate choice of the parameters (See text). Below 0.4 K, the leveling off of $1/T_1$ demonstrates the pure quantum tunneling regime.

of the magnetization has no effect on the transverse field dependence of $1/T_2$ due to the fact that it affects only the transverse component of the fluctuation of the magnetization.

4.6.2.2 Temperature dependence

For the temperature dependence of $1/T_2$, the data is fitted well above 1 K with Eq. (4.13), but it starts to deviate below 1 K as shown in Fig. 4.10. The discrepancy between the data and the theoretical curve can be resolved by adding the constant value of 1.6×10^3 s^{-1}. Thus, $1/T_2$ seems to level off at a constant value, as in the case of $1/T_1$. However, the origin of the leveling-off of $1/T_2$ cannot be the tunneling dynamics because its contribution from Eq. (4.18) is negligible at all temperatures. We argue below that the constant value of $1/T_2$ for $T \to 0$ i.e.,

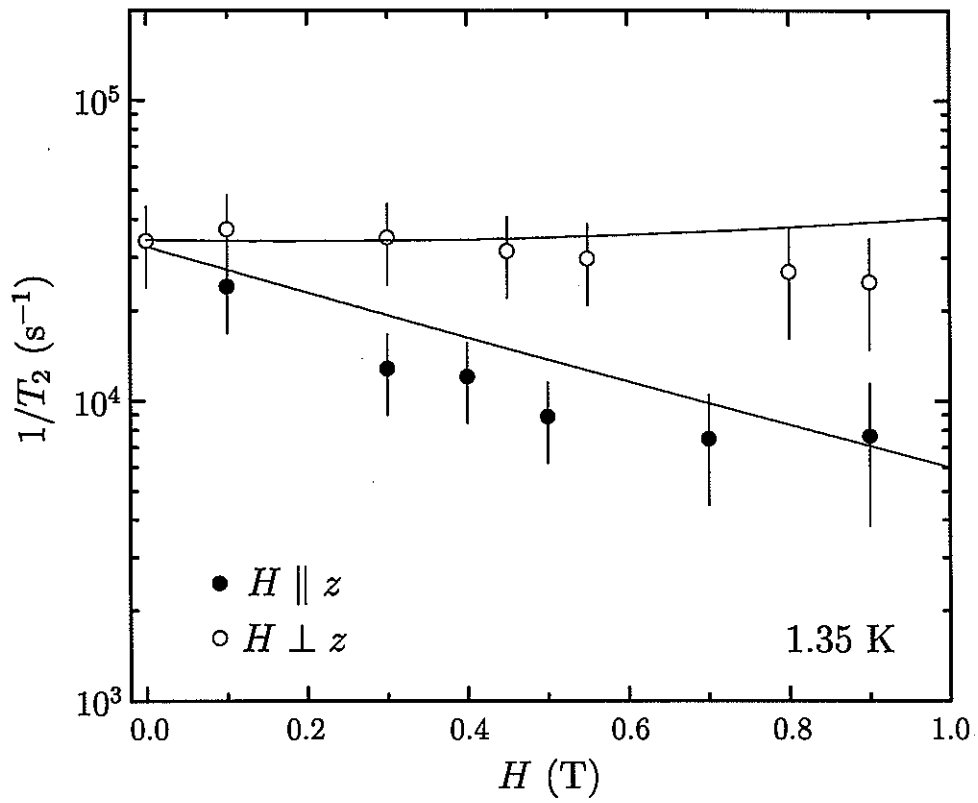

Figure 4.9 Field dependences of $1/T_2$ for both longitudinal and transverse directions. Theoretical curves were obtained from Eq. (4.13) with $\gamma_N h_z = 2 \times 10^7$ (rad Hz). It appears that the tunneling and the canting effects do not contribute to $1/T_2$.

1.6×10^3 s^{-1} arises from the nuclear dipolar interaction mostly between ^{57}Fe and ^{1}H nuclei.

The irreversible decay of the transverse magnetization (i.e., T_2 process) due to the nuclear dipolar interaction may originate from two contributions: (i) the dipolar interaction between like nuclei, (ii) the fluctuation of the dipolar fields arising from unlike nuclei. For ^{57}Fe NMR in Fe8, (i) should be negligible because the second moment M_2 due to ^{57}Fe nuclei is estimated to be of the order of 7×10^2 s^{-2}, which is four orders of magnitude smaller than $M_2 \sim 1.6 \times 10^7$ s^{-2} for ^{57}Fe-^{1}H interaction. Then, the contribution (ii) must be dominant one. In the weak collision fast motion approximation one can express $1/T_2$ in terms of the spectral density at zero frequency, $J_z(0)$, of the fluctuations of the hyperfine field. Since in the present case the hyperfine field in the dipolar interaction due to the ^{1}H nuclear moments at the ^{57}Fe site one can write $1/T_2 \approx M_2 J^0(0) \approx M_2 \tau_c$, where τ_c is a correlation time and M_2 is the second moment [47]

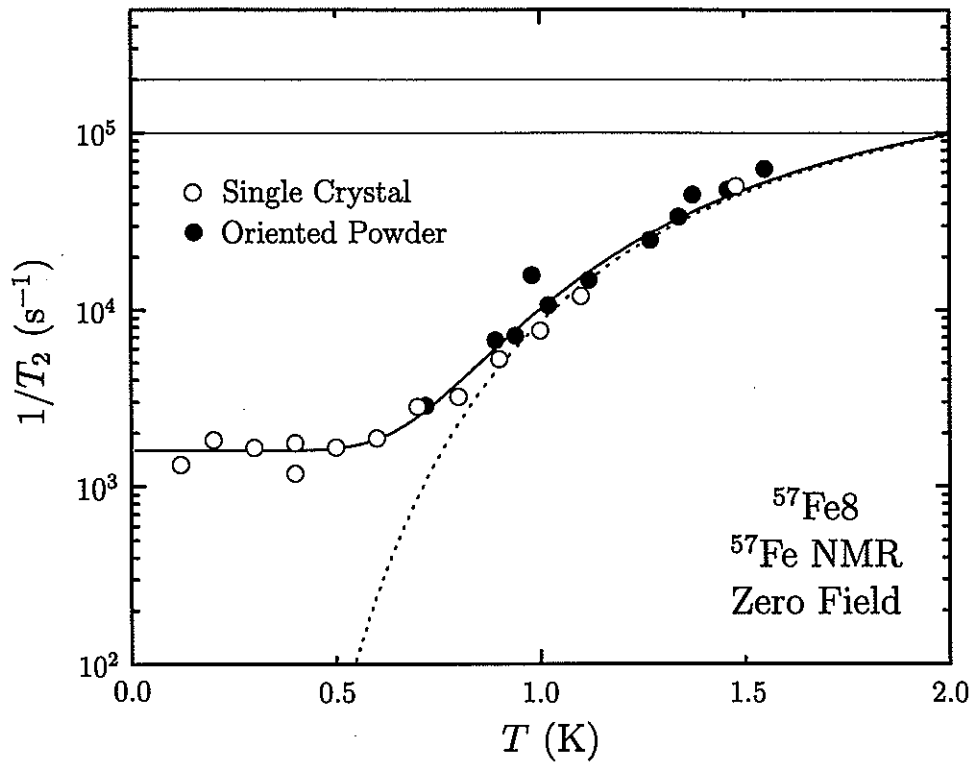

Figure 4.10 Temperature dependence of $1/T_2$. Dotted line was obtained from Eq. (4.13) with $\gamma_N h_z = 2 \times 10^7$ (rad Hz) and solid line was obtained adding the constant value 1.6×10^3 s^{-1}, which is ascribed to the nuclear dipole-dipole interaction between ^{57}Fe and ^{1}H nuclei, to Eq. (4.13). The horizontal lines indicate the range of T_2 values above which the echo signal becomes undetectable depending on the spectrometer used and the experimental conditions.

of the ^{1}H-^{57}Fe dipolar interaction. We should point out that the formula mentioned above is the same form with Eq. (4.8), and so it is valid only in the fast motion regime i.e., $\sqrt{M_2}\tau_c \ll 1$. If we identify τ_c with the proton T_2 value ($\sim 10^{-3}$ s) measured at low temperatures [119] then $\sqrt{M_2}\tau_c = 4$ indicating that the fast motion approximation is not applicable. Then one has to refer to the quasi-static approximation whereby the effect on ^{57}Fe T_2 arises from the dephasing of the Hahn echo due to the slow fluctuations of the ^{57}Fe–^{1}H dipolar interaction. By using the line narrowing approach [133] in the nearly static regime one has that the contribution to the

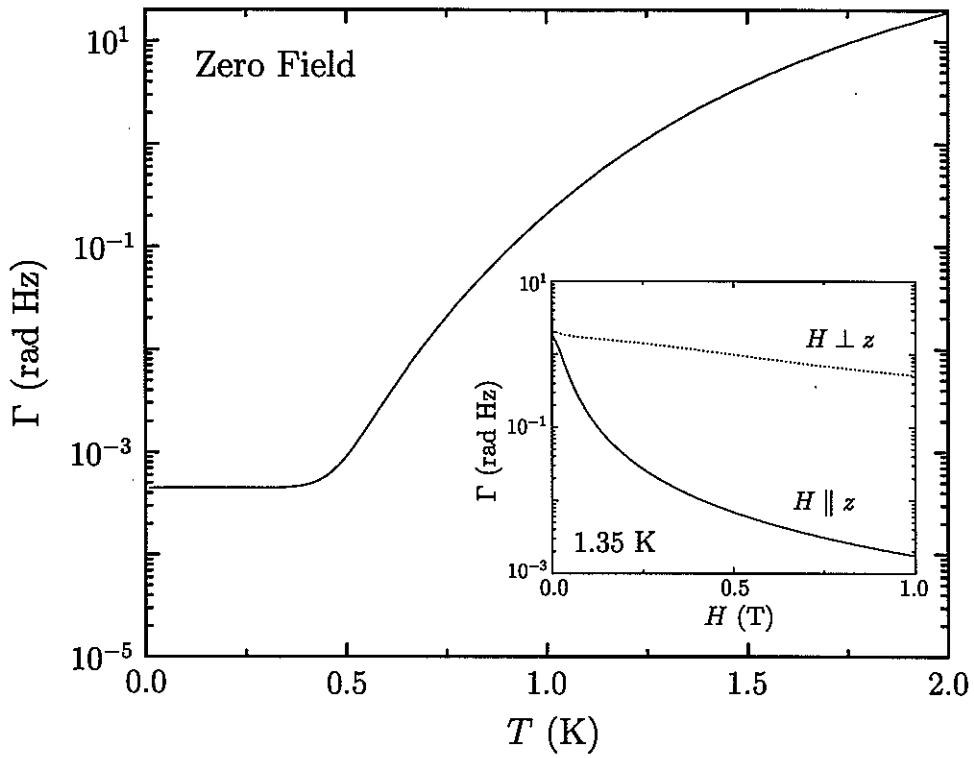

Figure 4.11 Calculated tunneling probability Γ versus T plot. In inset, Γ is plotted against H_z (solid line) and $H_\perp$ with the tilting angle, $\theta = 3°$ (dotted line) at 1.35 K.

decay of the echo signal can be expressed approximately as

$$1/T_2^{\text{eff}} = \left(\frac{M_2}{12\tau_c}\right)^{1/3}. \tag{4.21}$$

With the values quoted above for M_2 and τ_c one has $1/T_2^{\text{eff}} = 1.1 \times 10^3$ s^{-1} in excellent agreement with the low T limiting value of ^{57}Fe $1/T_2$ of 1.6×10^3 s^{-1}.

4.6.3 Comparison of ^{57}Fe relaxation rate in Fe8 with ^{1}H relaxation in Fe8 and ^{55}Mn relaxation in Mn12

As can be seen in Fig. 4.8 the ^{57}Fe $1/T_1$ vs. T in zero field levels off at low T reaching a constant T-independent value of about 10^{-3} s^{-1}. In Fig. 4.12 we show a comparison of our data with data in the literature about proton $1/T_1$ in Fe8 and ^{55}Mn $1/T_1$ in Mn12. In both cases a T-independent spin-lattice relaxation plateau was observed at values comparable to what predicted from our extrapolated fitting curve.

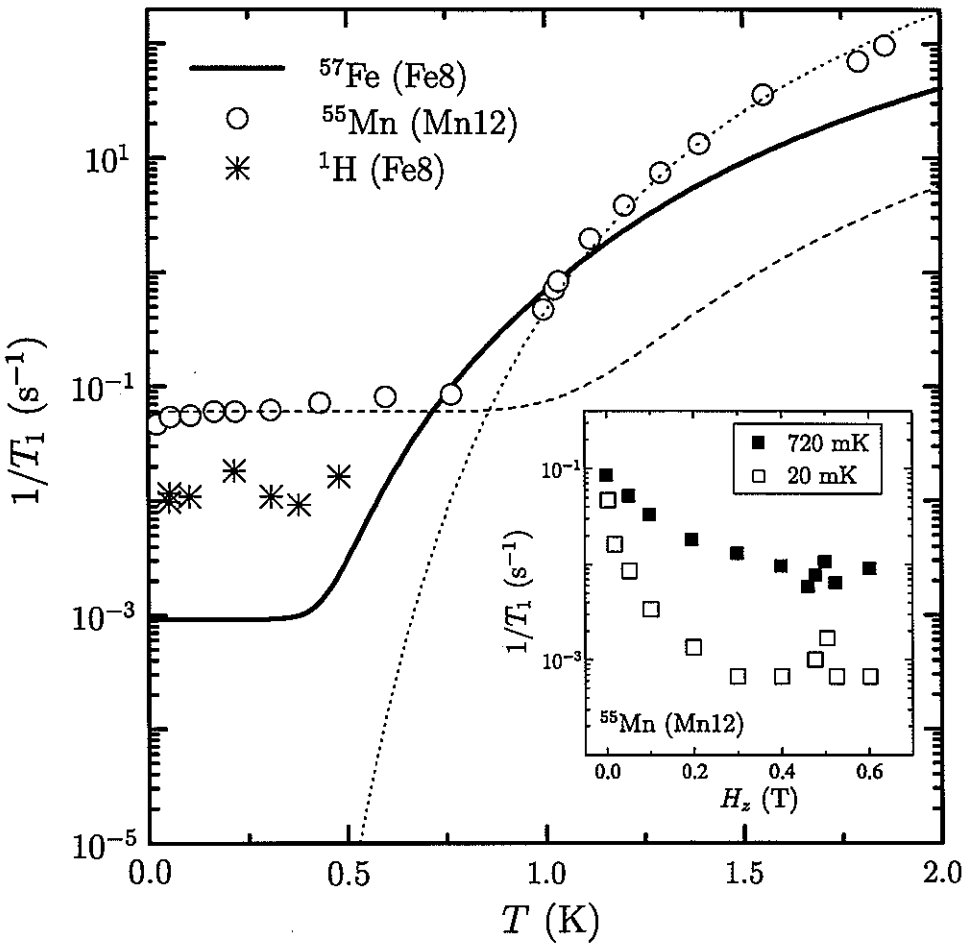

Figure 4.12 Comparison of temperature dependences of ^{57}Fe $1/T_1$ in Fe8 with ^{1}H $1/T_1$ in Fe8, extracted from Ref. [58], and ^{55}Mn $1/T_1$ in Mn12, extracted from Ref. [44]. ^{55}Mn data above 1 K is found to be proportional to $\exp(-12.1/T)$ (dotted line). Dashed line is the simulated result for the tunneling fluctuations in Mn12. Inset shows the longitudinal field dependence of ^{55}Mn $1/T_1$ at 20 mK and 720 mK, extracted from Ref. [134], demonstrating that the plateau found in Mn12 is really arising from the tunneling effect (see text).

Let us analyze ^{55}Mn $1/T_1$ in Mn12 qualitatively in the framework of our theoretical models. In Refs. [131] and [44], the ^{55}Mn relaxation data in Mn12 have been interpreted as arising from the thermal fluctuations [Eq. (4.12)], and the plateau found below 0.7 K has been attributed to the tunneling between $m = \pm 10$ ground states. As shown in Fig. 4.12, we find that ^{55}Mn $1/T_1$ data [44] above 1 K decreases with decreasing T in proportion to $\exp(-\Delta E_{\rm Mn}/T)$, where $\Delta E_{\rm Mn} \sim 12.1$ K is the energy difference between the ground and the first excited states (dotted line in Fig. 4.12). We emphasize that, due to much higher energy barrier (61 K) in Mn12 than in Fe8 (25 K), both the thermal [Eq. (4.12)] and the tunneling contribution [Eq. (4.17)] can be described in Mn12 by considering only the two lowest m states. This implies that it is difficult to establish the presence of a contribution of tunneling dynamics to the nuclear relaxation of ^{55}Mn only on the basis of the T dependence. Then one has to turn to the field dependence in longitudinal fields as it was done in Fe8. At 1.45 K no anomalous drop of $1/T_1$ at low fields could be observed in Mn12 [57, 131] indicating that at this temperature the spin phonon thermal contribution is still dominant. On the other hand, at lower temperature a fast initial drop of $1/T_1$ at low fields and a small enhancement at the first level crossing (~0.5 T) can be observed in ^{55}Mn relaxation (see inset in Fig. 4.12). This behavior is identical to the one observed for ^{57}Fe relaxation in Fe8 as shown in Fig. 4.5 and can thus be ascribed to phonon assisted tunneling. If one assumes for ^{55}Mn relaxation at low T a contribution given by Eq. (4.18) and Eq. (4.17) for the two lowest states ± 10 and ± 9 i.e. $A + B\exp(-\Delta E_{\rm Mn}/T)$ one finds the dashed line in Fig. 4.12 with a value for the ratio A/B comparable to the one in Fe8 (Fig. 4.8).

Regarding the comparison of the plateau's in Fig. 4.12 for the different cases one notes that the ^{55}Mn results in Mn12 seem to indicate a tunneling probability larger for Mn12 than for Fe8. This is surprising in view of the much smaller value of Δ_m^2 in Eq. (4.17) expected for Mn12 compared to Fe8 as a result of the higher anisotropy barrier and small in-plane anisotropy in the former of the two clusters. It have been suggested that the fast tunneling rate in Mn12 may arise from a limited number of fast tunneling molecules [44, 134]. We compare now the ^{57}Fe data and the ^{1}H data in Fe8 (see Fig. 4.12). Since the ^{1}H $1/T_1$ data [58, 119] were measured in zero external field the strong collision formula Eq. (4.18) should apply also for protons and

thus the two sets of data should measure directly the same effective tunneling probability. This is consistent only if one assumes that the prefactor, c, in Eq. (4.18) is one order of magnitude larger for ^{1}H than for ^{57}Fe. This conclusion, although surprising, cannot be refuted without a detailed calculation of the relaxation in the strong collision limit for both nuclei.

4.7 Summary and conclusions

A comprehensive ^{57}Fe NMR study has been carried out in order to investigate the static and dynamic magnetic properties in Fe8 molecular cluster.

The temperature dependence of the resonance frequency in zero field is well explained in terms of the average total magnetic moment of the molecule which is reduced by thermal fluctuations as the temperature increases. We have shown that the hyperfine fields at the nuclear sites are dominated by the negative core polarization term due to $3d$ electrons. From the fine structure of the spectrum within each Fe group, we find that the internal field at the nucleus is slightly different for each Fe site, whereby the difference can be easily accounted for by small differences in the covalent bonds, indicating a total lack of symmetry of the Fe8 molecule. We confirmed the internal magnetic structure of the cluster in its $S = 10$ ground state, as shown in Fig. 4.1. The ferrimagnetic spin configuration corresponding to the $S = 10$ ground state has been shown to be robust even when the external magnetic field is applied perpendicular to the easy axis of the cluster.

The quantum tunneling of the magnetization (QTM) was detected by measuring the nuclear spin-lattice relaxation rates of ^{57}Fe as a function of the temperature and of longitudinal field. We argue that the tunneling contribution to $1/T_1$ should be described in the framework of a strong collision theory. This leads to the remarkable result that at low fields and low T the relaxation rate is a direct measure of the tunneling rate. For the proper description of the tunneling effect, we propose a simple phenomenological model in terms of the tunneling probability that is determined by the tunnel splittings between pairwise degenerate $\pm m$ states. The experimental data are in good agreement with our theoretical calculations when both the thermal fluctuations due to spin-phonon interaction and the tunneling dynamics are included.

For the spin-phonon interaction we used values of the spin phonon coupling constant derived previously from proton NMR in Fe8. Regarding the tunneling effect we find that in order to fit the data one has to assume a large fourth order term in the in-plane anisotropy of Fe8. This result is, however, consistent with previous observations reporting a tunneling splitting much larger than predicted on the basis of published values of the anisotropy constants and the fact that the ^{57}Fe isotopic enrichment increases the tunneling splitting.

We compared our ^{57}Fe relaxation data in Fe8 to the ^{55}Mn relaxation in Mn12 to show that in both cases the $1/T_1$ is dominated by phonon assisted tunneling below 0.5 K while in Fe8 the tunneling dynamics can be observed even at intermediate temperatures (1–2 K). When the magnetic field is applied perpendicular to the main easy axis we find the unexpected result that the tunneling dynamics does not contribute to the measured $1/T_1$. We demonstrate that the negligible tunneling effect in the transverse field is due to the breakdown of the degeneracy of $\pm m$ pairs by an inevitable tilting of the sample off the xy plane. Finally, it turns out that the tunneling dynamics gives no effect on both the temperature and field dependences of $1/T_2$.

CHAPTER 5 Scaling behavior of the proton spin-lattice relaxation rate in antiferromagnetic molecular rings

(This chapter is mostly based on a paper accepted for publication in *Physical Review B* [135].)

In this chapter, we present new and refined data for the magnetic field (H) and temperature (T) dependence of the proton spin-lattice relaxation rate ($1/T_1$) in antiferromagnetic molecular rings as well as a new explicit scaling formula that accurately reproduces our data. The key ingredients of our formulation are (1) a reduced relaxation rate, $R(H,T) = (1/T_1)/(T\chi(T))$, given by $R(H,T) = A\omega_c(T)/(\omega_c^2(T) + \omega_N^2)$, where $\chi = (\partial M/\partial H)_T$ is the differential susceptibility, A is a fitting constant, and ω_N is the proton Larmor frequency, and (2) a temperature-dependent correlation frequency $\omega_c(T)$ which at low T is given by $\omega_c(T) \propto T^\alpha$, that we identify as a lifetime broadening of the energy levels of the exchange-coupled paramagnetic spins due to spin-acoustic phonon coupling. The main consequence are: (1) $R(H,T)$ has a local maximum for fixed H and variable T that is proportional to $1/H$; the maximum occurs at the temperature $T_0(H)$ for which $\omega_c(T) = \omega_N$; (2) for low T a scaling formula applies: $R(H,T)/R(H,T_0(H)) = 2t^\alpha/(1+t^{2\alpha})$, where $t \equiv T/T_0(H)$. Both results are confirmed by our experimental data for the choice $\alpha = 3.5 \pm 0.5$.

5.1 Introduction

The discovery that certain transition metal complexes ("magnetic molecules") act as individual nanomagnets [2] has prompted wide interest in the physics community. The individual molecules are shielded from each other by a shell of bulky ligands so that the magnetic interactions between neighboring molecules are very small and the observed magnetic properties

of bulk samples are very nearly intramolecular in origin. Antiferromagnetic (AFM) rings are magnetic molecules comprising an even number (N) of uniformly spaced paramagnetic metal ions arranged as a planar ring. The AFM rings can usually be described by the Heisenberg model of localized spins s interacting via nearest-neighbor exchange (the interaction term for two successive spins of the ring is $J\mathbf{s}_n \cdot \mathbf{s}_{n+1}$ where J is a positive energy and the spin operators are in units of $\hbar$) along with weak anisotropic terms. The energy eigenstates deriving from the Heisenberg Hamiltonian can be classified by the total spin quantum number S, and due to the small number of paramagnetic spins in the ring they are well separated in energy. The minimal energy for each S, as measured relative to the energy of the singlet $S = 0$ ground state, is well described by a so-called Landé rule [136], $E(S) = (\Delta/2)S(S+1)$, and it is convenient to picture these energies as defining a rotational band [137]. The constant Δ is the energy gap to the lowest $S = 1$ state and it is approximately $\Delta = 4J/N$. Often it is also possible to approximate the next one or two higher energy levels for each S in terms of rotational bands of successively higher energy. The crystal field anisotropy introduces splittings of the otherwise degenerate S levels which have been measured accurately by EPR and torque magnetometry [12]. The anisotropy is in most cases small compared to J and can therefore be neglected in the temperature range of our measurements. More generally, the structure of the low-lying excitations, the local spin dynamics, and the broadening of the quantum energy levels of AFM rings are of great interest in fundamental quantum magnetism and its applications.

NMR has proved to be a powerful tool to investigate the local spin dynamics in magnetic molecules, and a considerable body of results has accumulated over the past five years mostly on the dependence of the proton spin-lattice relaxation rate ($1/T_1$) on T and H [54, 138].

5.2 Experimental results and discussion

The general behavior found in AFM rings is that $1/T_1$ is approximately proportional to χT, where $\chi = (\partial M/\partial H)_T$ is the differential susceptibility, namely, on cooling it decreases monotonically from its high T saturated value and at very low T it is well approximated by $\exp(-\Delta/k_B T)$. However, a long-standing unexplained feature is that for a number of AFM

rings $1/T_1$ shows a strong peak superimposed on the χT behavior at a temperature of the order of J/k_B [138]. The peak is particularly noticeable upon defining a reduced relaxation rate $R(H,T) \equiv (1/T_1)/(T\chi(T))$. It has also been observed that in a number of AFM rings all $1/T_1$ data appear to overlap upon plotting $R(H,T)/R(H,T_0)$ versus $t = T/T_0(H)$ with $T_0(H)$ the temperature of the maximum in $R(H,T)$ for the given choice of H [139]. This finding prompted the idea that there may be some universal behavior underlying the peak of $1/T_1$ versus T in AFM rings.

Since many of the previous data [139] were incomplete and obtained for a limited range of external fields we here provide improved data for Fe6(Li), Fe6(Na), and Fe10, and we also present data for the first time for the AFM ring Cr8, all with a non-degenerate $S = 0$ ground state. In addition, we greatly extend the qualitative ideas of universal behavior suggested in Ref. [139] by providing an explicit formula for $1/T_1$. As discussed below our formula has its origins in the first-principles formula of Moriya based on two-spin time correlation functions, incorporates generic features of AFM rings in particular the existence of discrete magnetic energy levels due to the AF exchange between paramagnetic ions, and whose major premise is that these levels are lifetime broadened due to the coupling of the ion spins to the acoustic phonons of the host molecular crystals. In particular we show that all features of our data can be accurately reproduced by assuming that $R(H,T)$ is given by the Lorentzian-type expression:[1]

$$R(H,T) \equiv \frac{1}{T_1 \chi T} = A \frac{\omega_c(T)}{\omega_c^2(T) + \omega_N^2}, \tag{5.1}$$

where A is a fitting constant independent of both H and T, the width parameter $\omega_c(T)$ will be assumed to be an increasing function of T but independent of H, and ω_N is the proton Larmor frequency. We interpret $\hbar\omega_c(T)$ as the lifetime broadening of discrete energy levels originating in the coupling of the exchange-coupled ion spins to the host molecular crystal. In particular for low T we shall assume that $\omega_c(T) \propto T^\alpha$, where the exponent α will be determined by a best-fit procedure to our experimental data and, as seen below, we find $\alpha = 3.5 \pm 0.5$. This

[1] A Lorentzian expression for $1/T_1$, often called a BPP formula, is widely used in NMR (see e.g., Abragam [45] p. 457) and originates in the sampling of the spectral density of "lattice" fluctuations. The source of the χT factor and the width parameter $\omega_c(T)$ in Eq. (5.1) is briefly discussed in the text.

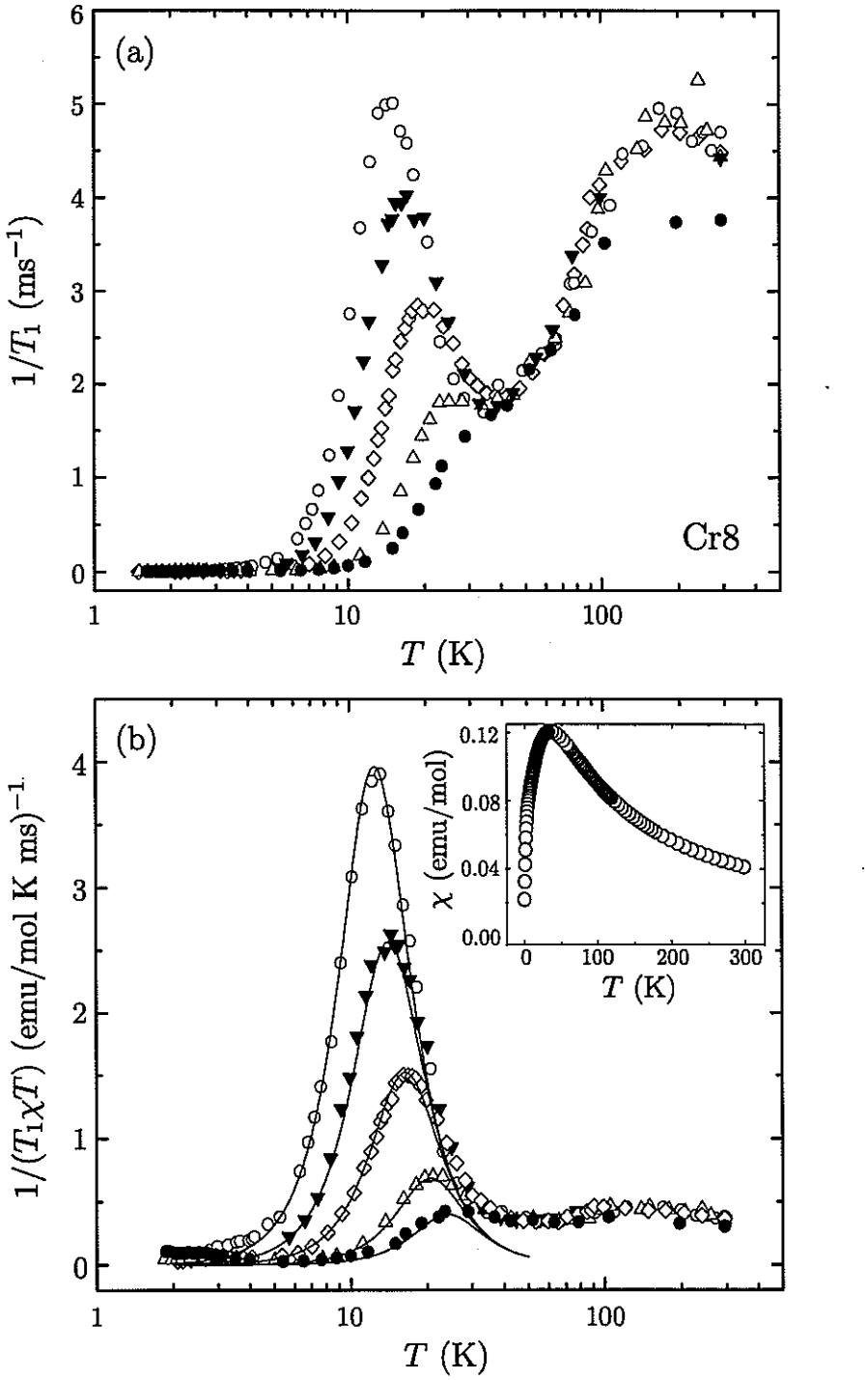

Figure 5.1 (a) ^{1}H $1/T_1$ versus T in Cr8; (○) 0.47 T (▼) 0.73 T (◇) 1.23 T (△) 2.73 T (●) 4.7 T. (b) $1/(T_1\chi T)$ versus T in Cr8. The inset shows the measured susceptibility versus T at 1.2 T. The solid lines correspond to Eq. (5.1) with $A = 1.0 \times 10^{12}$ (rad^{2}Hz^2), $C = 1.8 \times 10^4$ (rad Hz) and $\alpha = 3.5$.

numerical result suggests that the lifetime broadening at low T is due to spin-acoustic phonon coupling.

A key feature of Eq. (5.1) is that $R(H,T)$ has a local maximum for fixed H and variable T, occurring at the temperature, $T_0(H)$, for which $\omega_c(T)$ coincides with ω_N.[2] The corresponding maximum value of R is given by

$$R(H,T_0(H)) = \frac{A}{2\omega_N}, \tag{5.2}$$

namely proportional to $1/H$, in very good agreement with our experimental findings.

Moreover, from Eq. (5.1) we have for low T the scaling formula

$$\frac{R(H,T)}{R(H,T_0(H))} = \frac{2t^\alpha}{1+t^{2\alpha}}, \tag{5.3}$$

where $t = T/T_0(H)$. In particular, we note that according to Eq. (5.3), a plot of $R(H,T)/R(H,T_0)$ should be symmetric in the variable $\log(t)$.

The four AFM ring systems considered here are: (a) Cr8 $\equiv$ $[Cr_8F_8Piv_{16}]$ (HPiv = pivalic acid), Cr^{3+} ($s = 3/2$) ions, $J/k_B \cong 17.2$ K [21]; (b) Fe6(Li) $\equiv$ $[LiFe_6(OCH_3)_{12}(C_{15}H_{11}O_2)_6]B(C_6H_5)_4 \cdot 5CH_2Cl_2$, Fe^{3+} ($s = 5/2$) ions, $J/k_B \cong 21$ K [20]; (c) Fe6(Na)$\equiv$ $[NaFe_6(OCH_3)_{12}(C_{15}H_{11}O_2)_6]^+ClO_4^-$, $J/k_B \cong 28$ K [140]; (d) Fe10 $\equiv$ $[Fe_{10}(OCH_3)_{20}(C_2H_2O_2Cl)_{10}]$, Fe^{3+} ($s = 5/2$) ions, $J/k_B \cong 13.8$ K [11]. The measurements of $1/T_1$ have been performed with standard pulse Fourier Transform spectrometers. The recovery of the nuclear magnetization varies from almost exponential to strongly stretched exponential depending on the molecule and the range of T and H. In all cases the measured $1/T_1$ is an average value over the many protons in the molecule. However, due to the different types of recoveries one should allow for a possible systematic uncertainty of up to 50% in the absolute values reported. Details about the NMR measurements can be found in Refs. [54] and [138].

The experimental data for $1/T_1$ for the AFM ring Cr8 are shown in Fig. 5.1(a) for five choices of H, and the susceptibility data is given in the inset of Fig. 5.1(b). The corresponding values of the reduced spin-lattice relaxation rate $R(H,T)$ are given in Fig. 5.1(b). The solid

[2] $T_0(H)$ has been determined from the position of the maximum of $R(H,T)$ vs. T plot [Fig. 5.1(b)]. It is noted that the maximum in $1/T_1$ vs. T plot occurs always at slightly higher temperature than $T_0(H)$ [Fig. 5.1(a)].

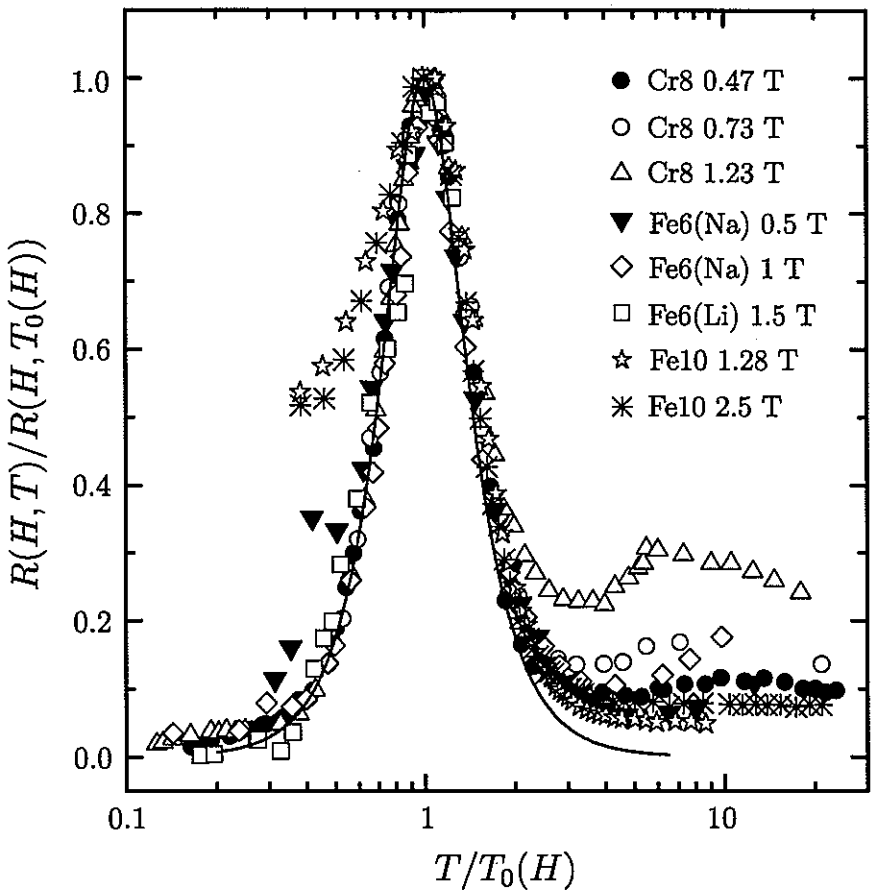

Figure 5.2 Proton relaxation rate, $R \equiv 1/(T_1\chi T)$, scaled by its maximum value (see text) versus $T/T_0(H)$ for the AFM rings and fields listed. The solid curve is given by Eq. (5.2) with $\alpha = 3.5$.

curves have been obtained using Eq. (5.1) with $A = 1.0 \times 10^{12}$ (rad^2 Hz^2), $C = 1.8 \times 10^4$ (rad Hz) and for low T we use $\omega_c(T) = CT^\alpha$, where the coefficient C and the exponent α are determined by a best-fit procedure; we find that $\alpha = 3.5 \pm 0.1$ for the Cr8 data. In Fig. 5.2 the solid curve is obtained using Eq. (5.3) for the choice of $\alpha = 3.5$ (solid curve). Also shown in Fig. 5.2 are our experimental data for the four AFM rings Cr8, Fe6(Na), Fe6(Li), and Fe10. Indeed, it would appear that all of the data are consistent with Eq. (5.3) and suggest that $\alpha \approx 3.5$ in all cases. The discrepancy for $T/T_0(H) > 2$ is not surprising since the power law dependence of ω_c on T is only expected to apply for low T. For very low T the discrepancies are thought to be due to different nuclear relaxation mechanisms which can be important when $\omega_c(T)$ becomes very small. In Table 5.1 we give the values of the parameters when the

data for the different AFM rings are fitted separately. It is noted that the parameter A varies only within a factor of 2 for the different rings. A can be identified with the average square transverse hyperfine field fluctuations. The interaction is the dipolar interaction between the protons and the magnetic transition ion averaged over all protons in the molecule. The values of A in the table are indeed of the correct order of magnitude for such an interaction and the fact that they are comparable for all AFM rings is consistent with the fact that the location of the protons with respect to the magnetic ion is on the average similar in all the molecules. On the other hand the constant C varies by almost two orders of magnitude for the different rings. This indicates that this parameter is strongly dependent on the magnetic properties of the AFM ring as will be shown further on.

For weak magnetic fields ($g\mu_B H \ll \Delta$) one expects [60] in general that Eq. (5.1) should be supplemented by a second Lorentzian, where ω_N is replaced by the electron Larmor resonance frequency ω_e. However, if $\omega_c(T) \approx \omega_N$ we have $\omega_c(T) \ll \omega_e$ and it follows that the contribution of the second Lorentzian is negligible by comparison. To confirm this experimentally we performed $1/T_1$ measurements on two different nuclei namely ^{1}H and ^{7}Li in the same AFM ring Fe6(Li). Given that $\gamma_H/\gamma_{Li} \approx 2.6$ we selected the fields in the ratio 1:2.6 so as to achieve the same value of ω_N. The resulting data for the two species are shown in Fig. 5.3 and they are both fitted by Eq. (5.1), again with $\alpha = 3.5$, shown as the solid curve. If in Eq. (5.1) one were to use ω_e the data for the two nuclear species would have to fall on two separate curves (solid curve for ^{1}H and dotted curve for ^{7}Li). These measurements thus provide a direct demonstration that the applied field H affects $R(H,T)$ only via ω_N.

Molecule	A (rad^{2}Hz^2)	C (rad Hz)	α
Cr8	1.0×10^{12}	1.8×10^4	3.5(0.1)
Fe10	1.9×10^{12}	1.8×10^5	3.2(0.2)
Fe6(Li)	1.2×10^{12}	1.1×10^4	3.5(0.5)
Fe6(Na)	1.8×10^{12}	2.9×10^3	3.5(0.2)

Table 5.1 The values of the parameters obtained from the best fit of the $1/T_1$ data using Eq. (5.1). Note that the value of C varies depending on α.

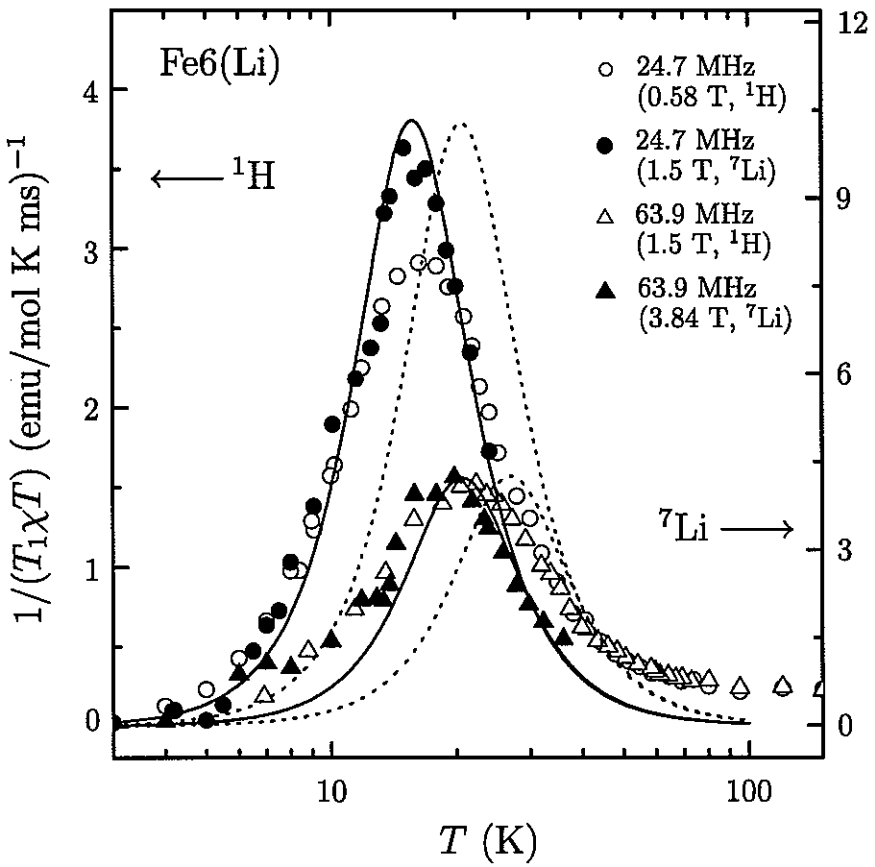

Figure 5.3 $1/(T_1\chi T)$ versus T in Fe6(Li) for ^{1}H NMR (left ordinate) and ^{7}Li NMR (right ordinate) for $\omega_N/(2\pi) = 24.7$ and 63.9 MHz. The solid curve represents Eq. (5.1) with $\omega_N = \gamma_N H$. If in Eq. (5.1) ω_N were replaced by $\omega_e = \gamma_e H$ the ^{1}H and ^{7}Li data would be expected to fall on the solid and dotted curves, respectively.

The use of a power law form for $\omega_c(T)$ is restricted to the low-T regime. However, if we suppose that Eq. (5.1) is valid over a broad temperature range we can extract the form of $\omega_c(T)$ using $R(H,T)/R(H,T_0) = 2\omega_N\omega_c/(\omega_c^2+\omega_N^2)$ in conjunction with $1/T_1$ data. The results are shown in Fig. 5.4 for the different AFM rings, where the independent variable is chosen as k_BT/Δ. This log-log plot shows very clearly that the power law behavior at low T and the subsequent, seeming saturation at high T is a universal feature of these rings and that $\omega_c(T)$ is indeed weakly H dependent. A remarkable feature of Fig. 5.4 is that in the low T (power-law) regime all of the data appear to coincide with a single curve, i.e., $\omega_c(T) = D(k_BT/\Delta)^\alpha$, with

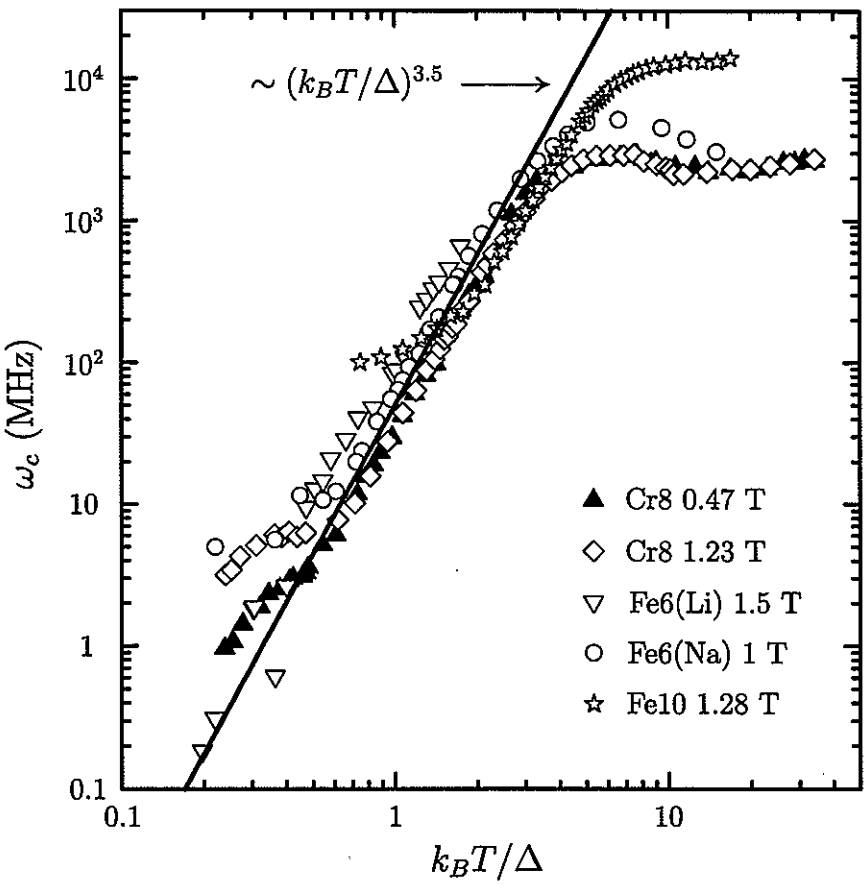

Figure 5.4 Correlation frequency ω_c extracted from the data and Eq. (5.1) plotted versus k_BT/Δ where $\Delta = 4J/N$ (see text).

a unique value of the constant D. Further work is needed on different specific systems to check whether this inference is in fact valid. If confirmed by further experiment this would be an important issue to be addressed as part of a quantitative theoretical calculation.

We now briefly discuss the theoretical basis for Eq. (5.1). According to the standard formula of Moriya [50, 51], which is based on a perturbative treatment of the hyperfine interactions between nuclear and paramagnetic spins, $1/T_1$ takes the form of a linear combination of the Fourier time transform, evaluated at ω_N, of the general two-spin equilibrium time correlation functions, weighted with the square of components of the nuclear-ion spin dipole interaction tensor. Since ω_N is very small compared to the frequency differences (of order $J/\hbar$) between those eigenstates of the exchange-coupled ion spins that are linked by single-spin operators, only quasi-elastic fluctuation terms of the spin correlation functions will contribute to $1/T_1$, as

only these allow for energy-conserving nuclear transitions [60]. However, the ion spins are also coupled to the lattice and this provides the source of the lifetime broadening $\hbar\omega_c(T)$ of the discrete magnetic energy levels and hence the Lorentzian broadening of the "elastic" peak. For AFM rings (even N) the ground state of the exchange-coupled ion spins is a non-degenerate $S = 0$ singlet state. The dominant contribution to $1/T_1$ at low temperatures, which originates from the quasi-elastic terms of both the auto- and pair two-spin time correlation functions, is therefore proportional to $e^{-\Delta/k_BT}$, or equivalently to χT. Finally, we remark that the familiar critical slowing-down effects associated with phase transitions [38] are absent in AFM rings and this too is due to the discreteness of the magnetic energy levels and the fact that only their lifetime broadening is probed by NMR.

Elsewhere we will report evidence that the same description appears to apply for the giant Keplerate magnetic molecule {Mo72Fe30} where 30 Fe^{3+} ions occupy the sites of an icosidodecahedron and the ground state is a non-degenerate $S = 0$ state [4]. On the other hand, for the magnetic molecule V12, (a 3-dimensional cluster, but the predominant exchange pathways link a central group of four spins $s = 1/2$) there is no evidence of a peak in $1/T_1$ at low T [141]. It is therefore certain that scaling behavior of the spin-lattice relaxation rate is by no means universal for magnetic molecules. It remains to develop a clear physical explanation for why scaling behavior occurs for certain magnetic molecules but not for others. It will also be important to clarify the role of the intrinsic spin of the magnetic ions. In this regard it would be very useful to synthesize a *bona fide* AFM ring system composed of spins $s = 1/2$. We are aware that a Cu^{2+} octanuclear $s = 1/2$ AFM ring, Cu8, has been measured and shows no peak in $1/T_1$ in the temperature range 4–300 K [142]. Since, however, Cu8 has a very large exchange constant $J/k_B \sim 1000$ K, the peak should be searched at very high T and thus Cu8 cannot be considered to be a *bona fide* $s = 1/2$ ring system for our purpose.

On the theoretical side, work is in progress [143] to calculate $\omega_c(T)$ using a detailed microscopic model for the interaction between the paramagnetic ions and the lattice. One of the goals of that work is to support or ultimately refute the apparent dependence of $\omega_c(T)$ on k_BT/Δ, at least for the AFM ring systems. Another goal is to establish the form of $1/T_1$ for

arbitrary fields when $g\mu_B H \ll \Delta$ is not fulfilled.

5.3 Summary and conclusion

In this chapter we have shown that the behavior of the proton spin-lattice relaxation rate for four different antiferromagnetic ring-type magnetic molecules can accurately be characterized in terms of a scaling law based on Eq. (5.1) and the related Eq. (5.3). A key quantity in this description is a correlation frequency $\omega_c(T)$ having what appears to be an S shape behavior which can be approximated at intermediate temperature by a power-law dependence on T. Such a temperature dependence suggests that the source of the correlation frequency is the coupling of the paramagnetic ions with acoustic phonons. The expected effect of that coupling is that the Heisenberg energy levels of the AFM ring acquire a frequency width which we identify with $\omega_c(T)$. The observed apparent power law dependence of $\omega_c(T)$ indicates that this quantity decreases rapidly with decreasing T, whereas it reaches values of the order of the proton Larmor frequency $\omega_N = \gamma_N H$ (i.e., 10^7–10^8 Hz) at relatively high T (i.e., 10–30 K). In this respect NMR, which probes very low frequency fluctuations, appears to be a unique tool for deriving quantitative information on the thermal broadening of the magnetic energy levels in some AFM rings.

CHAPTER 6 General summary

In this thesis, our main interest has been to investigate the spin dynamics and quantum tunneling in single molecule magnets (SMMs). For this we have selected two different classes of SMMs: a ferrimagnetic total high spin $S = 10$ cluster Fe8 and antiferromagnetic (AFM) ring-type clusters. For Fe8, our efforts have been devoted to the investigation of the quantum tunneling of magnetization in the very low temperature region. The most remarkable experimental finding in Fe8 is that the nuclear spin-lattice relaxation rate $(1/T_1)$ at low temperatures takes place via strong collision mechanism, and thus it allows to measure directly the tunneling rate vs T and H for the first time (see Chapter 4). For AFM rings, we have shown that $1/T_1$ probes the thermal fluctuations of the magnetization in the intermediate temperature range. We find that the fluctuations are dominated by a single characteristic frequency which has a power law T-dependence indicative of fluctuations due to electron-acoustic phonon interactions (see Chapter 5).

APPENDIX A $1/T_1$ in terms of the wave vector (q) components of the electronic spins

We can express Eq. (2.34) in terms of the q dependent correlation function of the electronic spins. By introducing normal coordinates,

$$\mathbf{S}_q = \frac{1}{\sqrt{N}} \sum_j \mathbf{S}_j \exp(i\mathbf{q} \cdot \mathbf{R}_j), \tag{A.1}$$

where $\mathbf{q}$ is a wave vector and N the number of magnetic ions in a crystal, we can express $1/T_1$ from Eq. (2.34) [49, 51, 54, 144],

$$\frac{1}{T_1} = \frac{(\hbar\gamma_n\gamma_e)^2}{4\pi} \int_{-\infty}^{+\infty} dt \cos(\omega_n t) \int dq \left(\frac{1}{4} A^{\pm}(q) \langle S_q^{\pm}(t) S_{-q}^{\pm}(0) \rangle + A^z(q) \langle S_q^z(t) S_{-q}^z(0) \rangle \right), \tag{A.2}$$

where $A^{\pm,z}(q)$ are the Fourier transforms of the spherical components of the product of two dipole-interaction tensors, and $S^{\pm} \equiv S_x \pm i S_y$. According to the fluctuation-dissipation theorem [145], a response function

$$R_q^{\alpha} = (S_q^{\alpha}(t), S_{-q}^{\alpha}(0)) \equiv \frac{1}{i\hbar} (\langle S_q^{\alpha}(t) S_{-q}^{\alpha}(0) \rangle - \langle S_q^{\alpha}(0) S_{-q}^{\alpha}(t) \rangle), \tag{A.3}$$

is related with the correlation function i.e.,

$$\int_{-\infty}^{+\infty} dt e^{-i\omega t} \langle S_q^{\alpha}(t) S_{-q}^{\alpha}(0) \rangle = E_\beta(\omega) \tilde{R}_q^{\alpha}(\omega) = \frac{E_\beta(\omega)}{(\mathrm{g}\mu_B)^2} \chi^{\alpha}(q) f_q^{\alpha}(\omega), \tag{A.4}$$

where $\alpha = \pm, z$, $E_\beta(\omega) = \frac{1}{2}\hbar\omega \coth(\frac{1}{2}\hbar\omega/k_B T)$, $f_q^{\alpha}(\omega) \equiv \tilde{R}_q^{\alpha}(\omega)/\tilde{R}_q^{\alpha}(0)$, $\tilde{R}_q^{\alpha}(\omega)$ is the Fourier transform of $R_q^{\alpha}(t)$, and $\chi(q) = (\mathrm{g}\mu_B)^2 \tilde{R}_q(0)$ is the static susceptibility. In the high temperature limit, we can approximate $E_\beta(\omega) \cong k_B T$. Then, Eq. (A.2) can be rewritten

$$\frac{1}{T_1} = \frac{(\hbar\gamma_n\gamma_e)^2}{4\pi \mathrm{g}^2 \mu_B^2} k_B T \left[\frac{1}{4} \sum_q A^{\pm}(q) \chi^{\pm}(q) f_q^{\pm}(\omega_e) + \sum_q A^z(q) \chi^z(q) f_q^z(\omega_n) \right]. \tag{A.5}$$

In the high temperature limit, on the further assumption of an isotropic response function, $\frac{1}{2}\chi^{\pm}(q) = \chi^z(q) = \chi(q = 0)$ and by taking a q-independent average value for the dipolar

hyperfine interaction of the nuclei with the electronic spins i.e., $A^{\alpha}(q) = A^{\alpha}$ [53–55]. Eq. (A.5) reduces to

$$\frac{1}{T_1} = \frac{(\hbar\gamma_n\gamma_e)^2}{4\pi g^2\mu_B^2} k_B T \chi(0) \left[\frac{1}{2}A^{\pm}\Phi^{\pm}(\omega_e) + A^z\Phi^z(\omega_n)\right], \tag{A.6}$$

where $\Phi^{\alpha}(\omega) \equiv \sum_q f_q^{\alpha}(\omega)$. This formula is the same as Eq. (2.35) which can be derived directly from the real space expression of the nuclear relaxation [Eq. (2.34)].

APPENDIX B Derivation of the correlation function for two-state random field fluctuation

Let us assume that the local field jumps randomly between the ground state with lifetime τ_0 and the excited state with lifetime τ_1. The time dependent fluctuating field $\Delta H_\alpha(t)$ with $\alpha = z, \perp$ can be described by pulse-like sudden jumps between the two field values as shown in Fig. B.1(a). Here we further assume that $\tau_0 \gg \tau_1$ and the magnitude of the field variation is fixed to h_α. As depicted in Fig. B.1(b), we may think of simple two level system labeled as states 1 and 2 in such a way that the average field $\tau_1 h_\alpha/(\tau_0 + \tau_1)$ is made zero.

In this simple system, one can express the correlation function as

$$G(t) = \langle H_\alpha(t) H_\alpha(0) \rangle = H_1[H_1 p_1(t) + H_2 p_2(t)], \tag{B.1}$$

where H_1, H_2 are the field values of the states 1 and 2, respectively,

$$H_1 = \frac{\tau_0 h_\alpha}{\tau_0 + \tau_1} \quad ; \quad H_2 = -\frac{\tau_1 h_\alpha}{\tau_0 + \tau_1} \tag{B.2}$$

and $p_1(t)$ and $p_2(t)$ are the ensemble average probabilities that in an ensemble in which the field was H_1 at $t = 0$, it will be H_1 or H_2 at time t. On the assumption that p_1 and p_2 satisfy the balance equation, we have

$$\begin{aligned} \frac{dp_1(t)}{dt} &= W_{21} p_2 - W_{12} p_1 \\ \frac{dp_2(t)}{dt} &= W_{12} p_1 - W_{21} p_2, \end{aligned} \tag{B.3}$$

where W_{ij} is the transition probability from state i to state j.

If at $t = 0$ the field is H_1 i.e., $p_1(0) = 1$ and $p_2(0) = 0$ (with normalization), one can obtain

$$\begin{aligned} p_1(t) &= \frac{\tau_1}{\tau_0 + \tau_1} + \frac{\tau_0}{\tau_0 + \tau_1} e^{-t/\tau_c} \\ p_2(t) &= \frac{\tau_0}{\tau_0 + \tau_1} - \frac{\tau_0}{\tau_0 + \tau_1} e^{-t/\tau_c}, \end{aligned} \tag{B.4}$$

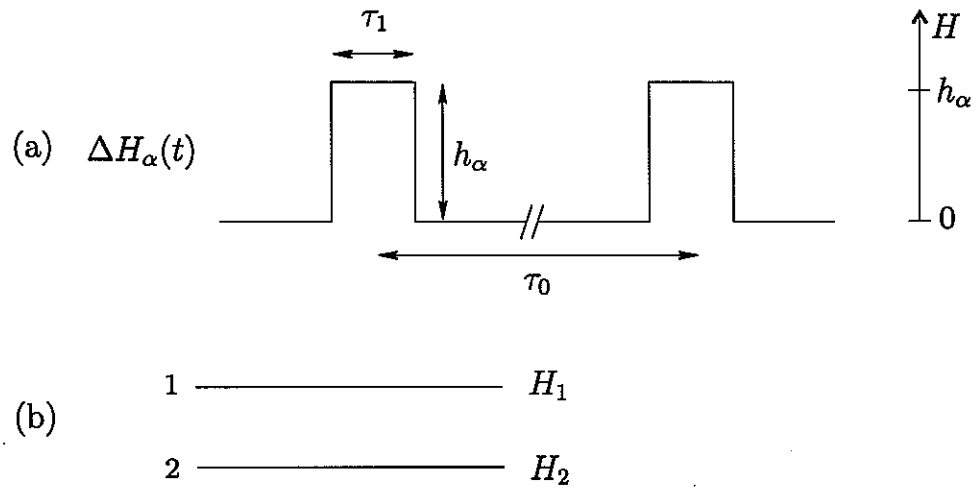

Figure B.1 (a) Fluctuating field $\Delta H_\alpha(t)$ with the magnitude h_α of the field jump and lifetimes τ_0 and τ_1. (b) Simple two level system for the field fluctuation of states 1 and 2.

where the correlation time τ_c is defined by the transition probabilities,

$$\frac{1}{\tau_c} = W_{12} + W_{21} \tag{B.5}$$

and we utilized the fact that $W_{12} = 1/\tau_1$ and $W_{21} = 1/\tau_0$.

Finally, with Eqs. (B.2) and (B.4) and some simple algebra, Eq. (B.1) becomes

$$\langle H_\alpha(0) H_\alpha(t) \rangle = \frac{\tau_0 \tau_1}{(\tau_0 + \tau_1)^2} h_\alpha^2 e^{-t/\tau_c}. \tag{B.6}$$

Note that the exponential time dependence arises from the assumed balance equation. Thus the expression for $1/T_1$ becomes:

$$\frac{1}{T_1} = \frac{(\gamma_n h_\perp)^2}{\tau_0} \frac{\tau_1^2}{1 + \omega_n^2 \tau_1^2}, \tag{B.7}$$

which can be compared with Eq. (2.39).

APPENDIX C Nuclear relaxation in strong collision limit

In most NMR measurements, the nuclear relaxation can be described by a perturbative approach (i.e., weak collision approach). It is obvious that the weak collision approximation is no longer valid if the local quantization field at the nuclear site reverses suddenly by, for example, the quantum tunneling of the magnetization.

This situation with a nuclear spin 1/2 is illustrated in Fig. C.1. The two Hamiltonians are given by $\mathcal{H}_{a,b} = \gamma_n \mathbf{H}_{a,b} \cdot \mathbf{I}$ where $\mathbf{I}$ is the nuclear spin vector. The corresponding eigenstates are $|\pm\rangle_a$ and $|\mp\rangle_b$, respectively, and it is obvious that $|\pm\rangle_a = |\mp\rangle_b$. If the change of the local field is very fast compared to the nuclear Larmor frequency, i.e., $dH_{\rm loc}/dt \gg \omega_n$, one may use the *sudden approximation*. In this case, since the nuclei (spin 1/2) cannot follow the change of the rapid reversal of the local field, the nuclear spin states cannot change, but the excited energy state becomes ground state, and vice versa, after the jump of the local field. Therefore the populations in the two nuclear states must fulfill the following relation:

$$N_a^{\pm} = N_b^{\mp}. \tag{C.1}$$

The rate equation for the populations for the Hamiltonian $\mathcal{H}_a$

$$\begin{aligned} \frac{dN_a^+}{dt} &= W\left(|-\rangle_b \rightarrow |+\rangle_a\right) N_b^- - W\left(|+\rangle_a \rightarrow |-\rangle_b\right) N_a^+, \\ \frac{dN_a^-}{dt} &= W\left(|+\rangle_b \rightarrow |-\rangle_a\right) N_b^+ - W\left(|-\rangle_a \rightarrow |+\rangle_b\right) N_a^-, \end{aligned} \tag{C.2}$$

where W denotes the transition rate. Also one can have similar equations for $\mathcal{H}_b$. It is easily seen that from Fig. C.1 W's should be symmetric. Therefore,

$$\begin{aligned} W(|+\rangle_a \rightarrow |-\rangle_b) &= W(|+\rangle_b \rightarrow |-\rangle_a) \equiv W^{\pm}, \\ W(|-\rangle_a \rightarrow |+\rangle_b) &= W(|-\rangle_b \rightarrow |+\rangle_a) \equiv W^{\mp}. \end{aligned} \tag{C.3}$$

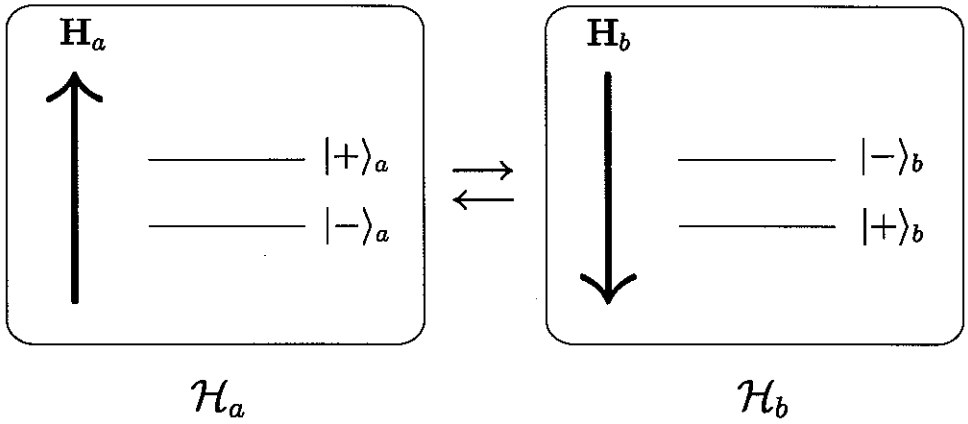

Figure C.1

Since $\omega_n \ll k_B T$ at all accessible temperatures i.e., the Boltzmann factor $e^{-\omega_n/k_B T} \sim 1$, one can write $W^{\pm} = W^{\mp} = \Gamma$ where Γ is the transition rate of the local field. From Eqs. (C.2) and (C.3), one can have

$$\begin{aligned} \frac{dM_a}{dt} &= -2\Gamma(M_a - M_0), \\ \frac{dM_b}{dt} &= -2\Gamma(M_b - M_0), \end{aligned} \tag{C.4}$$

where the magnetizations $M_{a,b}$ are given by the relationship $M_{a,b} = \gamma_n I(N^-_{a,b} - N^+_{a,b})$, and M_0 is the equilibrium magnetization. Here we assumed that $M_a = M_b$.

Thus, in this simple model, the nuclear spin-lattice relaxation rate $1/T_1$ is equivalent to 2Γ i.e., twice the transition rate of the local field:

$$\frac{1}{T_1} = 2\Gamma. \tag{C.5}$$

ACKNOWLEDGEMENTS

I would like to take this opportunity to express my thanks to those who helped me with various aspects of conducting research and the writing of this thesis. First and foremost, I thank my advisor Prof. Ferdinando Borsa for his guidance, patience and support throughout this research and the writing of this thesis. His insights and words of encouragement have often inspired me and renewed my hopes for completing my graduate education. He is not only the best physicist but also a great teacher I have ever met. He has never blamed my ignorance nor big mistake but gave me a patient guidance until I understand correctly an important thing and follow the right track by myself. I believe that it was a blessing that I had him as my academic advisor.

I acknowledge lots of experimental help of Robert Vincent who is one of the best expert in NMR equipments in the world. He has been a good advisor, technician, collaborator, and friend during five years in Ames.

I must also thank to Prof. R.G. Barnes. His knowledge in physics and incredible enthusiasm for research have impressed me in many times. I have learned a lot from him. I would also like to thank Dr. B.J. Suh who guided me to NMR research, for his precious suggestions and encouragement throughout the initial stage of my graduate career. His insights into physics and attitude to experiments taught me what a researcher ought to be. Dr. Z.H. Jang should also be thanked for many valuable helps both personally and experimentally. A special thanks should go to Dr. A. Lascialfari in Pavia, Italy, and Dr. Y. Furukawa in Sapporo, Japan. Without collaborations with them, this thesis could not have been completed. Also I am grateful to many colleagues throughout many years: B. Meyer, D. Procissi for his many useful assistance, A. Shastri and his beautiful family, M. Belesi for her friendship, and I. Rousokatzakis for many useful theoretical discussions. They are all good friends as well as good collaborators.

I would like to thank my PhD POS committee members for their efforts and invaluable

contributions to this work: professors M. Luban who is an excellent teacher and also good collaborator in theoretical parts of my NMR research, J. Schmalian who has inspired me to greater improvements in many occasions, J. Shinar, J. Qiu, and G. Miller. Also Prof. D.C. Johnston and Prof. P. Canfield should be thanked for their useful suggestions and discussions. I also would like to thank A. Cornia for providing the enriched Fe8 sample and a detailed description of the sample preparation.

Finally, thanks are due to my parents, parents-in-law, and my brother and sister in Korea for their loving guidance and mental support.

The United States Government has assigned the DOE Report number IS-T 2015 to this thesis. Notice: This document has been authored by the Iowa State University of Science and Technology under Contract No. W-7405-ENG-82 with the U. S. Department of Energy. The U. S. Government retains a non-exclusive, paid-up, irrevocable, world-wide license to publish or reproduce the published form of this document, or allow others to do so, for U. S. Government purposes.

October, 20, 2004

Ames, Iowa, USA

SEUNG-HO BAEK

Bibliography

[1] O. Kahn. *Molecular Magnetism.* VCH Publishers, VCH, New York, 1993.

[2] D. Gatteschi, A. Caneschi, L. Pardi, and R. Sessoli. *Science*, 265:1054, 1994.

[3] F. Le Gall, F.F. de Biani, A. Caneschi, P. Cinelli, A. Cornia, A.C. Fabretti, and D. Gatteschi. *Inorg. Chim. Acta*, 262:123, 1997.

[4] A. Müller, M. Luban, C. Schröder, R. Modler, P. Kögerler, M. Axenovich, J. Schnack, P. Canfield, S. Bud'ko, and N. Harrison. *ChemPhysChem*, 2:517, 2001.

[5] J. Sinzig, L.J. de Jongh, A. Ceriotti, R. della Pergola G. Longoni, M. Stener, K. Albert, and N. Rösch. *Phys. Rev. Lett.*, 81:3211, 1998.

[6] K.L. Taft and S.J. Lippard. *J. Am. Chem. Soc.*, 112:9629, 1990.

[7] J.S. Miller and M. Drillon, editors. *Magnetism: Molecules to Materials III*, Wiley-VCH, Weinheim, Germany, 2002.

[8] D. Gatteschi. *Phil. Trans. R. Soc. Lond. A*, 357:3079, 1999.

[9] D. Gatteschi and R. Sessoli. *J. Mag. Mag. Mat.*, 272-276:1030, 2004.

[10] A. Caneschi, D. Gatteschi, C. Sangregorio, R. Sessoli, L. Sorace, A. Cornia, M.A. Novak, C. Paulsen, and W. Wernsdorfer. *J. Mag. Mag. Mat.*, 200:182, 1999.

[11] K.L. Taft, C.D. Delfs, G.C. Papaefthymiou, S. Foner, D. Gatteschi, and S.J. Lippard. *J. Am. Chem. Soc.*, 116:823, 1994.

[12] A. Cornia, A.G.M. Jansen, and M. Affronte. *Phys. Rev. B*, 60:12177, 1999.

[13] O. Waldmann. *Europhys. Lett.*, 60:302, 2002.

[14] A. Chiolero and D. Loss. *Phys. Rev. Lett.*, 80:169, 1998.

[15] A. Caneschi, T. Ohm, C. Paulsen, D. Rovai, C. Sangregorio, and R. Sessoli. *J. Mag. Mag. Mat.*, 177-181:1330, 1998.

[16] M.-H. Julien, Z.H. Jang, A. Lascialfari, F. Borsa, M. Horvatić, A. Caneschi, and D. Gatteschi. *Phys. Rev. Lett.*, 83:227, 1999.

[17] D. Gatteschi, R. Sessoli, and A. Cornia. *Chem. Comm.*, 9:725, 2000.

[18] A. Cornia, M. Affronte, A.G.M. Jansen, G.L. Abbati, and D. Gatteschi. *Angew. Chem. Int. Ed.*, 38:2264, 1999.

[19] O. Waldmann, R. Koch, S. Schromm, P. Müller, I. Bernt, and R.W. Saalfrank. *Phys. Rev. Lett.*, 89:246401, 2002.

[20] M. Affronte, A. Cornia, A. Lascialfari, F. Borsa, D. Gatteschi, J. Hinderer, M. Horvatić, A. Jansen, and M.-H. Julien. *Phys. Rev. Lett.*, 88:167201, 2002.

[21] J. van Slageren, R. Sessoli, D. Gatteschi, A.A. Smith, M. Helliwell, R.E.P Winpenny, A. Cornia, A-L. Barra, A.G.M. Jansen, E. Rentschler, and G.A. Timco. *Chem. Eur. J*, 8:277, 2002.

[22] M. Affronte, T. Guidi, R. Caciuffo, S. Carretta, G. Amoretti, J. Hinderer, I. Sheikin, A.A. Smith, R.E.P. Winpenny, J. van Slageren, and D. Gatteschi. *J. Mag. Mag. Mat.*, 272-276:1050, 2004.

[23] A. Lascialfari, F. Borsa, M.-H. Julien, E. Micotti, Y. Furukawa, Z.H. Jang, A. Cornia, D. Gatteschi, M. Horvatic, and J. Van Slageren. *J. Mag. Mag. Mat.*, 272-276:1042, 2004.

[24] T. Lis. *Acta Cryst. B*, 36:2042, 1980.

[25] K. Wieghardt, K. Pohl, I. Jibril, and G. Huttner. *Angew. Chem. Int. Ed. Engl.*, 23:77, 1984.

[26] R. Sessoli, D. Gatteschi, A. Caneschi, and M.A. Nobak. *Nature*, 365:141, 1993.

[27] A.-L. Barra, P. Debrunner, D. Gatteschi, Ch. E. Schulz, and R. Sessoli. *Europhys. Lett.*, 35:133, 1996.

[28] J.R. Friedman, M.P. Sarachik, J. Tejada, and R. Ziolo. *Phys. Rev. Lett.*, 76:3830, 1996.

[29] L. Thomas, F. Lionti, R. Ballou, D. Gatteschi, R. Sessoli, and B. Barbara. *Nature*, 383:145, 1996.

[30] W. Wernsdorfer and R. Sessoli. *Science*, 284:133, 1999.

[31] D. Gatteschi and R. Sessoli. *Angew. Chem. Int. Ed.*, 42:268, 2003.

[32] D. Deutsch and R. Jozsa. *Proc. R. Soc. Lond. A*, 439:553, 1992.

[33] M.N. Leuenberger and D. Loss. *Nature*, 410:789, 2001.

[34] A. Leggett, B. Ruggiero, and P. Silvestrini, editors. *Quantum Computing and Quantum Bits in Mesoscopic Systems*, Kluwer, New York, 2004.

[35] F. Torres, J.M. Hernández, X. Bohigas, and J. Tejada. *Appl. Phys. Lett.*, 77:3248, 2000.

[36] J. Tejada. *Polyhedron*, 20:1751, 2001.

[37] F. Borsa. In K.A. Müler and A. Rigamonti, editors, *Local Properties at Phase Transitions*, page 607, North-Holland, Amsterdam, 1976.

[38] F. Borsa and M. Mali. *Phys. Rev. B*, 9:2215, 1974.

[39] Y. Furukawa, K. Watanabe, K. Kumagai, F. Borsa, and D. Gatteschi. *Phys. Rev. B*, 64:104401, 2001.

[40] Y. Furukawa, S. Kawakami, K. Kumagai, S.H. Baek, and F. Borsa. *Phys. Rev. B*, 68:180405(R), 2003.

[41] S.H. Baek, S. Kawakami, Y. Furukawa, B.J. Suh, F. Borsa, K. Kumagai, and A. Cornia. *J. Mag. Mag. Mat.*, 272-276:E771, 2004.

[42] T. Kubo, T. Goto, T. Koshiba, K. Takeda, and K. Awaga. *Phys. Rev. B*, 65:224425, 2002.

[43] Y. Furukawa, K. Aizawa, K. Kumagai, R. Ullu, A. Lascialfari, and F. Borsa. *Phys. Rev. B*, 69:14405, 2004.

[44] A. Morello, O.N. Bakharev, H.B. Brom, and L. de Jongh. *Polyhedron*, 22:1745, 2004.

[45] A. Abragam. *Principles of Nuclear Magnetism.* Clarendon Press, Oxford, 1961.

[46] C.P. Slichter. *Principles of Magnetic Resonance.* Splinger-Verlag, Berlin, 1990.

[47] J.H. Van Vleck. *Phys. Rev.*, 74:1168, 1948.

[48] J. Winter. *Magnetic Resonance in Metals.* Clarendon Press, Oxford, 1971.

[49] F. Borsa. In K.A. Müler and A. Rigamonti, editors, *Local Properties at Phase Transitions*, page 137, North-Holland, Amsterdam, 1976.

[50] T. Moriya. *Prog. Theor. Phys.*, 16:23, 1956.

[51] T. Moriya. *Prog. Theor. Phys.*, 28:371, 1962.

[52] J.H. Luscombe and M. Luban. *Phys. Rev. E*, 54:2266, 1996.

[53] A. Lascialfari, D. Gatteschi, F. Borsa, A. Shastri, Z.H. Jang, and P. Carreta. *Phys. Rev. B*, 57:514, 1998.

[54] F. Borsa, A. Lascialfari, and Y. Furukawa. Cond-Mat/0404378-9, 2004.

[55] A. Lascialfari, Z.H. Jang, F. Borsa, D. Gatteschi, and A. Cornia. *J. Appl. Phys.*, 83:6946, 1998.

[56] A. Lascialfari, Z.H. Jang, F. Borsa, P. Carretta, and D. Gatteschi. *Phys. Rev. Lett.*, 81:3773, 1998.

[57] Y. Furukawa, K. Kumagai, A. Lascialfari, S. Aldrovandi, F. Borsa, R. Sessoli, and D. Gatteschi. *Phys. Rev. B*, 64:094439, 2001.

[58] M. Ueda, S. Maegawa, and S. Kitagawa. *Phys. Rev. B*, 66:73309, 2002.

[59] Y. Furukawa, K. Watanabe, K. Kumagai, F. Borsa, T. Sasaki, N. Kobayashi, and D. Gatteschi. *Phys. Rev. B*, 67:064426, 2003.

[60] M. Luban, F. Borsa, S. Bud'ko, P. Canfield, S. Jun, J. Jung, P. Kögerler, D. Mentrup, A. Müller, R. Modler, D. Procissi, B.J. Suh, and M. Torikchvili. *Phys. Rev. B*, 66:054407, 2002.

[61] A. Cornia, A. Fort, M.G. Pini, and A. Rettori. *Europhys. Lett.*, 50:88, 2000.

[62] Y. Pontillon, A. Caneschi, D. Gatteschi, R. Sessoli, E. Ressouche, J. Schweizer, and E. Lelievre-Berna. *J. Am. Chem. Soc.*, 121:5342, 1999.

[63] W. Wernsdorfer, T. Ohm, C. Sangregorio, R. Sessoli, and C. Paulsen. *Phys. Rev. Lett.*, 82:3903, 1999.

[64] A.-L. Barra, D. Gatteschi, and R. Sessoli. *Chem. Eur. J*, 6:1608, 2000.

[65] C. Delfs, D. Gatteschi, L. Pardi, R. Sessoli, K. Wieghardt, and D. Hanke. *Inorg. Chem.*, 32:3099, 1993.

[66] R. Caciuffo, G. Amoretti, A. Murani, R. Sessoli, A. Caneschi, and D. Gatteschi. *Phys. Rev. Lett.*, 81:4744, 1998.

[67] A.-L. Barra, F. Bencini, A. Caneschi, D. Gatteschi, C. Paulsen, C. Sangregorio, R. Sessoli, and L. Sorace. *Chemphyschem*, 2:523, 2001.

[68] X. Martínez-Hidalgo, E.M. Chudnovsky, and A. Aharony. *Europhys. Lett.*, 55:273, 2001.

[69] A. Morello, F.L. Mettes, F. Luis, J.F. Fernández, J. Krzystek, G. Aromí, G. Christou, and L.J. de Jongh. *Phys. Rev. Lett.*, 90:017206, 2003.

[70] M. Ueda, S. Maegawa, H. Miyasaka, and S. Kitagawa. *J. Phys. Soc. Jap.*, 70:3084, 2001.

[71] A.K. Zvezdin, V.V. Dobrovitski, B.N. Harmon, and M.I. Katsnelson. *Phys. Rev. B*, 58:14733(R), 1998.

[72] A.J. Leggett. In L. Gunther and B. Barbara, editors, *Quantum Tunneling of Magnetization-QTM'94*, Kluwer, Netherlands, 1995.

[73] D. Gatteschi and R. Sessoli. In J.S. Miller and M. Drillon, editors, *Magnetism: Molecules to Materals III*, Wiley-VCH, Weinheim, Germany, 2002.

[74] D.A. Garanin. *J. Phys. A: math. Gen.*, 24:L61, 1991.

[75] P. Politi, A. Rettori, F. Hartmann-Boutron, and J. Villain. *Phys. Rev. Lett.*, 75:537, 1995.

[76] F. Hartmann-Boutron, P. Politi, and J. Villain. *Int. J. Mod. Phys. B*, 10:2577, 1966.

[77] N.V. Prokof'ev and P.C.E. Stamp. *Phys. Rev. Lett.*, 80:5794, 1998.

[78] N.V. Prokof'ev and P.C.E. Stamp. *J. Low. Temp. Phys.*, 104:143, 1996.

[79] W. Wernsdorfer, R. Sessoli, and D. Gatteschi. *Europhys. Lett.*, 47:254, 1999.

[80] J.J. Alonso and J.F. Fernández. *Phys. Rev. Lett.*, 87:097205, 2001.

[81] W. Wernsdorfer, R. Sessoli, and D. Gatteschi. *Europhys. Lett.*, 50:4, 2000.

[82] W. Wernsdorfer, A. Caneschi, R. Sessoli, D. Gateschi, A. Cornia, V. Villar, and C. Paulsen. *Phys. Rev. Lett.*, 84:2965, 2000.

[83] T. Ohm, C. Sangregorio, and C. Paulsen. *Eur. Phys. J. B*, 6:195, 1998.

[84] L. Thomas, A. Caneschi, and B. Barbara. *Phys. Rev. Lett.*, 83:2398, 1999.

[85] I. Chiorescu, R. Giraud, A.G.M. Jansen, A. Caneschi, and B. Barbara. *Phys. Rev. Lett.*, 85:4807, 2000.

[86] A.L. Burin, N.V. Prokof'ev, and P.C.E. Stamp. *Phys. Rev. Lett.*, 76:3040, 1996.

[87] F. Luis, J. Bartolomé, and J.F. Fernández. *Phys. Rev. B*, 57:505, 1998.

[88] A. Fort, A. Rettori, J. Villain, D. Gatteschi, and R. Sessoli. *Phys. Rev. Lett.*, 80:612, 1998.

[89] M.N. Leuenberger and D. Loss. *Europhys. Lett.*, 46:692, 1999.

[90] M.N. Leuenberger and D. Loss. *Phys. Rev. B*, 61:1286, 2000.

[91] Yu. Kagan and L.A. Maksimov. *Sov. Phys. JETP*, 52:689, 1980.

[92] I. Tupitsyn and B. Barbara. In J.S. Miller and M. Drillon, editors, *Magnetism: Molecules to Materals III*, Wiley-VCH, Weinheim, Germany, 2002.

[93] J. Villain, A. Würger, A. Fort, and A. Rettori. *J. Phys. I (France)*, 7:1583, 1997.

[94] N.V. Prokof'ev and P.C.E. Stamp. *Rep. Prog. Phys.*, 63:669, 2000.

[95] C. Sangregorio, T. Ohm, C. Paulsen, R. Sessoli, and D. Gatteschi. *Phys. Rev. Lett.*, 78:4645, 1997.

[96] E. del Barco, N. Vernier, J.M. Hernandez, J. Tejada, E.M. Chudnovsky, E. Molins, and G. Bellessa. *Europhys. Lett.*, 47:722, 1999.

[97] F. Luis, F.L. Mettes, J. Tejada, D. Gatteschi, and L.J. de Jongh. *Phys. Rev. Lett.*, 85:4377, 2000.

[98] F. Luis, F.L. Mettes, J. Tejada, D. Gatteschi, and L.J. de Jongh. *Polyhedron*, 20:1451, 2001.

[99] M.V. Berry. *Proc. R. Soc. Lond. A*, 392:45, 1984.

[100] E.N. Bogachek and I.V. Krive. *Phys. Rev. B*, 46:14559, 1992.

[101] J. von Delft and C.L. Henley. *Phys. Rev. Lett.*, 69:3236, 1992.

[102] A. Garg. *Europhys. Lett.*, 22:205, 1993.

[103] R. Shankar. *Principles of Quantum Mechanics.* Plenum, New York, 1994.

[104] A. Garg. *Phys. Rev. Lett.*, 83:4385, 1999.

[105] J. Villain and A. Fort. *Eur. Phys. J. B*, 17:69, 2000.

[106] C. Zener. *Proc. R. Soc. Lond.*, 137:696, 1932.

[107] S. Miyashita. *J. Phys. Soc. Jap.*, 64:3207, 1995.

[108] S. Miyashita. *J. Phys. Soc. Jap.*, 65:2734, 1996.

[109] E. Keçecioğlu and A. Garg. *Phys. Rev. Lett.*, 88:237205, 2002.

[110] E. Keçecioğlu and A. Garg. *Phys. Rev. B*, 67:054406, 2003.

[111] I. Mirebeau, M. Hennion, H. Casalta, H. Andres, H.U. Gudel, A.V. Irodova, and A. Caneschi. *Phys. Rev. Lett.*, 83:628, 1999.

[112] G.C. Papaefthymiou. *Phys. Rev. B*, 46:10366, 1992.

[113] E.M. Chudnovsky. *Science*, 274:938, 1996.

[114] H. De Raedt. *Phys. Rev. B*, 56:11761, 1997.

[115] F. Hartmann-boutron, P. Politi, and J. Villain. *Int. J. Mod. Phys. B*, 10:2577, 1996.

[116] F.L. Mettes, F. Luis, and L.J. de Jongh. *Phys. Rev. B*, 64:174411, 2001.

[117] E. del Barco, J.M. Hernandez, J. Tejada, N. Biskup, R. Achey, I. Rutel, N. Dalal, and J. Brooks. *Phys. Rev. B*, 62:3018, 2000.

[118] L. Sorace, W. Wernsdorfer, C. Thirion, A.-L. Barra, M. Pacchioni, D. Mailly, and B. Barbara. *Phys. Rev. B*, 68:220407(R), 2003.

[119] S. Maegawa and M. Ueda. *Prog. Theor. Phys. Suppl.*, 145:380, 2002.

[120] R.E. Watson and A.J. Freeman. *Phys. Rev.*, 123:2027, 1961.

[121] G.K. Wertheim, H.J. Guggenheim, and D.N.E. Buchanan. *Phys. Rev.*, 169:465, 1968.

[122] A.J. Freeman and R.E. Watson. In G.T. Rado and H. Suhl, editors, *Magnetism IIA*, Academic, New York, 1965.

[123] P. Gütlich. In U. Gonser, editor, *Mössbauer Spectroscopy*, Spinger-Verlag, Berlin, 1975.

[124] L. Cianchi, F. Del Giallo, G. Spina, W. Reiff, and A. Caneschi. *Phys. Rev. B*, 65:064415, 2002.

[125] L.R. Walker, G.K. Wertheim, and V. Jaccarino. *Phys. Rev. Lett.*, 6:98, 1961.

[126] V. Jaccarino. In W. Marshall, editor, *Theory of Magnetism in Transition Metals*, Academic Press, New York, 1967.

[127] J. Kortus, M.R. Pederson, C.S. Hellberg, and S.N. Khanna. *Eur. Phys. J. D*, 16:177, 2001.

[128] C. Kittel. *Introduction to solid state physics.* John Wiley & Sons, Inc., New York, 1996.

[129] H. Hori and S. Yamamoto. *Phys. Rev. B*, 68:54409, 2003.

[130] T. Kohmoto, T. Goto, S. Maegawa, N. Fujiwara, M. kunitomo, and M. Mekata. *Phys. Rev. B*, 49:6028, 1994.

[131] T. Goto, T. Koshiba, T. Kubo, and K. Awage. *Phys. Rev. B*, 67:104408, 2003.

[132] S. Alexander and A.Tzalmona. *Phys. Rev.*, 138:A845, 1965. See also A. Rigamonti and J.R. Brookman, Phys. Rev. B **21**, 2681 (1980).

[133] M. Takigawa and G. Saito. *J. Phys. Soc. Jap.*, 55:1233, 1986.

[134] A. Morello. *Quantum Spin Dynamics in Single-Molecule Magnets.* PhD thesis, Leiden University, The Netherlands, 2004. cond-mat/0404049.

[135] S.H. Baek, M. Luban, A. Lascialfari, E. Micotti, Y. Furukawa, F. Borsa, and J. van Slageren. *Phys. Rev. B*, 2004 (In press).

[136] A. Landé. *Z. für Physik*, 15:189, 1923.

[137] J. Schnack and M. Luban. *Phys. Rev. B*, 63:014418, 2000.

[138] A. Lascialfari, D. Gatteschi, F. Borsa, and A. Cornia. *Phys. Rev. B*, 55:14341, 1997.

[139] D. Procissi, B.J. Suh, E. Micotti, A. Lascialfari, Y. Furukawa, and F. Borsa. *J. Mag. Mag. Mat.*, 272-276:e741, 2004.

[140] A. Caneschi, A. Cornia, and S.J. Lippard. *Angew. Chem.*, 34:467, 1994.

[141] D. Procissi, A. Shastri, I. Rousochatzakis, M. Al-Rifai, P. Kögerler, M. Luban, B.J. Suh, and F. Borsa. *Phys. Rev. B*, 69:094436, 2004.

[142] A. Lascialfari, Z.H. Jang, F. Borsa, D. Gatteschi, A. Cornia, D. Rovai, A. Caneschi, and P. Carretta. *Phys. Rev. B*, 61:6839, 2000.

[143] M. Luban, F. Borsa, E.N. Economou, P. Kögerler, and I. Rousochatzakis. (unpublished).

[144] D. Hone, C. Scherer, and F. Borsa. *Phys. Rev. B*, 9:965, 1974.

[145] R. Kubo. *Rep. Prog. Phys.*, 29:255, 1966.

VITA

NAME: Seung-Ho Baek

DATE AND BIRTH PLACE: [redacted]

DEGREES AWARDED: B.S., Physics, Spring 1998; Kyung-Hee University, Seoul, Korea

PROFESSIONAL EXPERIENCE

Teaching assistent, Iowa State University, 1999-2001

Research assistent, Iowa State University, 2001-present

PROFESSIONAL PUBLICATIONS

1. "Direct measurement of the tunneling rate of the magnetization in Fe8 via ^{57}Fe nuclear spin-lattice relaxation by strong collision" **S.H. Baek**, F. Borsa, Y. Furukawa, Y. Hatanaka, S. Kawakami, and K. Kumagai, *Physical Review Letters* (submitted)
2. "Influence of lattice defects on the *d*-electron heavy fermion metal LiV_2O_4" D.C. Johnston, **S.H. Baek**, F. Borsa, and S. Kondo, (In preparation)
3. "Scaling behavior of the proton spin-lattice relaxation rate in antiferromagnetic molecular rings" **S.H. Baek**, M. Luban, A. Lascialfari, E. Micotti, Y. Furukawa, F. Borsa, J. van Slageren, and A. Cornia, *Physical Review B* (accepted)
4. "^{57}Fe NMR in oriented powder of Fe8 in zero and applied field" **S.H. Baek**, S. Kawakami, Y. Furukawa, B.J. Suh, F. Borsa, K. Kumagai, and A. Cornia, *Journal of Magnetism and Magnetic Materials*, **272-276**, E771 (2004)
5. "^{57}Fe-NMR determination of the local magnetic structure of the molecular nanomagnet Fe8" Y. Furukawa, S. Kawakami, K. Kumagai, **S.H. Baek**, F. Borsa, *Physical Review B*, **68**, 180405(R) (2003)
6. "NMR relaxation rates and Knight shifts in MgB_2 and AlB_2: Theory versus experiments" E. Pavarini, **S.H. Baek**, B.J. Suh, F. Borsa, S.L. Bud'ko, and P.C. Canfield, *Superconductor Science and Technology*, **16**, 147 (2003)
7. "NMR spectroscopy of the normal and superconducting of MgB_2 and compariosn to AlB_2" **S.H. Baek**, B.J. Suh, E. Pavarini, F. Borsa, R.G. Barnes, S.L. Bud'ko, and P.C. Canfield, *Physical Review B*, **66**, 104510 (2002).
8. "^{11}B NMR and relaxation in the MgB_2 superconductor" J.K. Jung, **S.H. Baek**, F. Borsa, S.L. Bud'ko, G. Lapertot, and P.C. Canfield, *Physical Review B*, **64**, 012514 (2001)